

UNIVERSITY OF OKLAHOMA

GRADUATE COLLEGE

STUDYING “FITNESS FOR SERVICE” OF THE SEALING ASSEMBLIES AND
CEMENT SYSTEM

A THESIS

SUBMITTED TO THE GRADUATE FACULTY

in partial fulfillment of the requirements for the

Degree of

MASTER OF SCIENCE

By

GEORGE OHENE KWATIA

Norman, Oklahoma

2018

STUDYING “FITNESS FOR SERVICE” OF THE SEALING ASSEMBLIES AND
CEMENT SYSTEM

A THESIS APPROVED FOR THE
MEWBOURNE SCHOOL OF PETROLEUM AND GEOLOGICAL ENGINEERING

BY

Dr. Saeed Salehi, Chair

Dr. Catalin Teodoriu

Dr. Ramadan Ahmed

© Copyright by GEORGE OHENE KWATIA 2018
All Rights Reserved.

Acknowledgements

I would like to express my sincere gratitude to God for enabling me to complete my thesis successfully.

I would like to express my gratitude to my supervisor and chair, Dr. Saeed Salehi, for his unwavering support, gusto and guidance throughout this research. I am indebted to him for his constructive criticism and suggestions in the completion of this thesis.

To Dr. Catalin Teodoriu and Dr. Ramadan Ahmed - my committee members, I am grateful for your assistance and directions during my degree and research.

My deepest gratitude goes to my family; without whom I could not have completed this thesis. To Chinedum Ezeakacha Peter, McCaskill Jeffery and any other person who supported me during my graduate program, I say thank you.

Table of Contents

Acknowledgements	iv
Table of Contents	v
List of Tables	x
List of Figures.....	xii
Abstract.....	xix
Chapter 1: Introduction.....	1
Overview	1
Motivation	1
Problem Statement.....	3
Study Objectives.....	4
Methodology.....	4
Chapter 2: Literature Review	6
Overview	6
Elastomers	6
Types and Composition of Elastomers.....	10
Elastomers in Oil and Gas Industry	16
Properties and Testing of Elastomers	20
Summary.....	33
Well Integrity and Cementing in Gas Hazard Zones.....	34
Gas Migration.....	37
Shallow Gas Loss of Well Control (LOWC)	43
Cement Design and Integrity	47

Gas Migration Additives	51
Cost Estimations and Effects	63
Summary.....	63
Chapter 3: Elastomer Experiment and Results	65
Research Methodology	65
Experimental Design	66
Experimental Investigations	67
Test Materials	67
Test Matrix	68
Test Sample Preparation Procedures	71
Elastomer Aging Experiment	71
Experimental Setup	71
Test Procedure	73
Elastomer Experiment Results	75
Performance of Elastomers.....	75
Hardness	76
Compression.....	81
Volumetric Swelling.....	89
Chapter 4: Cement Experiment and Results.....	96
Research Methodology.....	96
Scope of Work.....	97
Experimental Investigations	98

Test Materials	101
Cement Slurry Preparation Procedure	105
Slurry Formulations	105
Slurry Properties	105
Cement Gas Migration Experiment	108
Experimental Setup	108
Major Test Experimental Setup	108
Minor Test Experimental Setup	110
Test Procedure	111
Major Test Procedure	111
Minor Test Procedure	114
Cement Experiment Results	115
Pressure decline curves	128
Pressure decline curves by days	129
Pressure decline curves by days – 60 psi	129
Pressure decline curves by cycle	130
Pressure decline curves by ballooning	133
Predicting Effective or System Permeability (K) from decline curves	134
Small Setup 1	135
Class H and Fly Ash Cement Sample	140
Microsilica Cement Sample	142
Nanomaterial Cement Sample	145

Class H, Flyash, Latex and Nanomaterial Cement Sample.....	147
Class H, 1.5 liters / 100 kg commercial additive Cement Sample	148
Properties of Cement Samples.....	150
Rheology.....	150
Gas Transit time	152
Unconfined Compressive Strength and Ultrasonic Testing	154
Chapter 5: Summary and Conclusions	158
Elastomer Experiment Conclusions and Summary	158
Cement Experiment Summary and Conclusions	158
Recommendations	160
Abbreviation	163
References	165
Appendix A: Elastomers.....	175
Test Equipment and Testing Protocol	175
Hardness	175
Volumetric Swelling.....	176
Compression Test.....	177
Appendix B: Cementing.....	179
Calculations	179
Permeability prediction matlab code	181
Test Sample Preparation Procedure.....	181
Gas Transit Time	183
Rheology.....	184

Unconfined Compressive St Strength and Ultrasonic Testing 185

List of Tables

Table 1. Common general-purpose elastomers with structures (from Visakh et al., 2013).	14
Table 2. Some of the properties of typical elastomer in oil and gas industry.	18
Table 3. H ₂ S resistance of various elastomers, at their respective glass transition and high temperature performance (from Tynan, 2016).	24
Table 4. Experiment design details for the longevity test setup (from Qamar et al., 2012).	32
Table 5: Highlights of gas Migration additives	62
Table 6: Cost estimations for anti-gas migration additives	63
Table 7: Test parameters for aging experiments conducted	69
Table 8: Test parameters for aging experiments conducted	70
Table 9: Nomenclature of elastomer sample.	71
Table 10: Elastomer arrangement in autoclave shelves	75
Table 11: Test matrix 1 and parameters – Studying the effect of WOC and additives on 3ft experiments	99
Table 12: Test matrix 2 and parameters – Studying the effect of additives on 6ft experiments.....	99
Table 13. Test matrix 3 and parameters – Studying the effect of vibration and additives on 3ft experiments.	100
Table 14: Properties of baseline and gas tight slurries.	105
Table 15: Rheology of Class H base slurry and gas tight slurry.	106

Table 16: Leakage time for Setup 1 Experiment 1, Setup 1 Experiment 2, and Setup 1 Experiment 3.	124
Table 17: Leakage time for Setup 1 Experiment 1, Small Setup 1 Experiment 1 and Small Setup 1 Experiment 2.	138
Table 18. Rheological Properties of Tested Cement Slurries.....	151
Table 19: Ultrasonic Pulse Velocity (UPV) and Unconfined Compressive Strength (UCS) test results reported.	155
Table 20. Leak time for Major and Minor Setups	161
Table 21: Durometer readings for three days aging test.....	176
Table 22: Diameter and length readings for three days test.	177
Table 23: Stress vs. strain relationship of NBR before and after three days aging.	178
Table 24: Nomenclature for major experiment	182
Table 25: Nomenclature for minor experiment	182
Table 26: Recorded time for slurries to attain 100 lbf/100 ft ² and 500 lbf/100 ft ²	183

List of Figures

Figure 1. Molecular entanglement in high molecular weight polymer (a) Molecular entanglement in elastomer locked by cross linking (b) (from Drobny, 2007).	9
Figure 2. Structure of repeating units: a) NBR (top) and b) HNBR (bottom) (redrawn after James Walker, 2012, Issue 10.1)	15
Figure 3. Structure of repeating units: FKM Viton (a), FEPM Aflas (b), and FFKM Kalrez (c). (redrawn after James Walker, 2012, Issue 10.1).....	15
Figure 4. Some examples of elastomer failure caused by RGD (top row) and overload pressure (bottom row).....	19
Figure 5. Stress vs. Strain profile for elastomers (from James Walker, 2012, Issue 10.1).	20
Figure 6. Cross-section of cracks on the FKM O-ring elastomers after performance requirement test (from Chen et al., 2016).....	22
Figure 7. Cross-section of cracks on elastomer O-rings after high pressure RGD test at 3020F (from Chen et al., 2016).	23
Figure 8. Hardness vs. Temperature (from Jin et al., 2008).....	25
Figure 9. Nucleophilic reaction mechanism showing the breakdown of the acrylonitrile group in HNBR (redrawn after Cong et al., 2008).	26
Figure 10. Scanning Electron micrographs of NBR aged with H ₂ S (203°F, 168 hrs.) (from Fernández et al., 2016).	27
Figure 11. Scanning Electron Micrograph (SEM) of NBR aged with CO ₂ (203°F, 168 hrs.) (from Fernández et al., 2016).	28

Figure 12. SEM images of HNBR after aging at 0lbf (a), 1349lbf (b), and 2698lbf (c) (from Dajiang et al., 2017).	29
Figure 13. Swelling curves of button-shaped samples tested (a) 10% CaCl ₂ at 200°F (b) 45% NaBr at 200°F (from Wang et al., 2015).....	31
Figure 14. Shallow zone kick causes summarized in ExproSoft’s report to BSEE, 2017.	46
Figure 15. Potential leakage pathways in wellbores (from Salehi, 2013).	49
Figure 16: Dosage of microsilica needed at different cement slurry densities to withstand a maximum gas pressure of 125% of the water gradient (from Grinrod et al., 1988)....	57
Figure 17: Particle size distribution of raw samples. S1 – 333 kg/m ³ , S2 – 719 kg/m ³ , S3 – 582 kg/m ³ , S4 – 167 kg/m ³ (Daou and Piot, 2009).	59
Figure 18: Particle size distribution of cement and various microsilica additives (after Daou and Piot, 2009; Dylan Moore, 2015).	59
Figure 19: Schematic of autoclave cell setup (Ahmed et al., 2015).....	73
Figure 20: (a) Samples arranged in different shelves before lowering into the aging cell. (b)Schematic of sample arrangement inside the aging cell with legend. Shelves 1 to 6 are submersed inside brine, while shelves 7 to 12 are not, but still exposed to vapor from the brine.....	74
Figure 21: Effects of days on hardness of elastomer samples aged at 1000 psi, and at (a) 120 °F, (b) 180 °F.....	77
Figure 22: Effects of temperature on hardness of elastomer samples aged at 1000 psi, and after (a) 1 day, (b) 7 days.....	78

Figure 23: Effects of temperature on hardness of elastomer samples aged at 1000 psi, and after 3 days.	79
Figure 24: Effects of gas variation on hardness of elastomer samples aged at 1000 psi after 7 days.	81
Figure 25: Elastomer compression measurement at: 120 °F (a) after 1 day, (b) after 7 days, and 180 °F (c) 1 day, (d) 7 days.	83
Figure 26: PTFE compression measurement at after 1 day at 120 °F.	83
Figure 27: Effects of temperature on compression of elastomer samples after 3 days aging at 1000 psi, and at (a) 120 °F, (b) 180 °F	84
Figure 28: Effects of days on compression of elastomer samples aged at 1000 psi and 120 °F (a) actual strain values, (b) percentage increase in strain values.	85
Figure 29: Effects of days on compression (percentage strain) of elastomer samples aged at 1000 psi and 180 °F (a) actual strain values, (b) percentage increase in strain values.	85
Figure 30: Effects of temperature on compression of elastomer samples aged for 1 day at 1000 psi (a) actual strain values, (b) percentage increase in strain values.	86
Figure 31: Effects of temperature on compression of elastomer samples aged for 7 days at 1000 psi (a) actual strain values, (b) percentage increase in strain values.	87
Figure 32: Effects of gas variations on compression of elastomer samples aged at 1000 psi and 120 °F (a) compression measurement (b) percentage difference in compression measurements.	88

Figure 33: Effects of days on volumetric swelling of elastomer samples aged at 120 °F and 1000 psi, (a) compression measurement (b) percentage difference in compression measurements.	90
Figure 34: Effects of days on volumetric swelling of elastomer samples aged at 180 °F and 1000 psi, (a) compression measurement (b) percentage difference in compression measurements.	90
Figure 35: 1 Day aging in CO ₂ and H ₂ S with CH ₄ carrier at 1000 psi. (a) 120 °F and (b) 180 °F.	91
Figure 36: Viton Blistering taken with a Dino-Lite Digital Microscope.	92
Figure 37: Effects of temperature on percentage volumetric change in elastomer samples aged at 1000 psi, after (a) 1 day (b) 7 days (c) 3 days.....	93
Figure 38: Effects of gas variation on percentage volume measurements of elastomer samples aged at 1000 psi and after 7 days (a) volume measurement (b) percentage volumetric change.	95
Figure 39: Particle Size Distribution of various samples with Mastersizer 2000.	104
Figure 40: Gas Transit time for Class H base slurry and gas tight slurry.	107
Figure 41: Thickening time for gas tight slurry base slurry.	108
Figure 42: Schematic for gas migration setup (major test)	110
Figure 43: Schematic for gas migration setup (minor test).	111
Figure 44: (a) 3-foot whole Setup 1 Experiment 2 (b) Data acquisition card with sensors fitted.....	114
Figure 45: Position of leaks for Setup 1 Experiment 1 (a) and Small Setup 1 Experiment 2 (b).	115

Figure 46: Left – Positions 2 and 3 as they appear in Setup 1 Experiment 2. Right – Position 4 as it appears in Setup 1 Experiment 2.	117
Figure 47: Position 4 magnified as it appears in Setup 1 Experiment 2.....	117
Figure 48: Setup for ballooning inner pipe. Left – Connection from hand pump to inner pipe. Right – Hand pump used to pressure the inner pipe of Setup 1.	118
Figure 49: Left - Gas bubble travelling from cement sheath through water to surface. Right – Travelled gas bubble bursting at surface.	118
Figure 50: Leakage time of Experiment conducted on Setup 1 Experiment 1 before and after ballooning.....	122
Figure 51: Leakage time of Experiment conducted on Setup 1 Experiment 2 before and after ballooning.....	123
Figure 52: Pressure data for first 30 minutes of testing for S1E2C1T1 and S1E3C1T1 (a) Sensor 2 (b) Sensor 3.....	126
Figure 53: (a) Setup 1 Experiment 3 regular bubbling (b) rapid bubbling.....	126
Figure 54: Leakage time for Setup 1 Experiment 3 cycles and ballooning.....	127
Figure 55: Day 2 Setup 1 Experiment 1, Setup 1 Experiment 2 and Setup 1 Experiment 3 (Cycle 1 and Cycle 2 – 60 psi) – Sensor 2	130
Figure 56: Day 1, Day 2, Day 3 for Setup 1 Experiment 3 (Cycle 1 – 60 psi) – Sensor 2	132
Figure 57: Day 1, Day 2, Day 3 for Setup 1 Experiment 4 (Cycle 1 – 60 psi) – Sensor 3	133
Figure 58: S1E4 Sensor 3 ballooning vs. Day 1, Day 2, Day 3 for Setup 1 Experiment 4	134

Figure 59: Small Setup 1 Experiment 1 (a) Experiment 2 (b).....	136
Figure 60: Small Setup 1 Experiment 2.	137
Figure 61: Leak Positions for Small Setup 1 Experiment 6.	141
Figure 62: Fly ash cement showing leak position (Small Setup 1 Experiment 6).	141
Figure 63: Fly ash cement showing leak position (Small Setup 1 Experiment 6).	142
Figure 64: Leak Positions of Small Setup 1 Experiment 7	143
Figure 65: Cement after leak	145
Figure 66: Nanomaterial Cement Sample with leak position highlighted in red.	146
Figure 67: Leak positions in Small Setup 1 Experiment 9.....	147
Figure 68: Bubbling in Small Setup 1 Experiment 11	148
Figure 69: Leak positions for Small Setup 1 Experiment 11	148
Figure 70: No bubbling in SS1E12.	149
Figure 71: Gas Transit time for various slurry samples.	153
Figure 72: Days 1 and 3 results for Unconfined Compressive Strength (UCS) tests...	156
Figure 73: Bubble graph to depict leak time for major and minor tests.....	162
Figure 74: Digital Durometer Model DD-4.....	176
Figure 75: Digital Vernier Caliper.	177
Figure 76: Compression machine setup.	178
Figure 77: Schematic of sensor connection to data acquisition system.	183
Figure 78: Shear rate vs. Shear rate of various slurry samples.	184
Figure 79: Apparent viscosity graph for various slurry samples at 255.4 s^{-1}	184
Figure 80: Prepared samples for Unconfined Compressive Strength and Ultrasonic Cement Testing.....	185

Figure 81: Ultrasonic cement testing being carried out..... 185

Abstract

Well integrity is a crucial phase of well design and construction, as such multiple barriers are usually installed in wells to prevent any migration of formation fluids. One of these barriers include the elastomeric sealing system or seal assembly. Limited knowledge is available on elastomer behavior in harsh downhole conditions. Lack of adequate knowledge makes elastomer selection during well design a problematic phase. This thesis reviews literature on elastomer performance under various conditions and expounds on the chemical reactions involved in the failure mechanisms of elastomers. Experiments have also been conducted on three popular elastomers: Nitrile butadiene rubber (NBR), Ethylene propylene diene monomer (EPDM), and Fluoroelastomers (FKM) in the presence of hydrogen sulfide (H_2S), methane (CH_4), carbon dioxide (CO_2) and brine. The performance of these elastomers is also discussed. Experiments conducted help us make an informed decision thus classifying the elastomers based on the degree of degradation under these harsh downhole conditions.

The second barrier is the set cement. In Oil and Gas drilling operations, cement is used to maintain wellbore integrity by preventing the movement of formation fluids through the annular space outside the casing. However, in gas migration prone regions, cement sealability may be inadequate. The reduced sealability also makes such regions prone to well instability. This thesis reviews gas mitigation approaches according to published literature. Some slurry designs published in literature are used in the experiments and the results are reported herein. A novel gas tight cement slurry is designed to prevent gas migration. This cement slurry has been tested in different pipe sizes and has proven to mitigate gas migration of any sort.

Chapter 1: Introduction

Overview

This chapter provides a brief motivation for this thesis. It also describes the problem statement and unequivocal objectives of this study. The goal is to bring the reader to understand why this research is being conducted and to highlight the trajectory of this study. A brief methodology to the experiments conducted is also provided herein.

Motivation

NORSOK D-010 define well integrity as the “application of technical, operational and organizational solutions to reduce risk of uncontrolled release of formation fluids throughout the life cycle of the well.” (NORSOK, 2013). As a result, a breach in well integrity leads to the migration of formation fluids into the wellbore. In gas wells, uncontrolled migration of hydrocarbons can lead to sustained casing pressure. Sustained casing pressure (SCP), commonly known as sustained annular pressure (SAP) refers to the development of annular pressure at the surface which when bled off builds again. The presence of SAP in the well indicates communication between the casing and an unisolated zone in the formation. The presence of SCP is directly related to well age, with a 50% probability of a 15-year-old well to have considerable SCP in at least one of its installed casings (Brufatto, 2003). Some of recent incidents are related to loss of well control by failure in different barriers such as elastomer liner hangers and cement column. In 2013, an incident in shallow Gulf of Mexico region occurred resulting in a shallow gas well control incident at the Main Pass Block 295. A QC-FIT evaluation report revealed potential causes of the incident as due to casing hanger elastomeric seals, and cement column in conductor/surface liner annulus. With this in mind, we see that proper well

integrity is needed to prevent the migration of formation fluids. To ensure proper well integrity, well design and construction become a major concern of drilling.

During well design and construction, barrier requirements are driven based on potential downhole hazards. Two popular barriers used in oil and gas wellbores are the elastomer sealing system, and the cement column. Elastomer sealing systems are installed to hold pressure from the well up to the designated pressure and temperature ratings of the seal assembly (Davis, 2008; Gavioli, 2012; Chen et al., 2016) while the cement column is to prevent the movement of formation fluids through the annular space outside the casing. The concept of gas migration has been of major concern since the 1960s and various aspects including experimental and field case studies (Stone and Christian, 1974; Garcia and Clark, 1976; Cook et al., 1983; Al Buraik et al, 1998; Bour and Wilkinson, 1992), development of new products and techniques (Kucyn et al., 1977; Watters and Sabins, 1980; Cheung and Myrick, 1983; Siedel and Greene, 1985; Matthews and Copeland, 1986) and technical recommendations (Levine et al., 1979; Tinsley et al., 1980; Cheung and Beirute, 1982; Dean and Brennen, 1992) have been heavily dwelt upon. Also, with an increase complex offshore reservoir explorations, high performance sealing elastomers are in demand (Debruijin et al., 2008; Tanaka, 2007; Talyor, 1990).

However, much detail about elastomer performance with aging under harsh conditions is unavailable. There is also limited knowledge about suitable elastomers to use in corrosive and noncorrosive environments. On the other hand, a substantial amount of research has been performed on cement including thickening time, rheology, gas transition time, and compressive strength. Knowledge about cement being a primary barrier, and what type of cement recipe would mitigate gas migration is however

unavailable. These unanswered questions are what drive me to research on “fitness for service” of the sealing assemblies and cement system.

Problem Statement

Currently, the oil and gas industry is exploring and producing hydrocarbon from harsh environments. This has made shallow gas of much concern in many oil and gas regions of the world, including, the Pacific Rim, the Norwegian Continental Shelf (NCS), UK Continental Shelf, and the Gulf of Mexico (Moore and Hamilton, 1993). This is because shallow gas is encountered in the early stages of drilling the well before it is even possible to have the blowout preventer installed (Murray, 1995). Lécolier et al. (2010) argues that a substantial amount of the world’s remaining gas reserves has over 2% CO₂ and substantial amounts of H₂S. The presence of these gases has complicated well construction design. Appropriate well design procedures require careful selection of suitable elastomers that would not degrade when exposed to harsh downhole conditions. It is also imperative to have a cement system that can mitigate gas migration since shallow gas flow can lead to blowouts in the open hole section usually below the conductor or surface casing because of gas migration through the cement (Adams, 1990).

Oil field elastomers are vulnerable to acid attack and harsh downhole environments. Different physical and chemical mechanisms are involved in the deterioration of elastomeric properties. There are limited available studies that have been conducted to study the effects of H₂S, CO₂, and other harsh downhole conditions on elastomers. Published research on elastomer degradation mechanisms when exposed to these conditions are scarce (Cong et al., 2013). Thus, more studies are needed to ensure that elastomers are “fit for service” in the environments in which they are used.

Talabani et al. (1997) and Nelson and Guillot (2006) discuss that the root cause of gas migration is the pathways in the annulus through which the gas can migrate. Thus, the ability to seal off these pathways is the solution to formation fluid flows.

Study Objectives

This study is in two folds; the first part is in relation to elastomer performance while the later deals with cement system integrity. The objectives of this study would therefore be in two major folds – one in relation to elastomer study and the second in relation to cement system integrity study.

The objectives for the elastomer study include:

- To investigate if elastomers are “fit for service” for shallow well construction applications.
- To determine elastomer performances under downhole corrosive conditions.

The objectives for the cement system study include:

- Evaluate the cement system integrity as a primary barrier.
- Study the effects of gas migration additives in cement slurry performance.
- Develop a gas tight cement slurry that to mitigate flow of formation fluid.
- Report properties of new cement slurry design.

Methodology

Elastomer degradation strongly depends on the elastomer's chemical structure as well as the composition and abundance of liquid and gas phases they are in contact with. Cement sealability also strongly depends on the cement to casing bonds and available pores within the cement. To examine the relationship between elastomer degradation and downhole operating parameters such as temperature, exposure time, and acid gas variations. An

intensive theoretical and literature review was carried out. Multiple laboratory experiments and data analysis were also performed. The outcome of the theoretical analysis provided useful information in understanding the mechanisms that are involved in the elastomer degradation process. While the results shed light on elastomer selection for downhole conditions.

Also, in this study, different slurry designs have also been investigated, adding additives like latex, microsilica, nanomaterial, fly ash and bentonite. We have examined key properties of cement with respect to controlling gas migration, mechanisms for wellbore integrity failure, and the relationship between cement design and its integrity. The literature review helped access available information in comprehending oil well barriers from qualified personnel in the fields of chemistry, engineering, medicine, and oil and gas amidst others.

Chapter 2: Literature Review

Overview

This chapter will encompass the many research work that is related to this study. The goal is to bring to knowledge previous related works done and shed more light on the need for further research into the areas that have not been fully considered, using real time experimental data.

Elastomers

Elastomers are materials that exhibit rapid and large reversible strain, in response to a stress. Elastomers are an important class of polymers that have randomly distributed chains, which are connected by cross links in their molecular structure (Visakh, 2013). Elastomers are made up of long chains of monomers (i.e. typically consist of more than 300,000 monomer units) that have strong cross-linking bond with their neighboring chains that pulls the elastomer back into the original shape when the deforming force is removed. A more technical definition is provided by ASTM, which states, “An elastomer is a polymeric material which at room temperature can be stretched at least twice its original length and upon immediate release of the stress will return quickly to its original length.”

Formulation and processing method of elastomers impact their properties. Generally, basic characteristics of elastomers are determined by the type of polymer used in manufacturing and the nature and level of crosslinking occurring during vulcanization process. In high molecular weight polymers, they form entanglements by molecular intertwining as shown in Figure 1a. In cross-linked elastomer, many of these entanglements are permanently locked (Figure 1b). Additionally, the response of

elastomer materials to external forces are intermolecular, that is, “the externally applied forces are transmitted to the long chains through the linkage, and each chain acts like an individual spring in response to the external force” (Drobny, 2007).

Elastomers are arguably the most versatile of engineering materials as of today, and have multiple uses (Walker, 2011). Elastomers have diverse applications in nearly all disciplines of physical science and engineering. Mechanical engineers use elastomers for noise reduction and dampening, while electrical engineers use them for electrical and thermal insulation. In the oil and gas industry, elastomers are used as hydraulic seals, O-rings, packers, liner hangers and in many other downhole equipment. Elastomer seals are essential for zonal isolation in vertical and deviated wells. They are often used in liner hanger systems, and as packers which acts as a strong seal, preventing influx and channeling of hydrocarbon between the production casing and tubing (Davis, 2008 and Gavioli, 2012). The randomly distributed chains of elastomers prevent them from having a crystalline nature. In addition, the stiffness of rubber does not arise from bond stiffness, but from this disordering or entropic factor (Roylance, 2000).

Per Visakh et al. (2013) there are two major steps in elastomer processing. The first step involves the design of a mixing formulation for a specific end use. The second is the production process whereby rubber compounds are transformed into final products. In the rubber formulation, the raw material polymer can be softened mechanically by means of mastication, or chemically with the help of appetizers (peptization). Mastication is a mechanical method of breaking down the nerviness of rubber to reduce its viscosity for good dispersion of ingredients. Under these processing conditions, rubber chemicals, fillers, and other additives can be added and mixed with the polymer to form the uncured

rubber compound. Using a two-roll mill during distributive mixing, the rubber flows around the filler agglomerates. Therefore, penetrating the interstices between particles in the agglomerate, making it denser and immobile. Immobility tends to dampen the effective rubber content, while the incompressibility of the mixture allows a force of great magnitude to be applied to the mixture. The high force applied to the mixture, causes the agglomerates to fracture (dispersive mixing), and plasticizers are used to facilitate ease of filler incorporation. At the culmination of the mixing process, curatives are added to help cure the elastomer after which the mix is homogenized and sheeted out. The mixing procedure is usually carried out at a temperature of $77\pm 2^{\circ}\text{F}$, for optimum mixing conditions. To obtain a desired elastomer shape, an extruder is used to structure the rubber into the preferred shape. The extruder die is used in shaping the elastomer into the desired shape.

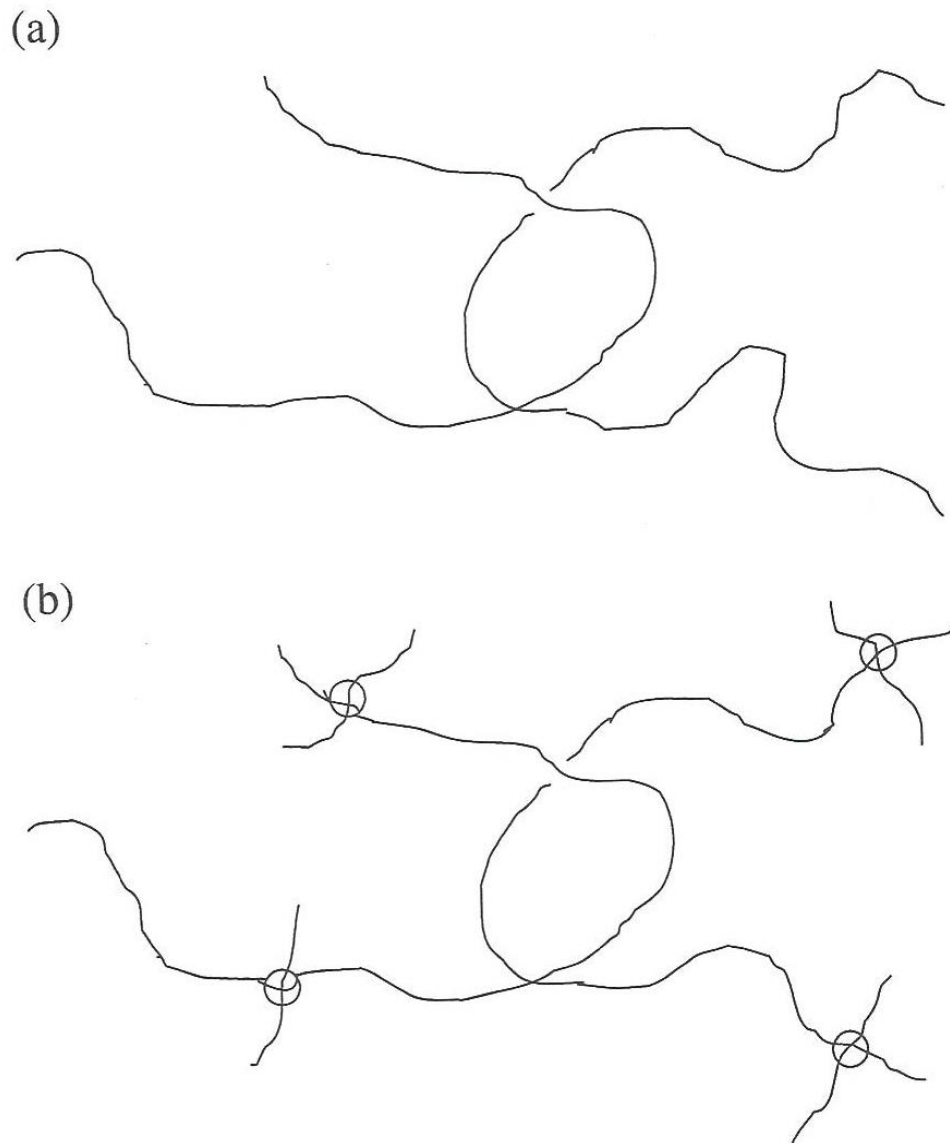


Figure 1. Molecular entanglement in high molecular weight polymer (a) Molecular entanglement in elastomer locked by cross linking (b) (from Drobny, 2007).

Types and Composition of Elastomers

Elastomers are often classified into two major categories, namely thermosets and thermoplastics. Thermosets are very common type of elastomers, which gain most of their strength after strong and permanent crosslinking (vulcanization) under elevated pressure and temperature. Thermoplastics undergo weaker crosslinking and behave like plastic materials; however, they exhibit common characteristics of elastomers such as good elasticity and flexibility. Most of elastomers used in oil field such as nitrile (NBR), hydrogenated nitrile (HNBR), fluorocarbon (FKM/Viton), perfluorocarbon (FFKM/Kalrez) and Tetrafluoroethylene propylene (FEPM/Aflas) are thermosets.

Other way to classify elastomers is group them into general purpose and special purpose elastomers. The general-purpose elastomers include: natural rubber, styrene-butadiene rubber (SBR), ethylene propylene diene monomer (EPDM), polychloroprene, and thermoplastic elastomers. Natural rubber (NR) is the most significant among general purpose elastomers. They are normally used after compounding with additives such as fillers, vulcanizing agents, and antioxidants. NR does not turn to abrade (wear), and has some features that makes it the most common type of elastomer. Some of these features include chemical resistance to acids, alcohols, and alkalis, electrical resistance, and shock absorption properties. NR has been extensively applied in the manufacturing of truck tires and tires of aircrafts, amongst others.

SBR is composed of styrene and butadiene. It exhibits a better resistance to abrasion, compared to natural rubber. EPDM, which is also a synthetic rubber like SBR, has a saturated polymer backbone structure that enables it to possess an outstanding resistance to heat, ozone, and weather changes. The non-polar nature of EPDM renders it

a bad conductor of electricity and resistant to polar solvents. However, this material is used in the manufacturing of steam hoses, roofing membranes, and electrical insulators. Polychloroprene, also known as chlorinated rubber, was first invented in 1930 by Arnold Collins (Britannica, 2009). They were formulated to be resistant to most inorganic acids, alkalis, salts, mineral oils, moisture, and fungus growth. The compound was also designed to have excellent flexibility, ozone resistance, as well as resistance to weather change. Chlorinated rubber paints are commonly used in marine, waste water applications, central processing unit socket insulation, bearings and seals for construction application, and waterproof seat covers in the automotive industry.

Thermoplastic elastomers are also considered to be general purpose elastomers. They include styrenic block copolymers (SBCs) and polyolefin thermoplastic elastomers (TPOs) (Visakh et al., 2013). SBCs are the economic thermoplastic elastomer used to manufacture footwear, sealants, and some adhesives. TPOs are a co-continuous phase system made up of polyolefin semi-crystalline thermoplastic and amorphous elastomeric components. The polyolefin semi-crystalline thermoplastic contributes to the strength of the elastomer, while the amorphous elastomeric components provide the flexibility of the elastomer (Killian, 2014). Table 1 shows some of the common general-purpose elastomers with their abbreviation and structures.

For the most part, general-purpose elastomers have proven to be useful in normal pressure and temperature conditions. However, advancement in technology, and the need for elastomers that can withstand harsh environmental and operational conditions led to the development of special purpose elastomers. Special purpose elastomers as the name implies, are elastomers that have specific applications in various fields. One of the

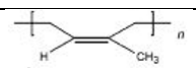
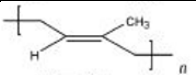
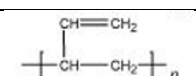
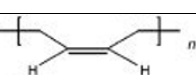
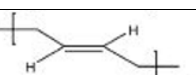
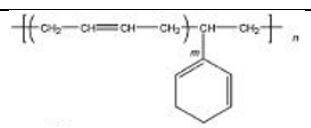
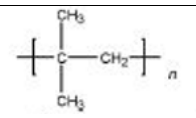
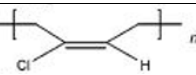
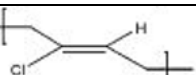
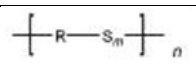
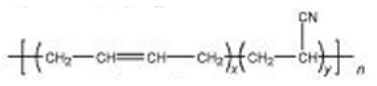
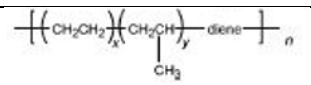
common special purpose elastomer is Isobutylene-co-isoprene, popularly known as butyl rubber and a copolymer of both isoprene and isobutylene monomers. It possesses a low permeability feature, which makes it desirable in airtight rubbers, and it can clean up oil spills when used as Elastol. Elastol is a long-chain polymer capable of mixing properly with spilled oil to form a physical polymer. Acrylonitrile butadiene rubber (NBR), popularly known as nitrile rubber is an important type of special purpose elastomer. Acrylonitrile and butadiene are the two monomers that influences the properties of NBR. The acrylonitrile (ACN) content is used to categorize NBR into low (less than 30% ACN), medium (30–45% ACN), and high (more than 45% ACN). The CAN content can vary from one manufacturer to another. Per Eriks Seals and Plastics (2017) the medium NBR is usually more applicable since low ACN improves flexibility at low temperature and high ACN content enhances the resistance to aromatic hydrocarbons. Generally, NBR elastomers have ultra-low gas permeability, enhanced ozone resistance, high temperature aging (40°F to 250°F), improved hardness, abrasion and tensile strength, as well as high resistance to aliphatic hydrocarbon fuels and oils. Figure 2 (a) shows the repeating chemical structure of NBR.

The saturated form of NBR is known as hydrogenated nitrile-butadiene rubber (HNBR) which is shown in Figure 2 (b). This material has the significant ability to resist heat (up to 320°F), maintain high physical strength, and retain its properties after long-term exposure to oil, chemicals, and heat. For these reasons, HNBR is widely used in oil and gas applications such as in blowout (BOP) preventers, Chevron seals, heat exchanger gaskets, oil field packers, paper mill rolls, and rotary shaft seals. Fluoroelastomers are another type of special purpose elastomers. They are fluorine containing polymers with

saturated structure which is obtained by polymerizing fluorinated monomers such as vinylidene fluoride, hexafluoropropene, and tetrafluoroethylene (Schweitzer P.A., 2000). Per ASTM D1418 standard, 80% of fluoroelastomers are referred to as FKM. The repeating chemical structure of FKM is shown in Figure 3a. There are some other types of fluorinated elastomers, such as perfluoro-elastomers (FFKM) shown in Figure 3c and tetrafluoro ethylene/propylene rubber (FEPM) shown in Figure 3b.

Fluoroelastomers are chemically more stable, and have desirable resistance to gas penetration, radiation, oil and chemicals. In addition, polysulfide rubbers are also considered special purpose elastomers with relatively high resistance to petroleum solvents, organic solvents, ultraviolet rays, ozone and aromatic fuels. HNBRs often fill the gap between NBRs and FKMs in many areas of application where resistance to heat and aggressive media are required simultaneously. They provide a lower cost alternative to FKM elastomers.

Table 1. Common general-purpose elastomers with structures (from Visakh et al., 2013).

Common name	Abbreviation	Structure of repeat unit
cis-1,4-polyisoprene	NR, caoutchouc	
trans-1,4-polyisoprene	Gutta percha	
1,2-polybutadiene	BR	
cis-1,4-polybutadiene		
trans-1,4-polybutadiene		
Butadiene styrene or styrene butadiene rubber	BS/SBR	
Butyl rubber	IIR	
cis-1,4-polychloroprene	CR	
trans-1,4-polychloroprene		
Polysulfide butadiene rubber	PSR	
Acrylonitrile butadiene rubber	NBR	
Ethylene propylene diene rubbers	EPDM	

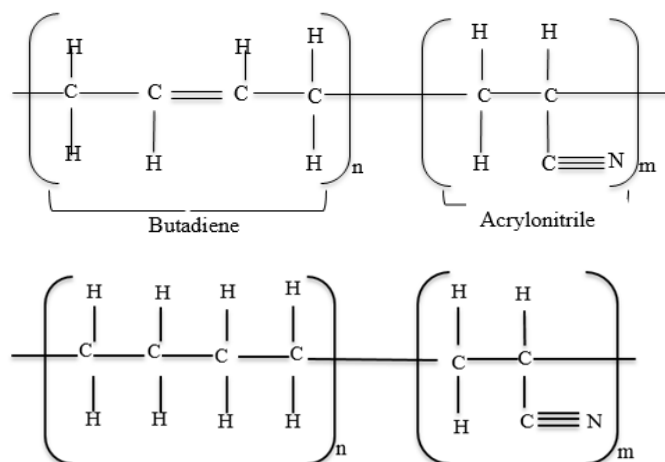


Figure 2. Structure of repeating units: a) NBR (top) and b) HNBR (bottom) (redrawn after James Walker, 2012, Issue 10.1)

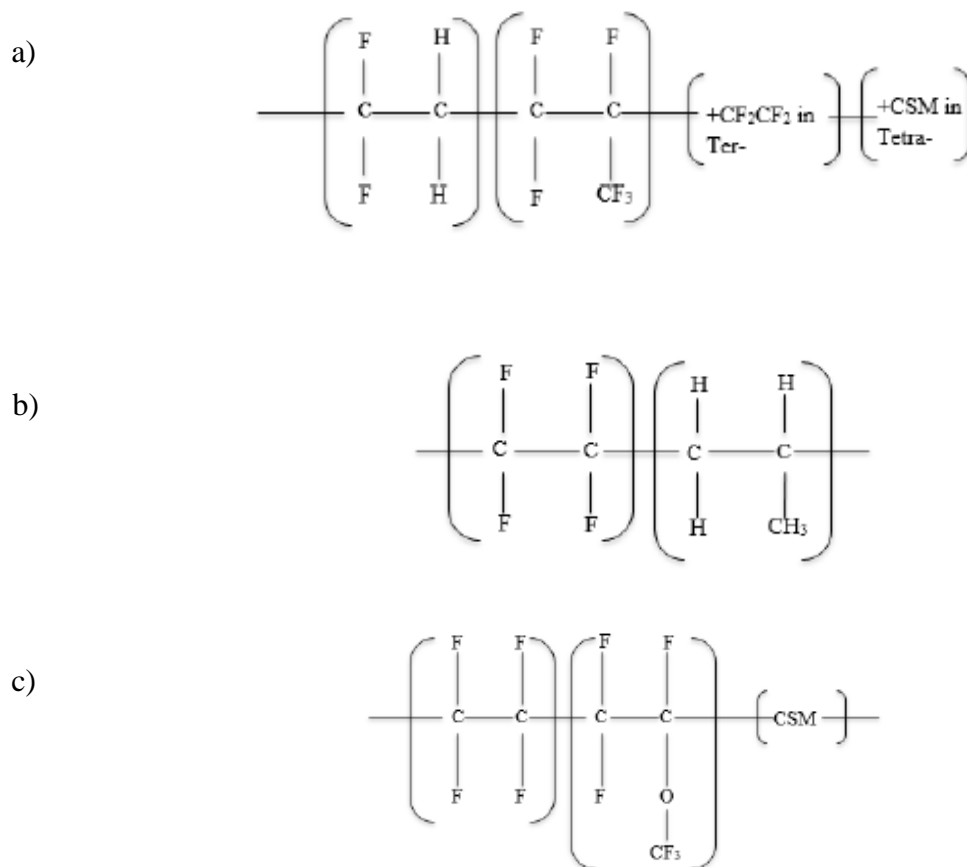


Figure 3. Structure of repeating units: FKM Viton (a), FEPM Aflas (b), and FFKM Kalrez (c). (redrawn after James Walker, 2012, Issue 10.1).

Elastomers in Oil and Gas Industry

Over the years, the exploration of complex offshore reservoirs has increased the need for high performance sealing elastomers (Debruijn et al., 2008; Tanaka, 2007; Talyor, 1990). Elastomer seals are essential for zonal isolation in vertical and deviated wells. They are often used either as O-rings (static seals) or energized seals (packers). Packers act as a strong seal, preventing influx and channeling of hydrocarbon between the production casing and tubing (Davis, 2008; Gavioli, 2012). O-rings fit to a predetermined sealing configuration with specific groove depth, width and clearance.

Harsh and challenging reservoir environments are driving the need for compatible elastomers, which require a comprehensive standard set of tests before obtaining approval. These tests are necessary to determine the seal performance at high pressures, wide temperature fluctuations, loading condition, and exposure to corrosive environment. Despite widespread use of elastomer in many oil field applications, their performance in HPHT corrosive condition is not well understood. In HPHT acidic environment, sealing elastomers can degrade considerably in a short period of time. Under harsh environment, elastomers quickly lose their performance due to thermal degradation and chemical attack.

The general coding nomenclature for elastomers follow standards such as ASTM-D1418/ISO-1629/ BSI-903/A26 53505 and other standards. The major stringent industry standards that can be applied to elastomer selection and testing are issued by following organizations:

1. American Petroleum Institute (API)
2. American National Standards Institute (ANSI)

3. American Society of Testing and Materials (ASTM)
4. American Society of Mechanical Engineers (ASME)
5. International Organization for Standardization (ISO)
6. National Association of Corrosion Engineers (NACE)

Selecting a suitable elastomer for an onshore or offshore operation requires evaluation of many inter-dependent elastomer characteristics. It is often a challenge to predict the life of an elastomer seal under harsh borehole environment due to physical and chemical changes in elastomer. Table 2 lists some of the acclaimed properties of typical elastomer in the oil and gas industry. The ability of elastomers to seal effectively depends on its physical and mechanical properties in downhole conditions. In most cases, elastomers are required to exhibit excellent performance, while retaining their physical properties at high and low temperature conditions, respectively. A good description would be the Joule-Thompson effect which occurs when there is a sudden pressure release in a subsea wellhead and blow out preventer (BOP); thus, leading to rapid change in temperature (Chen et al., 2016).

In downhole conditions, elastomers are often in a compressed state especially when they are used in liner hanger systems, BOPs, gaskets, and seals. Under these conditions, surrounding gas molecules tend to penetrate the pores of the compressed elastomer. A sudden release of the surrounding gases causes the gas molecules within the pores to expand and escape in what is known as rapid gas decompression (RGD) or explosive decompression. As shown in Figure 4, this phenomenon reduces the sealing integrity of elastomers because they experience harsh blistering and cracking, when the expanding surrounding gas energy exceeds the physical strength of the elastomer.

Elastomers with high temperature sealing performance and excellent rapid-gas-decompression (RGD) resistance, tend to have limited low temperature sealing performance due to their high modulus characteristics (Chen et al., 2016). It is often difficult to identify elastomers that have excellent rapid-gas-decompression resistance, and suitable for both high and low temperatures.

Table 2. Some of the properties of typical elastomer in oil and gas industry.

Elastomer Property	NBR	HNBR	Viton® (FKM)	Aflas® (FEPM)	Kalrez® (FFKM)
Max. Temperature (°F)	250	300	400	400	620
Tensile Strength (psi)	200-3500	1500- 3500	500- 2000	1900	2000
Steam Compatibility	Poor	Fair to Good	Poor	Excellent	Excellent
Brine High Density (Na/CaBR)	Poor	Fair to Good	Excellent	Excellent	Excellent
Brine Low Density (Ca/NaCl)	Excellent	Excellent	Excellent	Excellent	Excellent
Crude Oil. Sour (<2000 ppm H ₂ S)	Poor	Excellent	Fair to Good	Excellent	Excellent
Drilling Mud, Diesel Based	Fair to Good	Excellent	Fair to Good	Fair to Good	Excellent
Hydraulic Fluid, Oil/Water (HFA)	Fair to Good	Excellent	Poor	Excellent	Excellent

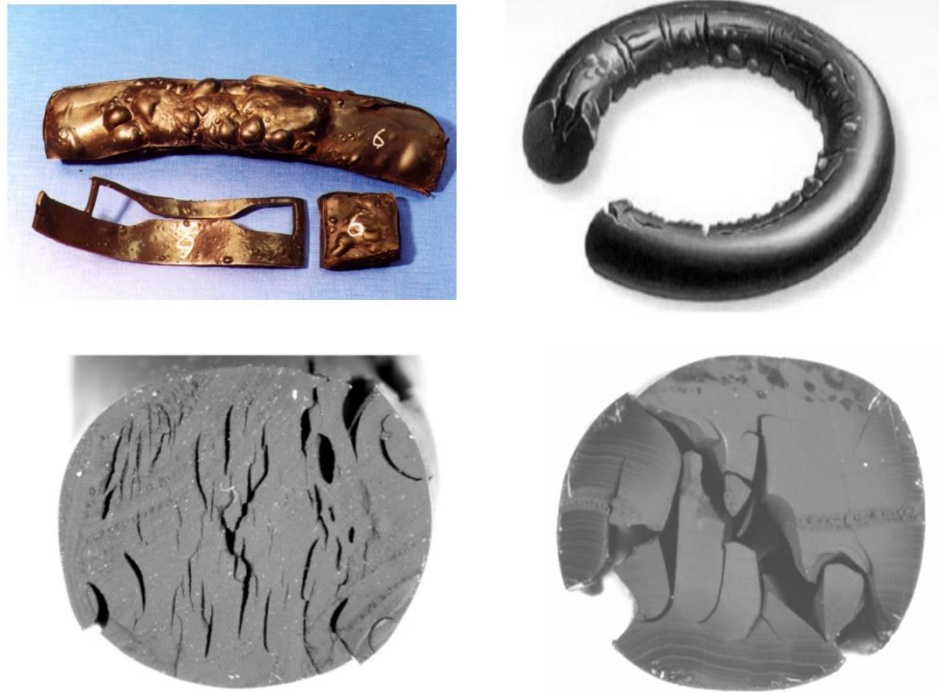


Figure 4. Some examples of elastomer failure caused by RGD (top row) and overload pressure (bottom row).

RGD occurs because of trapped-gas expansion when shear modulus of an elastomer is low. Under high-pressure, oil-field elastomers absorb methane, hydrogen sulfide and carbon dioxide; and subsequently they swell and lose their strength depending on temperature and duration of exposure. When pressure abruptly reduces, the dissolved gasses expand and bubble out quickly creating blisters and cracks in the material. HNBR is known for absorbing high level of hydrogen sulfide, which limits its applicability in some cases. Problems with RGD are often mitigated by slow depressurization, which allows the trapped gases to scape before expanding. In addition, proper elastomer material selection can mitigate the problem. In general, elastomers with high modulus and low permeability provide good RGD resistance.

Properties and Testing of Elastomers

Elastomers are viscoelastic materials, which implies that they exhibit both elastic and viscous properties when undergoing deformation. This behavior is shown in Figure 5. Unlike regular metals with the Young's modulus property, this is referred to as "modulus" for elastomers, which is the stress at any given strain. Per Schweitzer P.A (2000), the modulus of elastomers is generally measured at a specific elongation such as at 300% or lower. Elastomer's viscoelastic feature makes them responsive to compressive force that is critical to sealing efficiency.

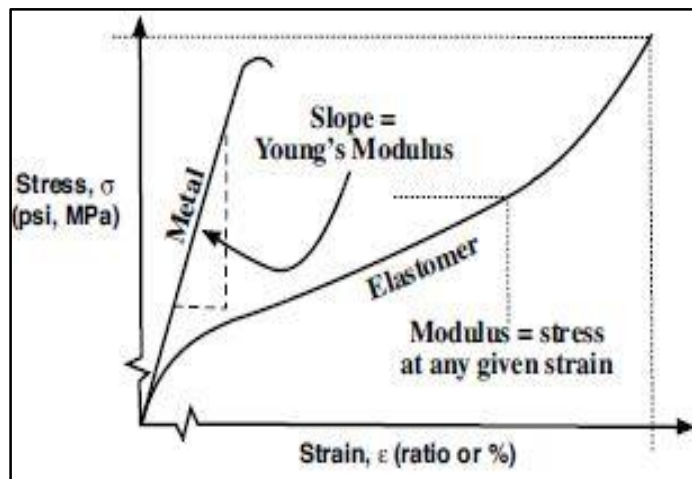


Figure 5. Stress vs. Strain profile for elastomers (from James Walker, 2012, Issue 10.1).

Recently, Wang et al. (2017) studied the sealing ability of elastomers using pressure-extrusion curves. Pressure-extrusion is the relationship between the pressure drop and the volume of extrusion of an elastomer. The curves were compared to the theoretically calculated finite elastic deformation of the seals, and the energy release rates of the cracks. In addition, they determined the elastic moduli, fracture energies, and sliding stresses of elastomers via experiments. They suggested that elastomers could have four modes of failure. The first is known as the front-end crack, which is initiated in front of the seal, and propagates through the length of the seal. The second failure is the local

crack, which occurs when a crack forms at the end of the elastomer and cuts the extruded elastomer. The third failure mode exists when the elastomer is not damaged but allows fluid to penetrate through the interface between the elastomer and the wall, causing fluid leakage. The final mode of failure is when the elastomeric seal escapes through the sealing site, because of deformation and pressure. They concluded that pressure-extrusion curves provide a good means of measuring the sealing abilities of an elastomer, since it corresponds with the theoretical calculations. Furthermore, study recommended this method for in-situ measurement of elastic modulus, sliding stress, and fracture energy, since they correspond to three distinct features on the pressure-extrusion curves.

Another method to characterize the sealing force of an elastomer at high and low temperatures is the compression stress relaxation (CSR) test (Tuckner, 2005). This approach provides more reliable correlations for sealing efficiency with respect to temperatures. However, it should be mentioned that the cross-links of an elastomer under compression, will break down after being contaminated by any corrosive environment for a long period. This will cause molecular chain displacement, chemical stress relaxation, and permanent deformation, leading to reduction in ability of elastomers to recover and questioning the elastomers sealing integrity (Dajiang et al., 2017). One other approach that is widely used to characterize elastomer properties is the inert gas pressurization test using nitrogen (Morgan et al., 2014; Severine and Grolier, 2005). Davies et al. (1999) compared the effects of nitrogen, air, and CO₂, on the tensile characteristics of NBR, Silicon rubber, and FKM. They performed tests at 580psi and discovered that nitrogen had minimal impact on the tensile properties. However, increase in pressure caused more nitrogen diffusivity within the elastomer impacting the elastomer testing results.

Apart from CSR and inert gas pressurization, glass transition temperature (T_g) is another important elastomer testing property. Glass transition temperature (T_g) is the temperature range at which an elastomer begins to change from a complete solid state into a soft and rubberier form (Overney, 2000). Chen et al. (2016) conducted an extensive investigation on the T_g and high-pressure CSR pattern of four different grades of HNBR and FKM elastomers, at low temperature. Additionally, high pressure nitrogen tests were conducted on the elastomers. In the high-pressure low-temperature confined CSR test, they observed that “HNBR-4” had the highest compression strain because of its low hardness and T_g . “HNBR-1” had the lowest compression strain because it was compressed below its T_g . For all FKM samples, lower strain was observed when compressed below the T_g . After the CSR tests, they concluded that “FKM-2” showed better performance compared to other FKM samples. This is explained by a soft and rubbery behavior under high compression strain, while displaying a high stress retention during the stress relaxation test. Their performance requirement test results indicated that all the FKM samples were cracked in the range of -20.02°F to 302°F , at 10,000psi. However, FKM-2 was an exception to this observation. Figure 6 shows the cracks as potential pathways for gas leakage, hence they are undesirable for sealing.

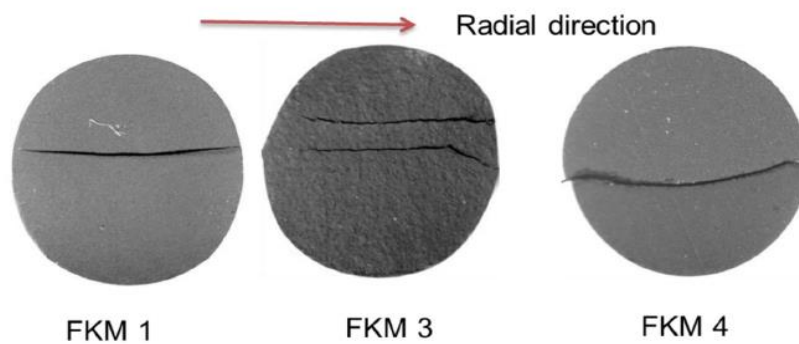


Figure 6. Cross-section of cracks on the FKM O-ring elastomers after performance requirement test (from Chen et al., 2016).

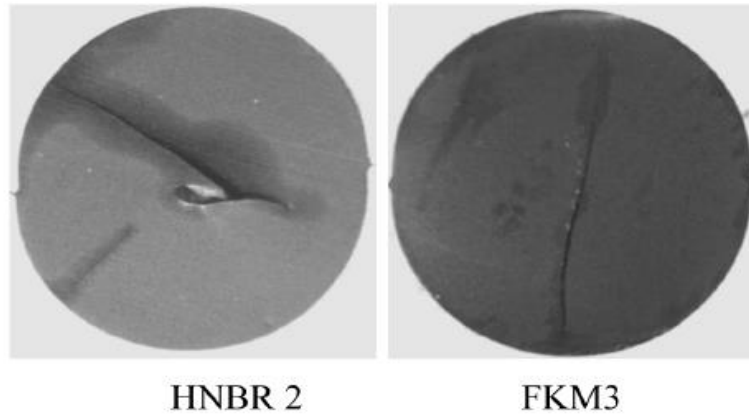


Figure 7. Cross-section of cracks on elastomer O-rings after high pressure RGD test at 3020F (from Chen et al., 2016).

Temperature is a critical factor that affects elastomeric properties. Chemical degradation of an elastomer will alter its sealing performance at low temperature (Tripathy, 1998). Experiments conducted in literature (Chen et al., 2016) using high-pressure nitrogen test at room temperature, showed no cracks and failure on the elastomer O-rings irrespective of the rate of release (3000psi/min). However, once testing conditions changed to 302°F, the results shown in Figure 7 reveal cracks that are longer than 80% of the cross-section diameter. In another study conducted to investigate temperature and corrosive fluid effect on elastomers, Tynan (2016) compared the reactivity of various elastomers to H₂S with their T_g, and high temperature performance, as shown in Table 3. It was suggested that low temperature and H₂S resistance, are two properties that can exist for the same elastomer type. This was similar to one of the author's previous observations in which an elastomer seal was selected with the combined qualities of high performance at low temperatures, excellent resistance to sour gas (H₂S), and a good amine corrosion inhibitor. Low temperature FFKM elastomer was chosen against FKM, because the design allowed for a life of 20+ years, while maintaining a

good low temperature resistance. Furthermore, study recommended FFKM as the most viable option for low temperature and H₂S conditions.

Table 3. H₂S resistance of various elastomers, at their respective glass transition and high temperature performance (from Tynan, 2016).

Elastomer Type	Resistant to H₂S	Glass Transition (T_g) °F	Upper Service Temp. °F
NBR	Most reactive	-22	248
Low Temp. HNBR	Most reactive	-40	320
HNBR	Less reactive	-22	356
FEPDM (TFE/P)	Non-reactive	41	482
Low Temp. FKM	Less reactive	-40	437
FKM	Most reactive	1.4	437
Low Temp. FFKM	Non-reactive	-22	464
FFKM	Non-reactive	32	500

Over the years, aging experiments have gained recognition as one of the commonly used methods for evaluating the behavior and performance of elastomers. These tests are conducted in special autoclaves by exposing testing samples to corrosive gas and liquid contaminants. Per Schweitzer P.A (2000), the properties of an elastomer can be destroyed only by chain growth or chain rupture. Some of the contributing agents to elastomer aging are: atmospheric ozone and moisture, heat, sunlight, CO₂, H₂S, CH₄, drilling fluids, and brine amongst other. These agents are used to evaluate the sealing integrity of elastomers. During elastomer aging, chain growth will usually decrease elongation and increase hardness and tensile strength, while chain breakage will have the reverse effect on these properties (Schweitzer P.A, 2000). Elastomer hardness is defined as the resistance of an elastomer surface to indentation by a Shore A durometer. Figure 8 shows that elastomer hardness tends to increase with an increase in temperature. Increase in hardness by temperature explained by mobility and crosslinking of the elastomer

molecular chain (Jin et al., 2008). Furthermore, study highlighted that changes in the order of the sulfur bonds occur with temperature increase.

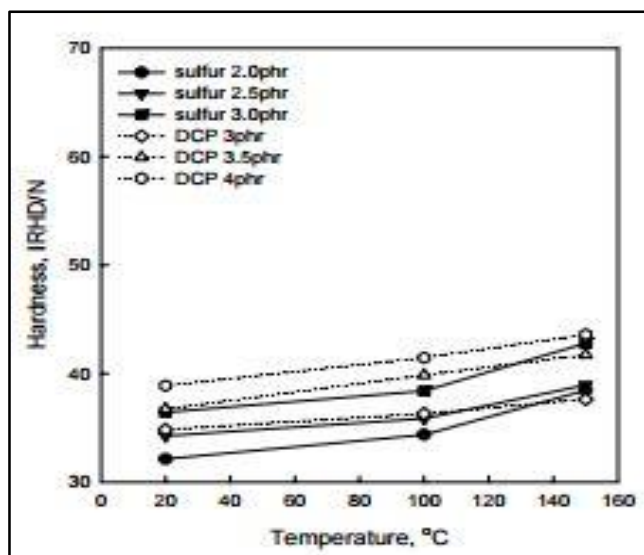


Figure 8. Hardness vs. Temperature (from Jin et al., 2008).

Cong et al. (2013) published experimental results of aging cell study for HNBR samples in aqueous solutions of H_2S and HCl . The authors used nuclear magnetic resonance, infrared spectroscopy, and X-ray photoelectron to analyze the samples. The H_2S experiment was carried out at 1000 ± 100 psi and $212^\circ F$, while the HCl experiment was carried out at $284^\circ F$. They observed that exposure of HNBR to HCl solution resulted in a slight reduction of tensile strength and ultimate elongation because of the hydrolysis of the $C \equiv N$ group to $-OH$ or $O=C-NH_2$. Once exposed to H_2S solution, all three parameters (tensile strength, ultimate elongation, and hardness) deteriorated significantly. Given the high reaction activity of H_2S , homolysis and heterolysis are two reactions of H_2S that may take place during elastomer degradation. Heterolysis converts H_2S into H^+ and HS^- . H^+ causes the acidic hydrolysis of the $C \equiv N$ group, while HS^- attacks $C=O$ due to its strong nucleophilicity, giving rise to $C=S$ and $C-C=S$ groups (Figure 9). During homolysis, H_2S can alter into mercapto radicals of $H\cdot$ and $HS\cdot$. $HS\cdot$ reacts with

macromolecule radicals of the elastomer that forms at high temperatures. It then forms to mercapto compounds. These compounds undergo further pyrolysis to form macromolecule radicals to react with mercapto radical (HS \cdot) in a continuous reaction cycle. This chain of reactions increases the C—S—C bonds. The breakdown of the triple bond in the CN group to double and single bond, as shown by these reactions, is responsible for the deteriorating properties of the elastomer. Studies showed that during exposure period to H₂S solution, the structure of HNBR will change due to formation of new chemical compounds.

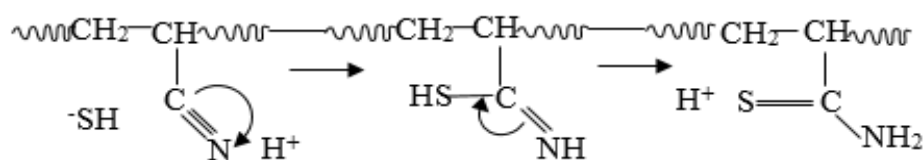


Figure 9. Nucleophilic reaction mechanism showing the breakdown of the acrylonitrile group in HNBR (redrawn after Cong et al., 2008).

Fernández et al. (2016) studied the elastomeric properties of two NBR's (high and low ACN) using two separate autoclave tests in liquid and gas contaminants respectively. They varied the concentration of crude oil compositions to obtain three liquid contaminants, while using H₂S and CO₂ as the gas contaminants. In the presence of crude oil, tests were conducted at 150⁰F and 1000psi, for 168 hours. After the crude oil aging, the results from their hardness test revealed no more than 5% change from the original elastomer hardness. A maximum volumetric swelling of 3.1% was recorded. Their compressive set test results showed high permanent deformation values within acceptable limits. Decrease in tensile strength and elongation at break was also recorded. The decrease in tensile strength was more severe with the NBR that was aged in the crude oil, which had the highest percentages of saturates and aromatics.

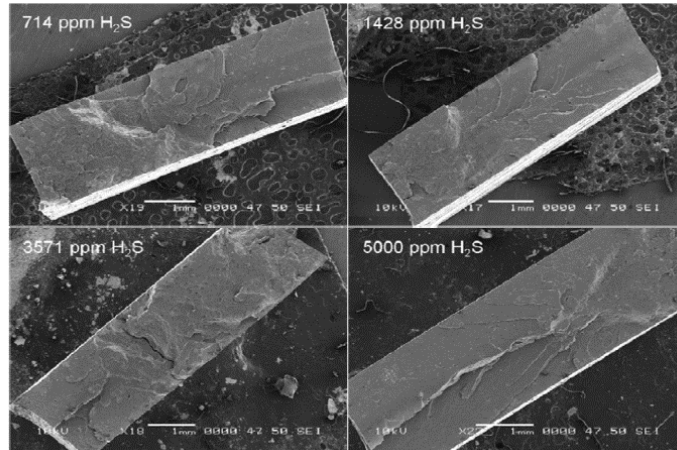


Figure 10. Scanning Electron micrographs of NBR aged with H₂S (203°F, 168 hrs.) (from Fernández et al., 2016).

Exposure of an elastomer to sour fluid conditions such as H₂S, at elevated temperatures, will accelerate aging and degradation. This process can provide some information about the long-term stability of elastomers (Tynan, 2016). In the H₂S aging experiments by Fernández et al. (2016), the H₂S concentration was increased from 714ppm to 5000ppm. A reduction in the elastic properties were observed, causing elastomers less retractable. Tensile strength and elongation at break properties decreased significantly with increase in H₂S concentrations. The SEM image in Figure 10 shows an increase in the brittle fracture surface with increase in H₂S concentration. The authors concluded that permanent deformation of the elastomer is a function of the H₂S concentration. In addition, they recorded an increase in the volumetric swelling and permanent deformation of the elastomers with increase in CO₂ concentrations. Increase in permanent deformation was finite and plateaued at very high concentrations of CO₂. Increase in hardness was recorded for low CO₂ concentrations. The SEM image in

Figure 11 shows a decrease in the brittle fracture surface of the NBR with increase in CO₂ concentrations.

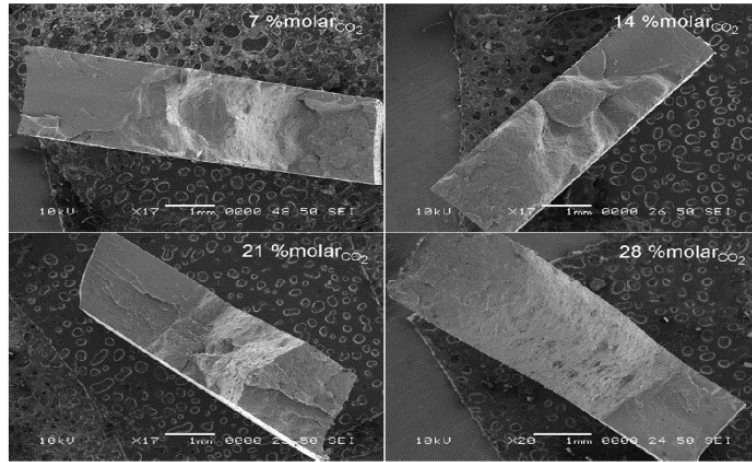


Figure 11. Scanning Electron Micrograph (SEM) of NBR aged with CO₂ (203°F, 168 hrs.) (from Fernández et al., 2016).

Dajiang et al. (2017) characterized NBR and HNBR samples by aging the elastomers in the presence of liquid and gaseous CO₂, under mechanical compression. Their control group sample was compressed at laboratory ambient temperature and pressure. Two separate groups of elastomers were aged in liquid and gaseous CO₂ respectively for 168 hours, at 230°F and a CO₂ partial pressure of 145 psi. Compared to the control samples, an increase in elastomer weight was recorded for the aged elastomers. Increase in weight was more pronounced with the elastomers that were aged in liquid CO₂. They also observed that the reduction in elastomer hardness was more severe in the gaseous contaminant, compared to the liquid contaminant. Samples were compressed by 25% of their original height for 24 hours at ambient temperature, and was left to recover for 30 minutes. They recorded compression set results in the range of 9.94% to 17% and 10.33% to 26.02% for NBR's aged in liquid and gaseous CO₂, respectively. Furthermore, study reported similar values for the HNBR samples

suggesting that mechanical loading will increase the damage in the elastomers in the presence of CO₂.

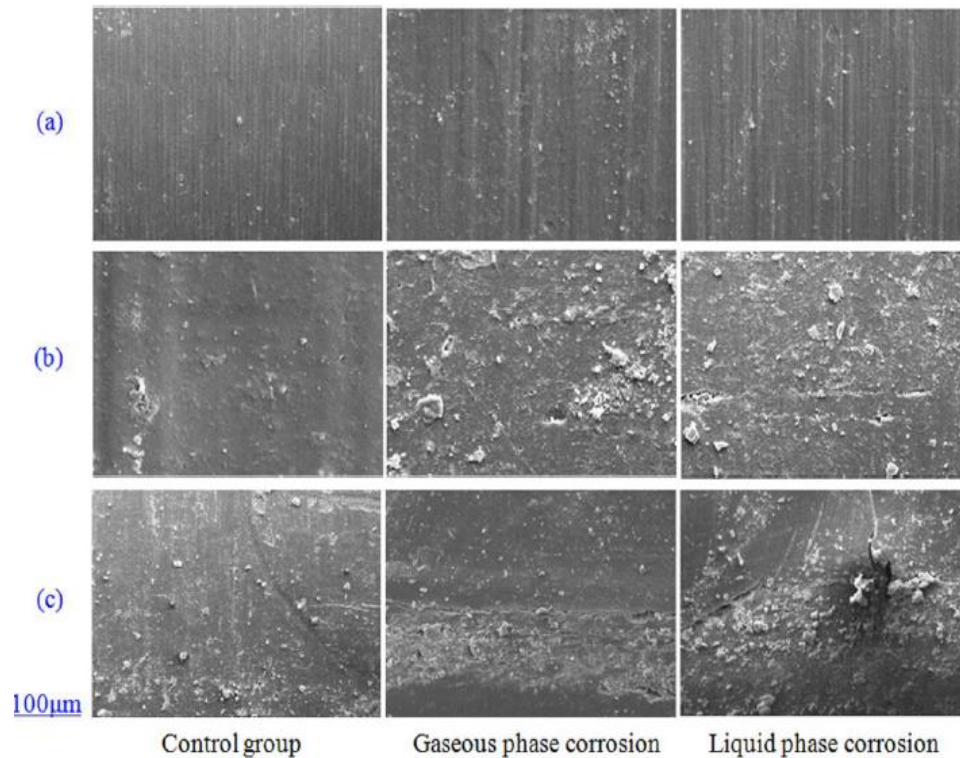


Figure 12. SEM images of HNBR after aging at 0lbf (a), 1349lbf (b), and 2698lbf (c) (from Dajiang et al., 2017).

In addition, Dajiang et al. (2017) observed slight deformation in the HNBR control group, compared to an obvious swelling and deformation revealed by the aged samples. Figure 12 shows HNBR SEM images, at various compressional loads. They observed holes, fractures, and more damage in the aged HNBR samples. Furthermore, their energy dispersive spectroscopy (EDS) results for the 2698lbf compressed samples showed decrease in the weight percent of the main constituent elements (C, O, Si, and Ca). They concluded that elastomer swelling, and damage tend to increase with increase in compressional load in liquid CO₂ corrosion, and appear to be more severe than gaseous CO₂ corrosion.

In addition, to corrosive gases, other contaminants such as drilling fluids can deteriorate elastomers. The behavior and performance of an elastomer can be impacted by drilling fluids contamination. Drilling fluids can alter the physical and chemical properties of elastomers that are used in drilling equipment severely affecting the equipment's life and function (Badrak, 1994). The degree to which drilling fluid can alter elastomeric properties and/or composition depends on the type of drilling fluid, temperature, pressure, and type of elastomer. For instance, during a drilling operation, positive displacement motors (PDMs) experienced chunking when the elastomer in the stator has reached its fatigue limit (Guidroz, 2011). Kubena et al. (1991) investigated performance of elastomers that are used in downhole drilling equipment, particularly PDMs. In their study, four elastomers (hydrocarbon, chlorinated, nitrile, and fluorinated elastomers) were contaminated with five non-aqueous fluids (NAF) base liquids (diesel oil, mineral oil, low aromatic content mineral oil, ester, and glycerol/water mixture). When a PDM is heated above the aniline point (1400 °F) of a diesel oil base fluid, the aromatic portion of the diesel will penetrate the elastomer compound, causing it to swell. Aniline point defined as the temperature at which a known volume of a clear aromatic compound (aniline), dissolves totally in a specific volume of oil to form a non-cloudy solution. High temperatures accelerated chemical attacks on stator rubbers, and hence reduces its mechanical properties. Previous field studies revealed that PDMs which were used with mineral/low-toxicity NAF, had twice the service life they would have had when used with diesel based NAF. Study concluded that no specific elastomer can fit to work in all types of drilling fluids.

Other corrosive fluids such as brine, can potentially influence the performance of an elastomer. Super absorbent polymers (SAP) often swell insufficiently when they are in contact with saline formation water (Bosma et al., 2006). Wang et al. (2015) developed a new water-swellaible elastomer that can swell in the presence of high salinity (20+ %) and divalent brines (CaCl_2 and CaBr_2). These new elastomers developed by mixing nanocomposite microgels with NBR. Figure 13 reveals that the new elastomer showed better swelling ratios compared to SAP (reference 1 and 2), in the CaCl_2 and CaBr_2 at 200°F. A similar performance was observed in presence of high level of brine. In addition, other test results revealed that new elastomer has better tensile strengths after swelling, as well as enhanced breaking elongation properties compared to the current water-swellaible elastomers.

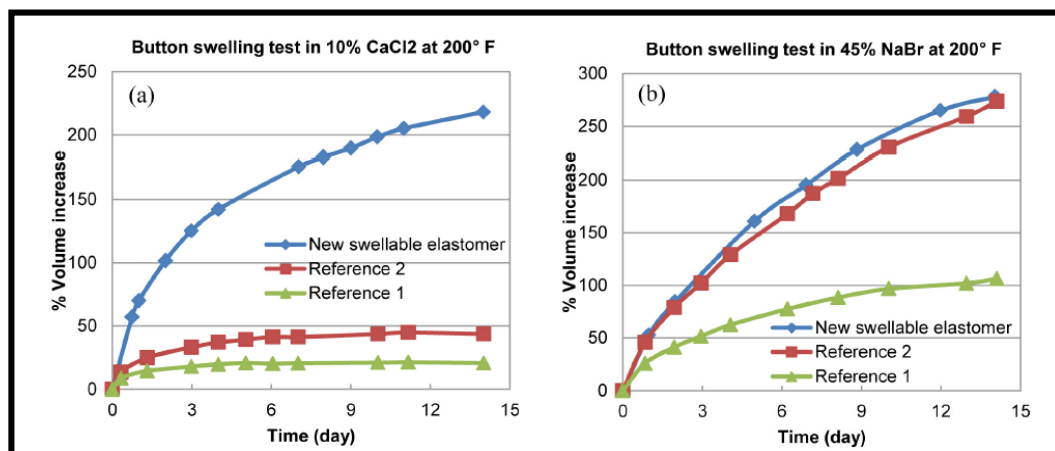


Figure 13. Swelling curves of button-shaped samples tested (a) 10% CaCl_2 at 200°F (b) 45% NaBr at 200°F (from Wang et al., 2015).

Another wide application of elastomers in downhole is expandable liners and swelling packers. These are used to control oil flow from each lateral, to improve total oil recovery. Qamar et al. (2012) conducted longevity tests on a full-scale rig. Table 4 shows the test matrix containing packers made from different swelling elastomers, exposed to

saline water or crude oil. The tests were conducted at different temperatures and 1000psi. W1 represents low-salinity while W2 and O1 represents high-salinity and oil-swelling elastomers respectively. The authors did not disclose the actual formulation of the elastomers for confidential purposes. However, their results showed that units 1, 2, and 6 failed, and did not seal within the first two weeks of the test. Unit 5 sealed then de-sealed, after several months of exposure. Unit 7 showed good sealing at lower pressures but failed at a pressure of 1000 psi. Units 3 and 8 had good sealing performance. They concluded that elastomers tend to swell and seal earlier when in contact with low salinity brine at high temperatures, compared to high salinity brine. Additionally, water-swelling elastomers swell and seal faster than oil-swelling elastomers (Qamar et al., 2012; Qamar et al., 2009; Pervez et al., 2012).

Table 4. Experiment design details for the longevity test setup (from Qamar et al., 2012).

Unit	Elastomer Type	Swelling Medium	Temperature
3½-in swell packer inside 7-in casing			
1	W2	12% brine	73°F
2	O1	Crude oil	73°F
3	W2	12% brine	122°F
4	O1	Crude oil	122°F
4½-in swell packer inside 7-in casing			
5	W2	12% brine	73°F
6	O1	Crude oil	73°F
7	W2	12% brine	122°F
8	W1	0.5% brine	73°F
9	W1	0.5 brine	122°F
Perspex demonstration unit			
10	W1		73°F

Summary

It can be summarized that currently there is a gap in understanding performance of elastomers in downhole conditions. Studies show accelerated degradation of elastomers in higher temperature and under different corrosive conditions such as CO₂, H₂S and HCL. Additionally, performance of elastomers is impacted differently by changing concentration of corrosive gases. In one study, tensile strength and elongation at break properties decreased significantly with increase in H₂S concentrations.

One particular study summarized effect of drilling fluid's contamination on elastomer properties. Drilling fluid can alter elastomeric properties and composition depending on the type of drilling fluid, temperature, pressure, and type of elastomer. Another study investigated sealing performance of expandable liners and swelling elastomers and concluded different behavior at low and high salinity brines.

It is crucial to know "fitness for service" of various elastomers in packers, casing seals, liner hanger and other downhole tools. One particular challenge is to know exact formulation and type of elastomers used in downhole equipment since formulation and processing method of elastomers impact their properties. Review of many of the manufacturers catalogues and websites indicates very little information disclosed as per exact formulation used in different downhole tools. In addition, limited data is available to assess performance of elastomers in downhole in forms of published testing data and laboratory procedures.

Furthermore, corrosive downhole conditions may accelerate failure of elastomers posing more challenges in applications of these materials in HPHT wells. Additionally, elastomer failures may result in underground loss of well control incident in harsh

downhole conditions. Therefore, an urgent need exists to conduct a comprehensive research study to investigate and assess the engineering design, performance, reliability and testing of the current and new elastomer material grades for offshore oil and gas activities.

Well Integrity and Cementing in Gas Hazard Zones

Shallow flows usually occur because of high pore pressures from undercompaction and overpressurization of sands during rapid depositions. They can consist of water, gas, and formation fines. Shallow flows are identified as one out of every five surface casings potential hazard (Bogaerts et al., 2012). They can jeopardize the integrity of a well by preventing hydraulic isolation after a cement job, leaving a path for flow into other shallow formations or sea beds. Gas leakage in the annulus has been recorded as a major hazard in drilling and completions operations. Shallow gas flow often results in well control issues. Shallow kicks can occur because of swabbing, core volume cutting, improper hole fill-up on trips, abnormal pressures, insufficient mud weight, gas cut mud, lost circulation during drilling or cementing, and gas migration through cement column. Shallow gas blowouts have been the major cause of the loss of offshore drilling rigs than any other type of well control problem. Records show that one out of three blowouts occur because of shallow influx (Adams and Kuhlman, 1990; Prince, 1990).

One of the major occurrences that can result from shallow flow is known as cratering. Cratering is the caving in of already drilled wells, and in such cases the drilling rig normally goes under with the collapsing well. Current well control practices usually call for the shutting in of a well when a kick is encountered, provided there is sufficient casing to contain the kick. However, in the presence of a shallow gas, casing strings may

not be set deep enough to keep the underground flow under control. The flow breaks through and disturbs the foundation of the rigs, leading to the formation of craters and the loss of both the rig and associated marine structures. A modern approach makes use of diverter systems that sidetracks the flow away from bottom supported rig platforms. In cases where the diverter is too restricted, the pressure created in the formation still exceeds the formation breakdown pressure, and a crater can still be formed irrespective of the fact that the well is not shut in. Although there is insufficient statistical information regarding cratering, they are mostly related to shallow gas blowouts. Design concerns and risks involving the cementing of shallow casing, sub mudline and liner systems are not new which at least two studies were conducted by MMS (Mineral Management Service) to address these issues. In 1986, Hughes compiled information in relation to blowout incidents. The author recorded that 82% of Texas blowouts, 77% of Louisiana blowouts, and the majority of the blowouts experienced in Outer Continental Shelf (OCS) showed presence of gas. Danenberger's study in 1993 showed that 58 out of the 83 blowouts that were encountered between the years of 1971 and 1991 on the OCS of the United States had gases associated with them. This was a strong indication of the severity of shallow gas flows and cratering, costing significant expenditure to the operators.

Bourgoyne et al. (1995) ascertained and described various probable sedimentary failure mechanisms that can lead to cratering. They developed correlations for the estimation of sediment breakdown resistance and to evaluate well design and well control procedures. Their sediment failure mechanism was subdivided into two sections: the first was for fluid migrations to unconsolidated sediments and the second was for crater formation. The mechanism for upward fluid migration include casing failure, failure of

the cement bond at the casing-sediment interface, rock tensile failure because of hydraulic fractures, rock shear failure in permeable zones, and upward fluid migration through fault planes. The recognized cratering mechanisms include borehole erosion, formation liquefaction, caving, and piping or tunnel erosion. They also showed how soil boring data can be useful in accurately estimating overburden stress and formation breakdown pressure. To prevent shallow gas kicks, use of seismic surveys were recommended to identify potential shallow gas zones prior to drilling. Using a heavier mud was recommended in shallow portions of the well.

Shallow gas is usually encountered at shallow subsurface depths of 300 ft with low fracture gradients. They often result to blowouts in the open hole section usually below the conductor or surface casing because of gas migration through the cement (Adams, 1990). Industry general practice allows the driller to close the well and circulate formation fluid influx out of the well. However, in shallow formations this action may result underground blowout or the formation being broached to the surface. Therefore, the gas is required to flow in a safe manner until the zone is completely isolated. This process can cause the erosion of plugs and pipework since the flowing gas is accompanied by large volumes of abrasive sand particles (Prince, 1990).

Some steps have been taken by the industry over the years in regards with shallow wells casing and cement design considerations. These include API RP 65 (Cementing Shallow Water Flow Zones in Deepwater Wells) and API RP 65 – Part 2 (Isolating Potential Flow Zones During Well Construction). Some other new standards such as API Recommended Practice (RP) 19LH (Liner Hangers) is currently being drafted by an API

subcommittee. Specifications of downhole liner hangers will be specified in this new standard.

Gas Migration

Gas migration is defined as gas entry into a cemented annulus with the potential to provide a flow path into the wellbore for gas, water and hydrocarbons. Gas migration can cause fluid flow through annulus, and surface. If not detected, gas flow will have severe consequences such as underground blowouts or if marginal it can cause sustained casing pressure. Drilling industry recognized this problem during the 1960s and since then intensive research has gone into investigating this problem. Various aspects of gas migration have been described in the literature as following:

- Experimental and field case studies (Stone and Christian, 1974; Garcia and Clark, 1976; Cook et al., 1983; Al Buraik et al, 1998; Bour and Wilkinson, 1992)
- Development of technical recommendations (Levine et al., 1979; Tinsley et al., 1980; Cheung and Beirute, 1982; Dean and Brennen, 1992)
- Developments of new products and techniques (Kucyn et al., 1977; Watters and Sabins, 1980; Cheung and Myrick, 1983; Siedel and Greene, 1985; Matthews and Copeland, 1986)
- Empirical prediction techniques (Sutton et al., 1984; Rae et al., 1989)

Gas migration phenomenon can be caused by numerous factors; and can occur at various times. Root causes of gas migration have been attributed to i) fall in annulus hydrostatic pressure; and ii) pathways in annulus through which gas can migrate (Nelson and Guillot, 2006). Primary causes of gas migration are related to the cementing process involving

several factors. Gas migration through a cemented annulus can be categorized into three types based on their migration path (Talabani et al., 1997). The first type occurs between the casing and the cement; a situation whereby gas molecules migrate through the void created between the casing and cement. A common practice to remedy this problem is adding the appropriate amounts of magnetite to the cement slurry. The second type of gas migration occurs through the void created between the cement and the wellbore wall. This void is created when the filter cake that is formed at the wellbore adversely affects the bonding process. Anchorage Clay and some other additives can be used to eliminate this problem in drilling. The third gas migration path exists because of hydrostatic pressure changes that appear in the cement during the setting phase. This is also referred to as primary gas migration when gas molecules migrate into the cement mainly because of loss of hydrostatic head. To better understand gas migration, Stiles (1993) proposes three stages of cementing: 1) during placement or immediate; 2) post-placement (short); 3) post-setting (long). It is important to understand all the physical and chemical process cement slurry goes through from liquid slurry to semi-solid and solid states. When the cement hydrostatic pressure in front of a large volume of gas “pocket” drops below the pressure in the gas zone, gas influx takes place (Pinto, 2012). On the other hand, secondary gas migration occurs much later after cement placement is complete. This is because of mechanical and thermal stresses which compromises the integrity of the hydraulic bond or the integrity of the cementing materials (Rupak, 2007). Per Mineral Management Service (MMS) safety alert (2003), annular flow related to cementing surface casing has been identified as one of the most frequent causes of the loss of well control incidents in the Gulf of Mexico. When zonal isolation is not achieved, and gas

molecules migrate behind casing, it charges the shallow formations. These shallow formations become a formidable challenge when there is little proximity between the pore pressure and fracture gradients in the operational mud window. In such situations, the gas can breach the casing, leading to a blowout. Here a review of major studies in literature regarding gas migration is presented:

Carter et al. (1973) presented a laboratory model of gas migration in deviated boreholes by focusing on properties of cement slurries needed for successful primary cementing jobs. Their research showed that the parameters directly related to gas migration include cement filtration control, borehole mud removal, and effective hydrostatic head (hydrostatic pressure exerted by the mud, spacer, and cement slurry). In addition, the study presented factors that reduce gas migration during and after primary cementing. These factors summarized as centralization of casing strings and increased flow rates during displacement amongst others.

Garcia et al. (1976) presented findings of a fieldwork study. This study was done to trace gas migration as it occurred in the wellbore. The investigations showed that gas migration occurs under two conditions. The first is when there is fluid loss in the cement slurry. Secondly, there is an uneven setting of the slurry, such that there is absence of hydrostatic head communication between the bottom of the hole and the mud column directly above the set cement. They provided guidelines to predict formations that have potentials for gas migration. Furthermore, the study recommended practices that curb annular gas flow.

Christian et al. (1976) presented a method to calculate the allowable filtrate loss rate for a cement slurry during various stages of cementing. They stated that without fluid-

loss control, cement slurries may be unsuccessful in transmitting full hydrostatic pressure before their initial set. The authors showed that increasing concentrations of fluid-loss additives yield to lower cement permeability and lower gas migration's potential. In addition, their field results demonstrated that gas migration can be successfully prevented with cement slurries that have a fluid loss in the range of 50 ml/30 minutes. Cook et al. (1977) in a similar study showed that filtrate loss control is just as important as the slurry thickening time or its compressive strength development. Both studies concluded that maximum fluid loss control should be used in cement slurries when cementing across zones varying in pressure. This would help to minimize gas leakage.

Webster et al. (1979) based on laboratory tests and field results identified the relationship between water separation in a cement slurry and loss of hydrostatic head of the cement. They observed that the use of clay in regulated amounts can be used to control the amount of free water in cement slurries. They concluded that reduction of free water to zero eliminates the potential of flow after a cementing job.

Bannister et al. (1983) simulated a wellbore model to study the incursion of gas into cement. Two design approaches were used to reduce gas conductivity (the relationship between gas flow and loss of hydrostatic pressure). One of these approaches was to deposit impermeable cement filter cake against the formation. The other approach involved the use of a self-activating slurry that interacts with incoming gas to form an impermeable barrier. Results from their investigation showed that the impermeable filter cake deposition, hinders gas invasion so far as it is in place, but once broken, gas flow becomes unhindered and rapid.

Cooke et al. (1983) presented field measurements of annular pressure and temperature during primary cementing operations. Pressure and temperature measurements were conducted in seven wells via sensors to investigate the causes of fluid migration behind casings. They highlighted multiple causes of fluid migration, but focused on one, 'the loss of pressure in a cement before the cement sets'. Their investigations disclosed that annular pressure measurements indicated fluid entry into the wellbore when the formation pore pressure exceeds the pressure exerted by the cement. The sensors showed the extent of vertical movement of the migrated fluid. The study concluded practical steps that can be followed to help minimize flow induced by loss in annular pressure.

Beirute et al. (1990) presented a method to scale down field wellbore parameters to laboratory conditions for accurate testing of cement recipes to be used for controlling gas migration. Their method assumed the gas bearing formation to have substantial permeability, gas volume, and thickness to invade the annulus and pressure-charge the cement. The study concluded some criteria for selecting cement slurries in wells with potential gas migration problems.

Bour et al. (1992) presented an analytical method to quantify the potential and severity of gas flow. They showed that appropriate gas migration control cementing systems can be designed once the flow potential has been established. Compressible cement was recommended for use to combat gas migration problem. Al-Buraik et al. (1998) discussed solutions to shallow gas migration problems with the use of lightweight latex slurries, and right-angle set (RAS) latex slurries amongst others.

Most recently, Bois et al. (2017) presented a gas migration model that investigates two different stages of fluid and porous solid in the life of a cement slurry. Their models allowed for the computing of cement properties, and state of stress, at any depth and time. In addition, models showed that the opening of a micro-annulus is not necessarily associated with gas migration. However, gas will invade the cement sheath when the cement pore pressure drops below the pore pressure of the formation. The study highlighted importance of gas flow rate and diffusivity in the cement sheath. Furthermore, they concluded that gas may use multiple leakage paths during migration to reach the surface leading to shallow gas blow out or leaking into another reservoir.

Overall, optimizing cement mix design and process can help in mitigating gas migration. It must be noted that not a single factor alone can prevent gas migration, but rather a combination of factors - depending on the well condition - is required. Some of the key properties of cement in context of controlling gas migration can be summarized as:

- Fluid loss
- Gel strength development
- Cement shrinkage
- Permeability
- Free fluid (free water)
- Mud removal
- Microannulus
- Mechanical and chemical failure of cement sheath

Shallow Gas Loss of Well Control (LOWC)

Shallow gas blowouts are the most common types of blowouts, and ideally require a case-by-case analysis to develop the most appropriate control techniques. However, records have shown that shallow gas blowouts have similarities in their causes. Adams et al. (1990) showed that shallow gas blowouts have some form of relationship with cementing operations. They provided information about drilling procedures, equipment selection, and response procedures from various rigs in cases of shallow gas blowouts. Some of the recorded causes were: bridging and diverter system failures, flow outside casing, and cratering. Some documented gas handling or kill techniques include: kick prevention, shut-in on shallow flows, use of pilot holes, heavy and dynamic-heavy slug, dynamic kill, and incorporating the measurement while drilling (MWD) approach. Studies recommended a shallow hazard survey prior to drilling a proposed location. Mud weights and casing setting depths should be optimized to handle possible influx and well control. Riserless drilling or the use of riser connectors that can release at high angles is a viable alternative. Adams et al. (1990) concluded that pilot hole drilling with controlled rate of penetration (ROP), offers a better chance of early detection. Prince et al. (1990) discussed the drilling procedures to reduce the probability of a shallow gas kick. The study concluded operational procedures such as controlling rate of penetration and mud circulation rates for circulating gas out of the well in timely manner. In addition, slowing down tripping process was recommended to reduce risk of swabbing.

Field surveys carried out as far back as in the 80s show that annular gas flows accompanying cementing defects (incomplete sheaths in annular space) are major problems in shallow casing strings. Tinsley et al. (1980) provided some data on the

remedial costs of wells due to gas flows. Another study conducted by Martinez and McDonal (1980) discussed the most hazardous form of gas migration as the one behind the conductor or surface casing reaching the surface in a very short period of time. They described some distinct occurrences resulting to annular gas flow as followings:

- Insufficient historical information on hazardous locations,
- Unsuccessful cement mixtures or cementing procedures,
- Inadequate hole preparation, mechanical devices and procedures during cementing,
- Unreliable cement slurries,
- Insufficient cement column hydrostatic pressure,
- Inability to detect channel location in the annulus.

Furthermore, studies showed annular gas flows due to drilling fluids displacement. Some of the factors that affects mud displacement include: mud conditioning, mechanical devices on the casing, casing movement, cementing techniques, slurry design, change in velocity due to eccentric annuli, washouts, variable filter cakes, and inclined holes. Drilling mud that has not been successfully displaced but remains in the wellbore-casing annulus can become a channel for gas flow. Although the displacement efficiency of mud is dependent on the fluid flow model, it also depends on the mechanical conditions such as the effect of casing string rotation or reciprocation; where casing rotating helps remove gelled mud, and thus prevents gas migration.

In a study conducted by the Petroleum Safety Authority (PSA) Norway on the review of well control incidents from 2003 to 2010 on the Norwegian Continental Shelf (NCS), it was revealed that more than 28% of well control incidents were due to technical failures

such as technical well design (cement, casing, and plugs) and improper primary barrier/mud column (PSA Report, 2011). Shallow gas incidents were quite significant. During the period of study (2003-2010), 146 well control incidents were registered from which more than 18 were categorized as shallow gas or high-risk shallow gas. The study recommended to include shallow gas, pore pressure and length of casings as typical topics for the risk review.

In the United States OCS, several shallow gas well control incidents have been reported. One of the incidents of shallow depth occurred in February 2013, at the Main Pass Block 295 in the Gulf of Mexico. District investigation of the incident concluded the cause due to the 18" liner top seal assembly and cement barrier between the conductor casing and surface liner. A QC-FIT evaluation report published in 2014 (BSEE, 2014) revealed potential causes of the incident as due to casing hanger seals, and cement column in conductor/surface liner annulus. The key findings from investigation report revealed the followings; 1) lack in robustness of current industry practices and regulations related to pressure testing, 2) quality control on downhole pressure equipment design, testing and realistic rating in situations of loss of well control incident and lifetime conditions; and 3) review and analysis of well design regarding shallow liner hanger sealing assembly, and the need for improving best industry practices.

In a recent ExproSoft's report to BSEE on updates of loss of well control incidents (LOWC), incidents grouped into two categories. The first category is called shallow zone LOWC events. These occur before the installation of the blowout preventer (BOP) on the wellhead. The second category is deep zone LOWC, and they occur after the BOP has been landed on the wellhead. The report stated that approximately 50% of LOWC that

occurred during drilling, were shallow events. For the deep zone drilling incidents, approximately one half of the kicks that occurred were detected late. In the same section, BOP failure accounted for 50% of the incidents while the rest were because of formation and cement failure. Shallow zone incidents typically occurred due to unexpected high well pressure or during the cement setting process. ExproSoft’s report classifies major causes for shallow zone kicks as i) unexpected high well pressure or too low of mud weight; ii) annular losses (swabbing); iii) poor cement; and iv) unknown (Figure 14). The report further recommends some important factors to focus on in shallow zone drilling such as awareness of shallow gas, cement waiting time, cement fluid loss and annulus pressure while waiting on cement.

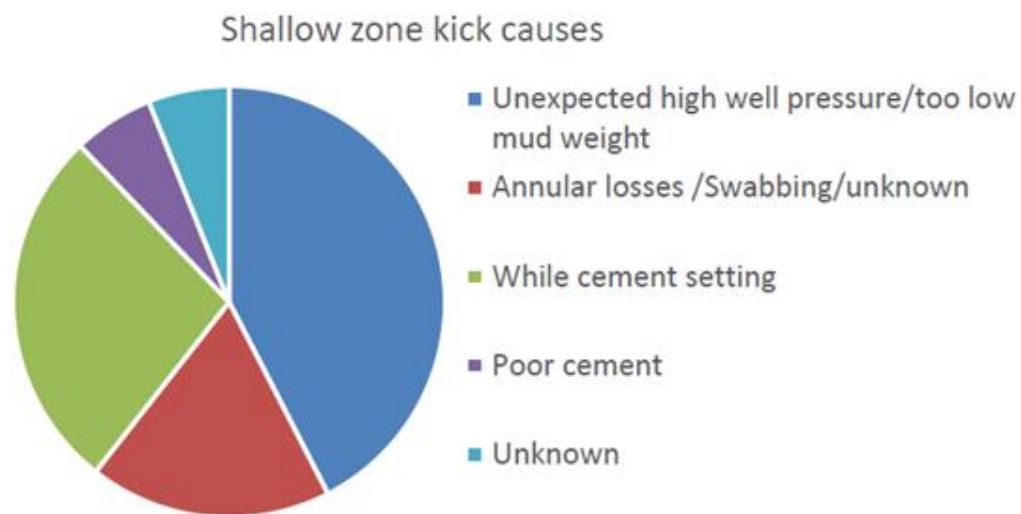


Figure 14. Shallow zone kick causes summarized in ExproSoft’s report to BSEE, 2017.

Review of loss of well control incidents while tripping at US OCS shows at least two incidents in 2013 and 2014. A kick incident occurred at Vermilion Block 356 of GOM for the Rowan Louisiana in 2014. The root-cause analysis showed that while short trip, and stuck pipe in “Gumbo” layers, the over-pull caused reduction in wellbore pressure

and “swab” effect. The investigation panel (BSEE 2015a) reported causes of loss of well control incidents due to:

- Existence of high risk “shallow gas”
- Short trip in the high-risk zone and swab effect

The investigation panel also recommended more robust and comprehensive hazard analysis in high risk drilling such as shallow gas, developing proper operational procedures, reduce drilling rate in high risk zones and more training to crew in detecting and mitigation of such hazards.

In another incident in 2013, the crew for Walter Oil and Gas Corporation while “tripping out” encountered a kick which was elevated to blowout. The BSEE investigation panel (BSEE, 2015b) made following recommendations (BSEE) as cause of initial loss of well control:

- Improper and insufficient completion fluid density
- Ignoring effect of temperature on brine density
- Failure to detect kick in early stages

Important to consider is lack of alternative protocols in fast well control events where the crew cannot accomplish some of the early steps.

Cement Design and Integrity

Well construction often require that conductor pipes be cemented in unconsolidated and relatively young geological formations. Weak formations and pressured sands tend to present narrow margins between pore pressures and fracture gradients. These tight drilling margins pose multiple challenges in managing weighted mud, equivalent circulating density (ECD), and drilling shallow over pressured formations with a riser. If

these pore pressures cannot be controlled, the zone begins to flow large volumes of salt water, which carry with it pieces of unconsolidated formation. Such flows can lead to washouts, ineffective cementing, hole re-entry issues, damaged casing, and sand compaction. One of the critical factors to consider in cement design for shallow flows is transition time. Transition time is the period during which the cement slurry changes from being a true hydraulic fluid to the point where it is solid enough to prevent annular gas flow.

Sabins et al. (1982) developed test techniques to study the beginning of transition period and conducted tests to delineate the condition of cement that would prevent gas migration. If cement pressure, adjacent to a high-pressure gas zone is maintained at a value equal to or greater than the gas reservoir pressure, then annular gas flow can be prevented. Once the pressure in the annulus is less than the pressure of an adjacent gas reservoir, gas entry can begin to occur (Tinsley et al., 1980). Their tests showed that critical static gel strength can occur 10 minutes after stopping the cement pumps. Additional results showed that for normal thickening times and slurries with low fluid loss, SGS (static gel strength) stabilized from 21 lbf/100ft² to 104 lbf/100ft². The authors emphasized that once an increase in SGS occurs, it can reach values exceeding 250 lbf/100ft² within one hour.

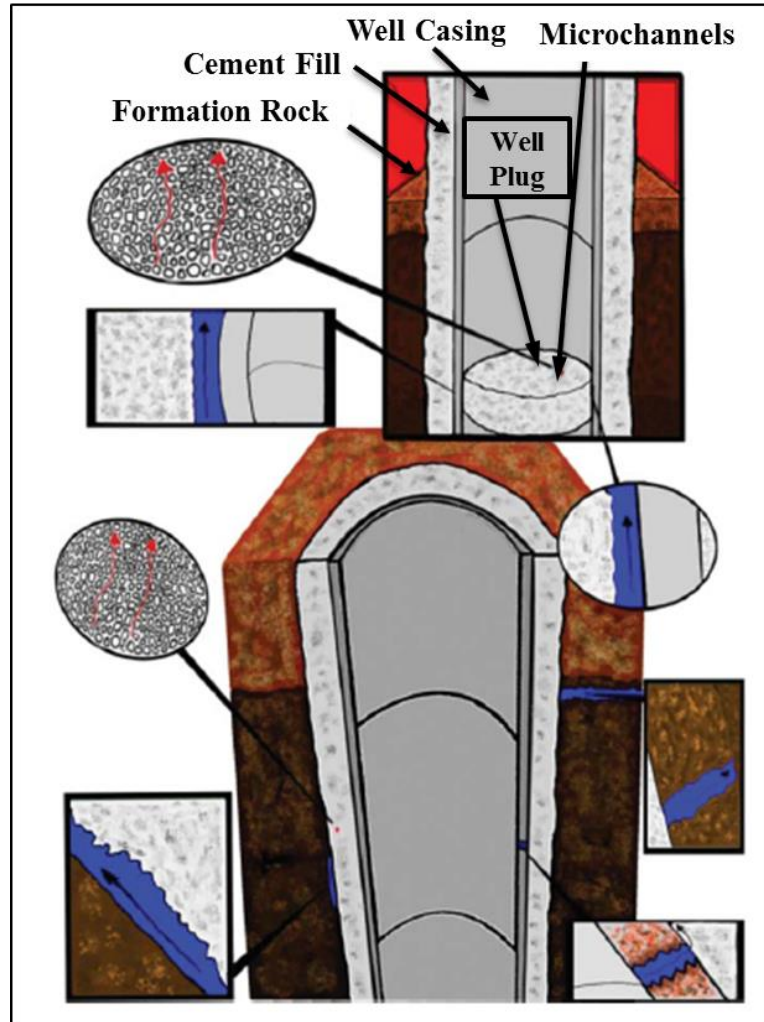


Figure 15. Potential leakage pathways in wellbores (from Salehi, 2013).

It is important to mention that cement must remain in its slurry form until it is fully displaced to the desired downhole location. However, after placement, cement should set fully and develop adequate compressive-strength within a brief period. To test the effects of thickening time on early compressive strength and gel-strength development, Sabins et al. (1986) studied a variety of cement slurries in a wide range of well conditions. These slurries included lightweight filler type cements, neat cement slurries with fresh and seawater, fly-ash slurries, and silica-stabilized slurries with fluid loss additives and dispersants. In their evaluations, static gel strength commenced

immediately after static conditions. This static gel strength development of the cement slurry offered some vital information. The first was the gas flow potential, while the second was the gel strengths above which the cement would subject the formation to excessive pressure. They emphasized that the static gel strength of cement slurry is more closely related to the type of cement slurry than the thickening time. However, with thickening times exceeding of 10 hours, gel strength development is restrained. The authors concluded that most of the tested slurries developed static gel strengths greater than 100 lbf/100 ft² in less than 20 minutes, and a reasonable increase in thickening times does not significantly change 12 and 24-hour compressive strengths.

Shallow water flows (SWFs) are major shallow drilling hazards that have led to the abandonment of prospective wells (Eaton, 1999). In additions, SWFs are common in deep-water GoM operations. Shiflet et al. (2005) discussed a three-component technique that has been developed to mitigate gas migration in three wells in the Eugene Island Block 273 gas field. The first component in this technique was to drill a gauge hole, while the second component involved mixing and pumping the correct cement slurry. The final process was the ability to utilize mechanical barriers to create obstructions to the gas migration. The three-component technique eliminated gas migration into the cement column of the three wells. Unsuccessful zonal isolation in shallow flow situations can result in the loss of a well and/or expensive remedial work. Cement systems like foam cement and optimized particle size distribution (PSD) cement have been used to control shallow flows in oil and gas wells. Irrespective of the cement system, O'Leary et al. (2004) highlighted the properties of a typical cement slurry for preventing shallow flows, and can be summarized as: 1) no free fluid, as free fluid would lead to cement slurry

volume reduction as the water is removed, 2) the slurry should be stable with complete absence of slurry settling or sedimentation, which causes density differentials in the cement, and leads to insufficient hydrostatic pressure for well control, 3) the slurry is recommended to have a fluid loss of 20–50 ml/30 minutes, since rheology, thickening time, and density are dependent on the available fluids, 4) sufficient thickening times for uniform cement placement around the casing, and 5) short critical hydration period.

Gas Migration Additives

Surfactant and foam cements have been used over the years to prevent gas migrations and to mitigate SWF. Surfactant cement is a conventional slurry to which a foam generating surfactant is added. The surfactant immobilizes gases from the formation by converting them into highly viscous low mobility foam, while lowering the slurry's surface tension to prevent bubbles from coalescing and being mobile. Developed in 1973 by the Institut Francais du Petrole (IFP), surfactant cements were deployed as a means of curbing gas migration economically. Harder et al. (1992) explored the use of ethoxylated nonyl phenols (ENP) as a counter-active surfactant in cement slurries. Thickening time, rheology, consistency, fluid loss, non-destructive and destructive compressive strengths were tested at varying levels of OBM contamination with several OBMs. The range of ENP concentrations were from 0.5% to 2.0% by volume of slurry. The authors observed that some cement slurries with 30+% OBM percentage would not produce any compressive strength until over 48 hours of wait on cement (WOC) time. One surfactant free slurry with 40% OBM revealed a 24-hour compressive strength of 700 psi, while the same slurry with 2% ENP developed a compressive strength of 1470 psi after 24 hours. They recorded major improvements in rheological compatibility for all OBM samples

and controlled high yield points by adding small amounts of ENP. Hibbeler et al. (1993) described some case studies regarding the cost effectiveness of surfactant cements. The major properties of a good surfactant are: excellent compatibility with the cement, high tolerance to calcium or pH sensitive environments, appropriate effect on slurry transition time, and gas blocking ability at a range of temperatures and pressures. They tested two surfactants: Ethoxylated Lauryl Ether (ELES) and Ethoxylated Nonyl Phenol (ENP). The ENP surfactant revealed unsatisfactory results because it caused longer transition time, high free water, and was ineffective in gas control. ELES demonstrated right angle setting between 120°F to 190°F. The right-angle set is a cement property that characterizes the change in cement slurry consistency from 30Bc to 100Bc in a short time. It is characterized by a 90° bend in a cement consistency versus time. Concentrations from 1.0% to 2.5% by volume of mix water was found to be optimum. They also observed that ELES surfactant reduced slurry's plastic viscosity and yield point while increasing the thickening time. Surfactant cements tend to block gas flow at the cement-formation interface, while providing cost effective gas control.

Cowan et al. (1993) made use of numerous surfactant additives to improve the performance properties of cement. Some surfactants used included ENP, Ethoxylated C12-C15 linear alcohol sulfate, Coco amidopropyl betaine, and Nonionic fluorocarbon surfactant blend. These surfactants were added to Portland cement with varying concentrations. Interfacial sealing tests were conducted on them and the surfactants proved to improve interfacial sealing between cement and pipe. To control fluid loss, they also combined surfactants like Sodium n-decyl sulfate, Sodium lauryl sulfate, Ammonium perfluoroalkyl sulfonate, Alkylether hydroxypropyl sultaine, Deceth-4

Phosphate, Nonoxynol-6 Phosphate, Alkyl phosphate ester, and Cocoamidopropyl with polymers. This combination enabled them to obtain the desired fluid loss at a lower cost. In conclusion they discussed how surfactants lead to less shrinkage. The cement with surfactant had approximately 3% less shrinkage compared to cement slurries without surfactants at the same temperature.

Faul et al. (2000) designed lightweight foamed-cement (LFC) slurry systems that uses only liquid additives with Portland cement, creating a low-density slurry with relatively short transition times. For SWF preventative cement compositions, the desired thickening time is 3-5 hours at 65°F, and a compressive strength of 400-500 psi at a temperature of 55°F is required. They obtained two Class “A” Portland cements from different suppliers, and all slurries were foamed to 12 lbm/gal. Their results showed a shorter transition time for LFC systems, and this helped to prevent potential SWFs, while maintaining zonal isolation and adequate cement placement time. For large scale testing, Class H cement was foamed to 12.5 lbm/gal for large scale tests. The thickening time at 65°F was 4.17 hours. Compressive strength was recorded as 360 psi and 600 psi, at 45°F and 55°F respectively.

Traditional compressible fluids (foamed cements containing nitrogen) have been discussed as one of the cementing systems for mitigating shallow gas and liquid flows. However, this approach has generated safety concerns, complicated logistics, lack of reliability, placement problems, and long-term integrity issues. To eliminate these concerns, special cement systems based on packing volume fraction and ratios of sized particles have been developed and used successfully in the Gulf of Mexico. This special cement system called as particle size distribution (PSD) system (O’Leary et al., 2004).

They concluded that the PSD system had early gel strength and compressive gel strength development because of the low water content. In addition, low density features minimized risk of lost circulation incidents in shallow-flow prone zones. Furthermore, set cement exhibited ultra-low permeability ensuring zonal isolation throughout the entire life of the well. Another study in Offshore Kalimantan reported application of a particle-size slurry system (Hartoni et al., 2000). The area of Offshore Kalimantan is characterized by low fracture pressure and shallow gas zone problems; therefore, the new slurry system was able to handle these issues.

In addition to foam and surfactant containing cements, salted cements are also used to mitigate dissolution in massive salt environments that have the tendency to compromise the cement sheath to formation bonding. In addition, they can be applied to cement unconsolidated and loose offshore shallow pressure zones, with high tendency of shallow breakouts and shallow fluid influx. First applications of salted cement discussed by Carter et al. (1966). After setting, cement expansion occurs because of internal pressure exerted by salt crystals. In a recent study, Teodoriu et al. (2015) investigated the effects of salt concentration on the thickening time, compressive strength, elastic modulus, and set cement permeability of API Class-G cement. They observed that the 5% by weight of water (BWOW) salted cement slurry had the shortest thickening time and the highest compressive strength. Authors reported 32% increase in strength after 24 hour and 72 hours, and 11% increase after 7 days. Strength retrogression was observed at elevated temperatures between 1 and 7 days, and the cement failed between 212°F and 302°F. Low NaCl concentrations between low and moderate temperature and pressure conditions yielded desired setting speed, hydraulic integrity, rheology, and excellent

accelerating effects on Portland cement hydration. Furthermore, they concluded that 5% \pm 2.5% BWOW NaCl concentration had the best effects on the tested cement properties.

Cement with latex and elastomer powders are reported in literature for use in mitigating gas migration. Latexes are aqueous dispersions of polymer particles such as surfactants which impart stability to dispersion. The mechanism of latex in cementing can be described as an acting impermeable polymer barrier when hit by gas. This, helps in mitigating gas flow in the cement column. Other latex benefits include acting as a fluid loss control agent and/or a lubricant. Studies have shown latex improving shear-bond strength of cement (Parcevaux and Sault, 1984). These additives were first introduced by Parcevaux et al. (1984). Latex field applications have been presented in several studies reported in the literature (Evans, 1984; Rae, 1987; Drecq and Parcevaux, 1988). In a recent study, Kelessidis et al. (2014) presented laboratory studies on two slurry systems one including latex additives. They conducted their assessment on two non-foamed cement slurries at room and elevated temperatures and pressures. The first slurry was a Class-G neat cement and the second slurry was a Class-G cement mixed with micronized silica, and latex. They recorded low fluid loss for the second slurry, compared to its original form at all pressure and temperature conditions. In addition, the second slurry showed prolonged dormant time but had a shorter transit time. The prolonged dormant time provides an extended time for cement slurry placement, while quick transit time indicates a better cement-water cohesive bond. Study concluded that a combination of micronized silica and latex will initially retard hydration in the acceleration period due to the coalescence of the latex particles in the slurry, and thus forming a plastic film that covers the C-S-H gel.

In addition to using latex as cement additive, elastomer powders were used to counteract pressure changes during the setting phase of cement. Talabani et al. (1997) observed that adding an elastomer rubber powder to the cement would eliminate cement-body micro fractures with an optimum cement elastomer mixture. The selection of the appropriate elastomer powder during a cement job can eliminate micro cracks in the cement by eliminating the pressure variation in the setting process of the cement.

Grinrod et al. (1988) discussed the use of microsilica in the creation of a gas tight cement slurry. Microsilica (silica fume) is a byproduct of silicon and ferrosilicon production. It has a bulk density of 400 to 500 kg/m³ and specific gravity of 2.2. It is composed primarily of vitreous silica, having SiO₂ content ranging from 85 to 95%, and a particle size distribution range of 0.02 to 0.5 µm, with an average of 0.15 µm. This fine particle size allows packing between the cement grains resulting in an improved microstructure of the cement matrix. When used in various concentrations with varying densities (Figure 16) they found out that microsilica had the ability to mitigate gas migration by immobilizing the pore water within the cement matrix. They explained that microsilica gives better strength and bonding, reduced permeability, improved durability and provides less strength retrogression.

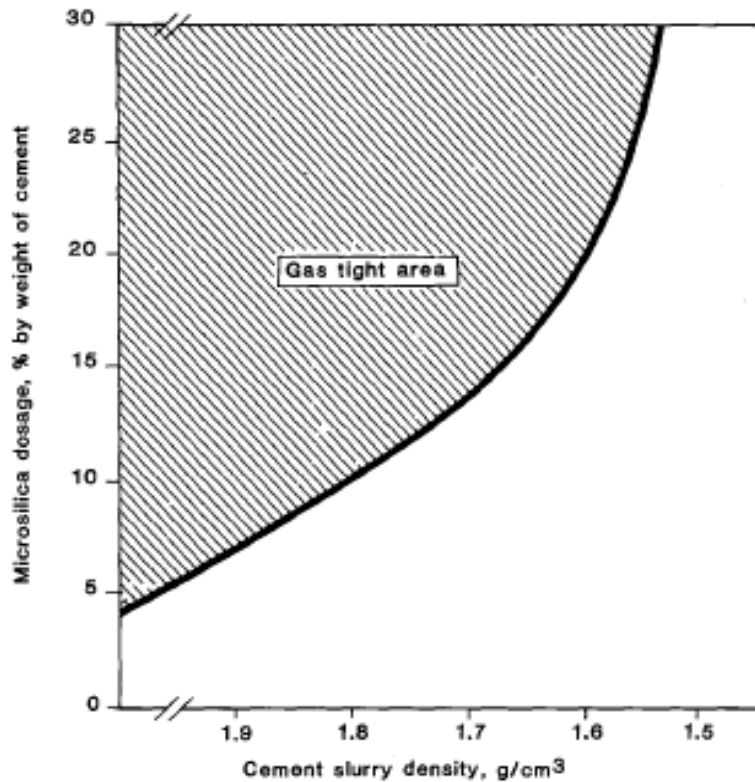


Figure 16: Dosage of microsilica needed at different cement slurry densities to withstand a maximum gas pressure of 125% of the water gradient (from Grinrod et al., 1988).

Skalle and Sveen (1991) state that despite microsilica shows positive effect on cement permeability it does not produce gas tight cement at higher temperatures. They also go ahead to investigate other cement additives and document that though bentonite reduced the amount of free water, it acted as a contaminant because it reduced the bonding strength of the cement. Latex also according to their research reduced bonding strength significantly.

Daou and Piot (2009) review typical uses of microsilica in oilfield cements. They paid particular attention to the influence of material grade - degree of densification on slurry behavior and set cement properties. They clarify the dispersability of densified microsilica in cement slurry by observing the set microsilica cement microstructure. This

was done with a scanning electron microscope coupled with an energy dispersive spectrometer. They demonstrated that, contrary to public belief, not all microsilica are the same. Microsilica comes in two major forms – undensified and densified microsilica. Undensified microsilica has bulk density typically $200 - 350 \text{ kg/m}^3$ while densified microsilica has a bulk density typically $500 - 700 \text{ kg/m}^3$. They document that densified microsilica does not disperse into small particles when mixed in a cement slurry. Therefore, densified and partially densified grades which are popular because they can be handled easily, do not provide the performance required for adequate zonal isolation as is expected of microsilica cement. According to their research, densified microsilica behaves as a completely inert material and not as a reactive one. Thus, is practically useless as lightweight material or an antisepting agent. They presented the particle size distribution of varied densification of microsilica. This is shown in Figure 17.

Figure 18 shows the particle size distribution of cement with undensified and densified microsilica. In conclusion they stated that only moderately compacted microsilica with a bulk density of approximately 300 kg/m^3 would be helpful in developing a good cement performance.

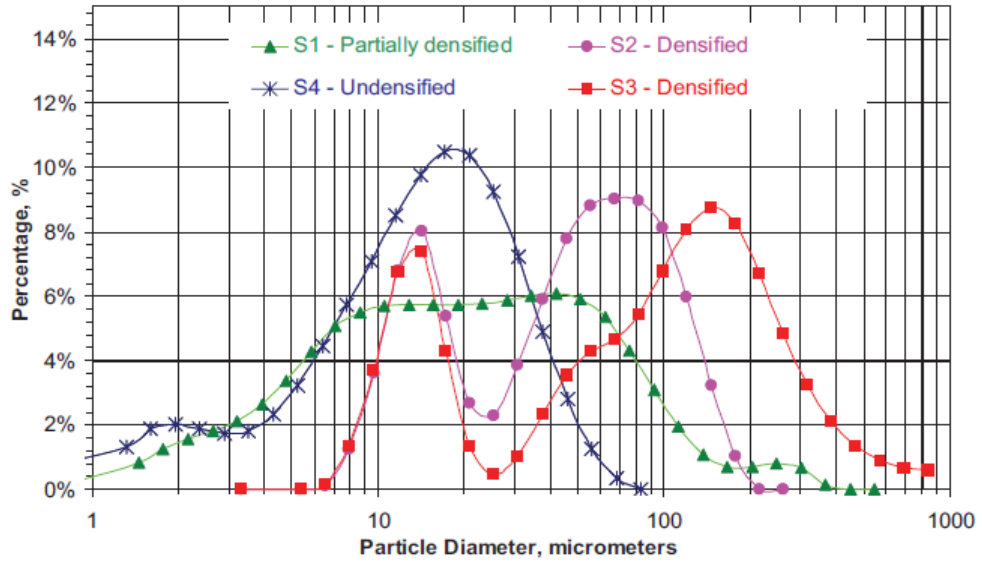


Figure 17: Particle size distribution of raw samples. S1 – 333 kg/m³, S2 – 719 kg/m³, S3 – 582 kg/m³, S4 – 167 kg/m³ (Daou and Piot, 2009).

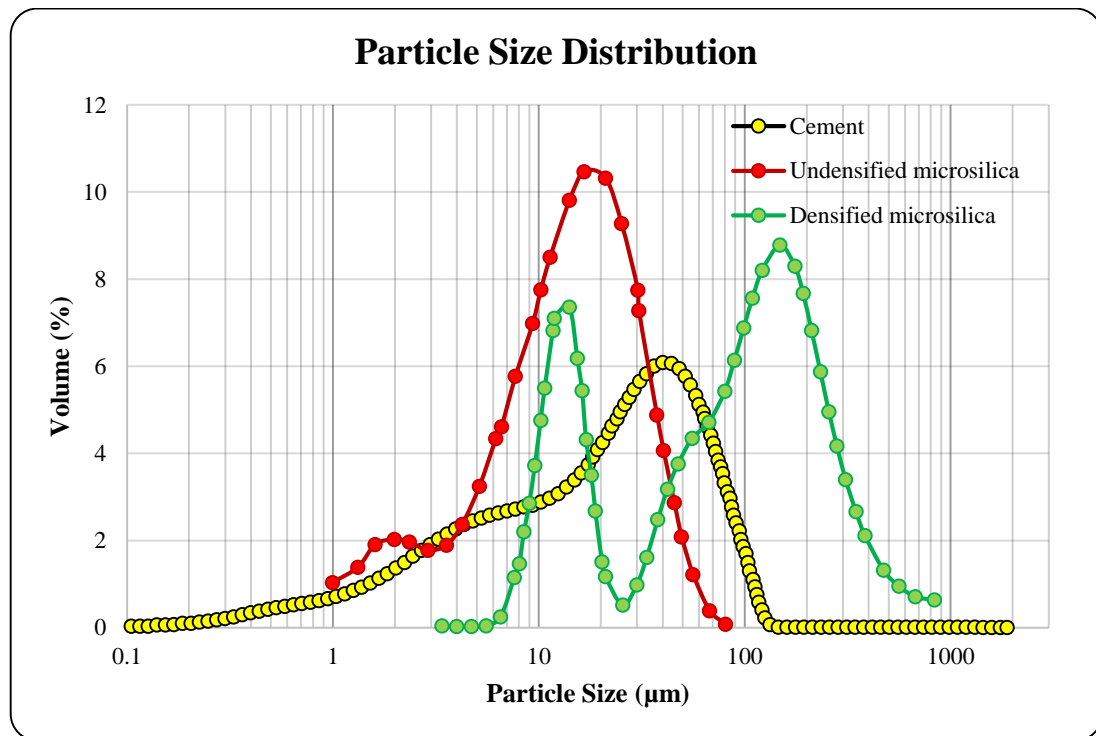


Figure 18: Particle size distribution of cement and various microsilica additives (after Daou and Piot, 2009; Dylan Moore, 2015).

Al-Yami et al. (2009) discussed a cement formulation to prevent gas migration in high pressure – high temperature (HP/HT) wells. The additives they used included silica,

manganese tetraoxide, expansion additives (magnesium oxides burned at 2192 °F), hematite and silica sand. The cement slurries that prevented gas migration had formulations with 45% BWOC of Mn_3O_4 , and 45% CWOC hematite with different ratios of silica sand and silica flour. The best formulation was Class G cement with 45% BWOC hematite, 5% BWOC expansion additive, 10% BWOC silica sand, 25% BWOC silica flour, 45% BWOC Mn_3O_4 , 3.5 gals/sack gas blocker, 0.5 gals/sack gas block stabilizer, 1.2% BWOC high temperature retarder, 0.45% BWOC low temperature retarder, and 0.3% BWOC fluid loss additive. The concluded that a cement with this formulation would prevent gas migration in an HP/HT well. At high temperatures,

Shakirah (2008), presented that magnesium oxide (MgO) has proven to provide expansion force in the cement matrix thereby decreasing the probability of microannuli creation. This expansive force within the cement matrix is because magnesium oxide hydrates to form magnesium hydroxide – which occupies more space than the original MgO. However, this hydration is only achievable at high temperatures of 550 °F and would not be beneficial at temperatures below 140 °F.

Abbas et al. (2013) discussed the use of Hydroxypylmethylcellulose (HPMC) – a cellulose based gelling and thickening agent – as a gas migration agent. They found HPMC to have the ability to develop an impervious barrier while preventing the amount of free water in the cement system. With lab experiments they confirmed that HPMC based cement slurries were gas tight, having the ability to prevent gas migration up to 150 psi. Their lab work showed that for HPMC polymer concentrations of 0.2 to 0.55 gals/sack, the cement pore pressure remained at a constant 16 psi with a continuous injection of 150 psi gas for up to 8 hours. Additional advantages to the use of HPMC

slurry included; its ability to control fluid loss up to 190 °F, and an increase in thickening time for up to 2 hours.

Calloni et al. (1995) discussed the use of Carbon black as a gas migration additive in cement. Carbon black is a paracrystalline carbon that is produced as a byproduct of incomplete combustion of heavy petroleum products like coal tar. They documented that concentrations as low as 4% BWOC of carbon black was enough to prevent gas migration in all formulations. The particle size of Carbon black ranges from 10 to 200 nm and a surfactant (formaldehyde-condensed naphthalene sulfonate, sulfonated cumarone or indene resins) is necessary for its dispersion (Petroleum Engineering's Guide). The biggest advantage associated with the use of carbon black was the economic prospects. Some patented work on the chemicals used for cement gas migration inhibition include: Ganguli (1992) – a copolymer of 2-acrylamido-2-methyl-1-propane sulfonic acid (AMPS), *N*-vinylacrylamide, and acrylamide (AAm) that reduced the occurrence of gas channeling, and Kuksov et al. (1992) – a mixture of lignosulfonates, alkali-treated brown coal, and organic silicon compounds that was able to reduce the permeability of cements.

Phosphorated aluminum powder can also be used as an anti-gas migration. It reacts with calcium hydroxide in the cement slurry producing hydrogen gas which swells the cement slurry. This swelling in turn prevents the channeling of gas in the cement (Wang 1996; Bortsov 1997a; Bortsov 1997b).

Table 5: Highlights of gas Migration additives			
Additive	Advantages / Pros	Disadvantages / Cons	Application / Uses
Surfactant or foam eg. Ethoxylated nonyl phenols (ENP), Ethoxylated Lauryl Ether (ELES)	Low density, Converts gas into immobile fluid, Economical, Improves rheological properties, right-angle setting between 120°F and 190°F, less shrinkage, high tolerance to calcium or pH sensitive environments, appropriate effect on slurry transition	Longer transition time, high free water	
Salt	Cement expansion, 5% BWOC improves cement compressive strength	Can compressive cement sheath to formation bonding	Salt environments, cement unconsolidated and loose shallow pressure zones
Latex	Fluid loss control, acts as a lubricant, improves shear-bond strength	Reduces bonding strength significantly	
Elastomer rubber powders	Counteract pressure changes during setting phase of cement, eliminates cement - body micro fracture with an optimum cement elastomer mixture		
Microsilica	Control free water immobilizes pore water within the cement matrix, reduces permeability, less strength retrogression	Does not produce gas tight cement at elevated temperatures, can be an inert material with wrong densification	
Bentonite	Reduces amount of free water	Reduces bonding strength of cement	
Magnesium oxide (MgO)	Provides expansion force in cement matrix	Not beneficial temperatures below 140°F	
Cellulose eg. HPMC	Fluid loss control upto 190°F, develops imperious barrier		
Carbon Black	Highly economical		

Cost Estimations and Effects

Since anti-gas migration additives generally increase the overall cost of a cement slurry design, this sections seeks to perform a cost estimation of some anti-gas migration additives. This provides the read a holistic view of their cement slurry design cost depending on the stand they take. It is to be noted that these reported prices (Table 6) are subject to change depending on the company, season and year of enquiry.

Table 6: Cost estimations for anti-gas migration additives

Cement anti-gas migration additive	Cost estimate
Fly ash	\$15 - \$40 per ton / 0.75 to 2 cents per pound
Latex	\$26 per gallon
Microsilica	\$400 - \$1000 per ton
Nanomaterial	\$480 - \$650 per ton
Carbon black	\$1054 per ton

Summary

Successful casing and cementing programs are especially critical for the shallow or top hole sections of a well. It will be very challenging to control a well when broaching of wellbore fluids occur. The presence of gas in the formation is a key consideration for designing casing and cements. Gas migration is a complex phenomenon which poses several challenges in terms of loss of well control incidents. Several factors such as cement properties, design, cement hydration and other operational conditions such as mud removal and pumping impact gas migration. Decades of research on gas migration has

provided the oil and gas industry with solutions ranging from using special additives in cement, improving operational procedures and improving cement mixture designs. However, no single solution still exists to fit all downhole cases.

Many of loss of well control incidents have occurred due to gas migration either through the cement column, faulty equipment, faulty casing, and failure in different well construction barriers. Some of the recent LOWCs in the UC OCS include MP 295 incident in 2013 and Vermilion block 356 in 2014, which are examples of shallow gas incidents. A recent report classifies different major causes of shallow zone kicks such as unexpected high well pressure, annular losses (swabbing), poor cement, and other unknown factors. Some important factors to focus on with respect to shallow zone drilling include awareness of shallow gas, cement waiting time, cement fluid loss and annulus pressure while waiting on cement.

Chapter 3: Elastomer Experiment and Results

The possible failure of elastomers in a wellbore makes it imperative to understand the various elastomer degradation mechanisms and develop methods to reduce the degradation. Hence, the objectives of this study are:

- To investigate if elastomers are “fit for service” for shallow well construction applications.
- To determine elastomer performances under downhole corrosive conditions.

Research Methodology

To achieve these objectives, both theoretical and experiment approaches have been considered in this study. Elastomer degradation strongly depends on the elastomer's chemical structure as well as the composition and abundance of liquid and gas phases they are in contact with. In this study, we have examined the relationship between elastomer degradation and downhole operating parameters such as temperature, exposure time, and acid gas variations. The outcome of the theoretical analysis provided useful information in understanding the mechanisms that are involved in the elastomer degradation process.

In addition to the theoretical analysis, experimental investigations were conducted to study the degrading behavior of elastomers in acidic environments. The degree of degradation was measured as the change in critical properties of the elastomer such as hardness, volumetric swelling, and compression. These investigations were used to determine whether elastomers are “fit for service” for a given set of downhole conditions, based on their performance.

Experimental Design

Elastomers are sensitive to downhole conditions (temperature, pressure, acid gas variations, and acid gas concentration). To perform tests under simulated borehole conditions, elastomer-aging experiments were carried out at varying temperatures from 120 °F to 180 °F. Pressure was kept constant at 1000 psi, with two fluid phases - a vapor and brine phase. For each experiment, the same types of elastomers were used. Half of them immersed in the brine phase and the other half exposed to the vapor from the brine (vapor phase). The gas variations included methane (CH₄), hydrogen sulfide (H₂S), and carbon dioxide (CO₂). Some experiments were conducted with 100% CH₄, 100% H₂S (500 ppm) with methane carrier, and 100% CO₂. Subsequent experiments were conducted with a mixture of the three gases, 50% CO₂ and 50% 500 ppm H₂S with methane carrier. Aging duration to quantify the effects of time on elastomer degradation was 1 and 7 days. Some experiments were also conducted with an aging duration of 3 days to study the patterns in the changing properties. Four different elastomers (NBR, EPDM, FKM, and PTFE) were considered in the investigation.

To quantify the level of degradation, properties (hardness, volumetric swelling, and compression) of aged and intact samples were measured and compared. In addition, a Dino-Lite Digital Microscope was used in observing the morphology and blistering of severely damaged elastomers. Two types of elastomer sizes were prepared to carry out the experiments. Cylindrical samples of thickness (height) 0.33-in and 1-in were selected based on preliminary tests and results. The 0.33-in thick elastomer was for compression measurements, while the 1-in thick elastomer was used for swelling and hardness measurements. All elastomers had a constant diameter of 0.75-in.

Experimental Investigations

Test Materials

To achieve successful aging experiment of elastomers, information from literature and published reports were applied accordingly. The elastomers were exposed to H₂S, CO₂, and CH₄ in either brine or vapor phase. This was done at a constant pressure of 1000 psi and varying temperature of 120 °F and 180 °F. A brief description of materials used in the elastomer aging experiment and their specific roles are presented in this section.

Elastomers

Four elastomers were used: NBR, EPDM, FKM, and PTFE. These elastomers were selected because they are widely used in oil and gas applications such as blowout preventers (BOP), packers, liner hangers, heat exchanger gaskets, paper mill rolls, rotary shaft seals, hoses and cable jacketing in hydraulic/pneumatic systems amidst others. The behavior of these elastomers was studied when exposed to harsh conditions to determine whether they are “fit for service”.

Brine

Two percent brine was used for the experiments. This is because the salt concentration averages from 14 to 36 ppt in the Gulf of Mexico (LaMourie et al., 2005). This approximates to 2.5% brine concentration. In this study, brine was used as the liquid corrosive medium to provide more information on elastomer degradation in the presence of liquid and vapor media. The presence of brine creates the opportunity to explain why elastomers would degrade differently based on their surrounding medium.

Gases

H₂S, CO₂, and CH₄ were the gases used for conducting the experiments. These gases were selected because they are predominant gases associated with shallow wells in the Gulf of Mexico. Furthermore, these gases are known to be commonly used in elastomer aging experiments, based on the materials and methods from previous studies.

Test Matrix

Nine test categories consisting of 288 experimental samples have been conducted to examine the effects of temperature, aging, and the presence of H₂S, CO₂, and CH₄ on the degradation of oilfield elastomers. Table 7 and Table 8 summarizes all test parameters of the experiment. Aging test 5 (T5) was conducted with 100% CH₄. Aging test 6 (T6) was conducted with 100% CO₂, and aging test 7 (T7) was conducted with 100% H₂S with methane carrier. Remaining aging tests were conducted with a mixture of the three gases, 50% CO₂ and 50% 500 ppm H₂S with methane carrier. Physical properties (hardness, volumetric swelling, and compression) of intact and aged samples were measured to assess the level of damage and performance of the elastomers. There are five independent variables: 1) Type of elastomer: NBR, EPDM, FKM, and PTFE, 2) Aging period: one and seven days, 3) Liquid contaminant: brine phase and vapor phase, 4) Sample length: 0.33-inches and 1-inch, 5) Temperature: 120°F and 180°F. Each test sample is given a unique nomenclature, which is discussed in subsection “test sample preparation procedure”.

Table 7: Test parameters for aging experiments conducted							
Age-Day	Phase	Length	T1 (120°F)	T3 (180°F)	Age/Phase	T8 (120°F)	T9 (180°F)
One	Vapor phase	L1 (0.33-in)	N1V1T1	N1V1T2	Three Days/Vapor Phase	N3V1T1	N3V1T2
		L1 (0.33-in)	E1V1T1	E1V1T2		E3V1T1	E3V1T2
		L1 (0.33-in)	V1V1T1	V1V1T2		V3V1T1	V3V1T2
		L1 (0.33-in)	P1V1T1	P1V1T2		P3V1T1	P3V1T2
		L2 (1.0-in)	N1V2T1	N1V2T2		N3V2T1	N3V2T2
		L2 (1.0-in)	E1V2T1	E1V2T2		E3V2T1	E3V2T2
		L2 (1.0-in)	V1V2T1	V1V2T2		V3V2T1	V3V2T2
		L2 (1.0-in)	P1V2T1	P1V2T2		P3V2T1	P3V2T2
		L1 (0.33-in)	N1B1T1	N1B1T2		Three Days/Brine Phase	N3B1T1
	L1 (0.33-in)	E1B1T1	E1B1T2	E3B1T1	E3B1T2		
	L1 (0.33-in)	V1B1T1	V1B1T2	V3B1T1	V3B1T2		
	L1 (0.33-in)	P1B1T1	P1B1T2	P3B1T1	P3B1T2		
	L2 (1.0-in)	N1B2T1	N1B2T2	N3B2T1	N3B2T2		
	L2 (1.0-in)	E1B2T1	E1B2T2	E3B2T1	E3B2T2		
	L2 (1.0-in)	V1B2T1	V1B2T2	V3B2T1	V3B2T2		
	L2 (1.0-in)	P1B2T1	P1B2T2	P3B2T1	P3B2T2		
	L2 (1.0-in)	Brine Phase					

Table 8: Test parameters for aging experiments conducted							
Age (Days)	Phase	Length	T2 (120°F)	T4 (180°F)	T5 (100% CH ₄ @120 °F)	T6 (100% CO ₂ @120 °F)	T7 (100% H ₂ S @120 °F)
Seven	Vapor phase	L1 (0.33-in)	N7V1T1	N7V1T2	N7V1T1M	N7V1T1C	N7V1T1H
		L1 (0.33-in)	E7V1T1	E7V1T2	E7V1T1M	E7V1T1C	E7V1T1H
		L1 (0.33-in)	V7V1T1	V7V1T2	V7V1T1M	V7V1T1C	V7V1T1H
		L1 (0.33-in)	P7V1T1	P7V1T2	P7V1T1M	P7V1T1C	P7V1T1H
		L2 (1.0-in)	N7V2T1	N7V2T2	N7V2T1M	N7V2T1C	N7V2T1H
		L2 (1.0-in)	E7V2T1	E7V2T2	E7V2T1M	E7V2T1C	E7V2T1H
		L2 (1.0-in)	V7V2T1	V7V2T2	V7V2T1M	V7V2T1C	V7V2T1H
	Brine Phase	L2 (1.0-in)	P7V2T1	P7V2T2	P7V2T1M	P7V2T1C	P7V2T1H
		L1 (0.33-in)	N7B1T1	N7B1T2	N7B1T1M	N7B1T1C	N7B1T1H
		L1 (0.33-in)	E7B1T1	E7B1T2	E7B1T1M	E7B1T1C	E7B1T1H
		L1 (0.33-in)	V7B1T1	V7B1T2	V7B1T1M	V7B1T1C	V7B1T1H
		L1 (0.33-in)	P7B1T1	P7B1T2	P7B1T1M	P7B1T1C	P7B1T1H
		L2 (1.0-in)	N7B2T1	N7B2T2	N7B2T1M	N7B2T1C	N7B2T1H
		L2 (1.0-in)	E7B2T1	E7B2T2	E7B2T1M	E7B2T1C	E7B2T1H
	L2 (1.0-in)	V7B2T1	V7B2T2	V7B2T1M	V7B2T1C	V7B2T1H	
	L2 (1.0-in)	P7B2T1	P7B2T2	P7B2T1M	P7B2T1C	P7B2T1H	

Test Sample Preparation Procedures

Elastomer samples were cut into the appropriate sizes (0.33-in or 1-in length) from 10 feet elastomer rods. Sample sizes are kept with a 15% margin of error before they are accepted to be used for any tests. All measurements including hardness, compression, diameter, length, and weight are taken and recorded in a Microsoft excel file. Measuring procedures are followed as stated in the “Test equipment and testing protocols” found in Appendix A. The sample nomenclature or sample identification code follows the independent variable listing in the order from 1 to 5 found in section “Test Matrix” in Appendix A. Table 9 describes the nomenclature for identifying samples.

Table 9: Nomenclature of elastomer sample.

N1V1T1				
N	1	V	1	T1
NBR sample	1-day aging period	Vapor phase contaminant	First sample length	First temperature

This nomenclature is written on each test sample bottle, after which the elastomer sample is placed in its corresponding sample bottle. For each elastomer aging test, a total of 32 samples were prepared and grouped into their 4 sections based on their type. Upon completion, the elastomers were ready to be moved to the autoclave for testing. All test equipment and setup protocol are discussed in the Appendix A.

Elastomer Aging Experiment

Experimental Setup

To simulate elastomer aging under corrosive downhole conditions, a test setup was developed. The schematic of the setup is shown in Figure 19. The setup consists of four components. The first is an aging cell with 3-liter capacity. The second component

comprises of three gas cylinders filled with test gases (CO_2 , CH_4 , and H_2S with CH_4 carrier). The third component is a gas injection cylinder (250 ml capacity) for accurate control of the composition of the gas inlet in the aging cell. Finally, there are measuring instruments and a data acquisition (DAQ) system. The cylinder is separated into two chambers via an injection cylinder equipped with a floating piston. The upper chamber of the cylinder is connected to an oil pump and reservoir, while the lower chamber is used to meter and inject the gas phase into the aging cell. The hydraulic oil flows back to the oil reservoir when the lower chamber is refilled with gas coming from one of the test gas cylinders. Piston location is determined from the liquid-level measured in the oil tank. During the aging test, elastomer samples were placed in the cell using round multilayer - raked shelves. The cell is partially filled with brine and the elastomers to be exposed to the liquid medium phase are immersed in the brine. The cell lid is put in place and the gas inlet line is connected. Gas injection begins by opening the valve between the injection cylinder and aging cell. Gas is injected into the cell repeatedly (in a selected sequence) until the cell pressure (P_2) reaches the desired value.

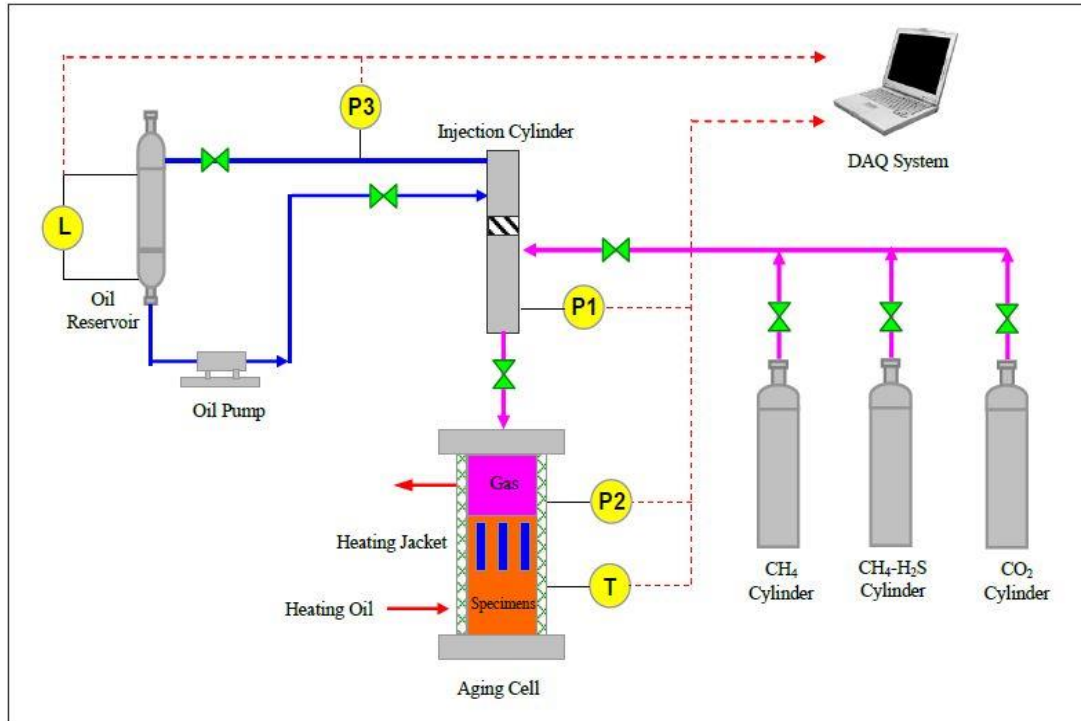


Figure 19: Schematic of autoclave cell setup (Ahmed et al., 2015).

Test Procedure

Figure 20 (a) and (b) shows the arrangement of the elastomers before and after lowering the elastomers in the autoclave cell respectively.

Table 10 shows the elastomer type and their arrangements in the shelves. The autoclave cell is equipped with a sample racking system that has 12 shelves, out of which the bottom two shelves are kept empty during aging experiments. The full length (inside) of the aging cell is 30-in. Prior to lowering the rack, the cell is filled with 2% NaCl (by weight) solution up to a level of 15-in. The samples were arranged on the racking system, 4 samples per shelf as shown in Figure 20 (a), and then lowered carefully into the cell. As shown in Figure 20 (b), 16 samples were completely immersed in the brine, while the remaining 16 were exposed to any vapor from the brine phase. The remaining 15-in space

of the autoclave was used for gas injection. The autoclave was sealed and heated to the desired temperature by circulating heating oil through the heating jacket. During temperature ramp-up, the autoclave cell was flushed twice with nitrogen, 15 minutes for each flush. The goal of the nitrogen flush is to remove any trapped air within the system. When the autoclave temperature reaches the selected test matrix temperature, the gas injection was initiated. The gas compositions are 50% CO₂ and 50% H₂S with a CH₄ carrier. The combined target pressure is 1000 psi. First, the CO₂ is injected up to 500psi, followed by the H₂S with CH₄ carrier until 1000 psi is achieved.

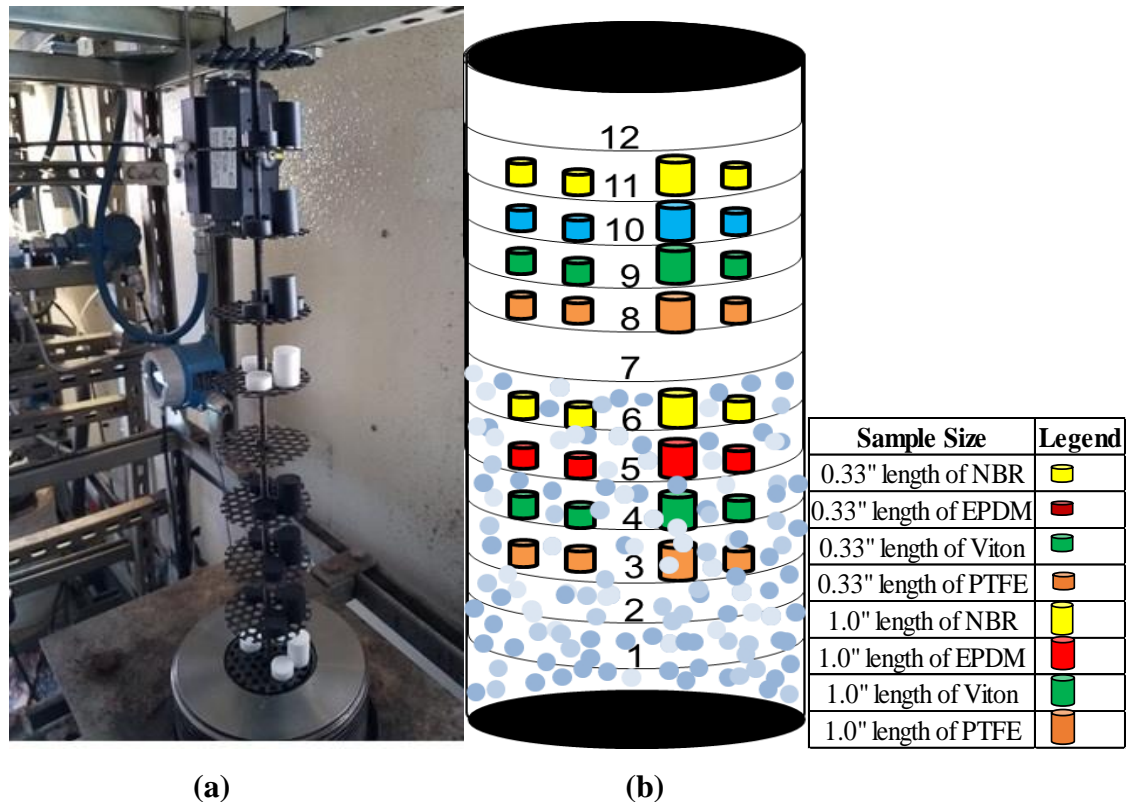


Figure 20: (a) Samples arranged in different shelves before lowering into the aging cell. (b)Schematic of sample arrangement inside the aging cell with legend. Shelves 1 to 6 are submersed inside brine, while shelves 7 to 12 are not, but still exposed to vapor from the brine.

Table 10: Elastomer arrangement in autoclave shelves

Shelf	Sample	Shelf	Sample
1	Empty	7	Empty
2	Empty	8	PTFE in vapor phase
3	PTFE in brine phase	9	Viton in vapor phase
4	Viton in brine phase	10	EPDM in vapor phase
5	EPDM in brine phase	11	NBR in vapor phase
6	NBR in brine phase	12	Empty

Elastomer Experiment Results

This section summarizes the results from the elastomer experiments conducted. The results comprise of all useful data collected during elastomer aging studies. It shows elastomer degradation in terms of change in performance of three indications: hardness, compression, and volumetric swelling. The parameters varied include days (1, 3, and 7 days), temperature (120 °F and 180 °F), and corrosive gases (CO₂, H₂S, and CH₄).

Performance of Elastomers

An elastomer's performance in oil and gas wells is determined by its sealing integrity. Elastomer seals are essential for zonal isolation in both vertical and deviated wells. The ability of an elastomer to perform this function is determined by its hardness, volumetric swelling, and compression. Generally, elastomer hardness increases with an increase in temperature due to cross-linking of elastomer chain (Jin et al., 2008). Swelling is the volumetric change in an elastomer after aging. Initially, elastomers swell on exposure to temperature. However, with an increase in temperature volumetric swelling decreases due to the decrease in elastomer elongation because of chain growth (Schweitzer P. A., 2000). The compression test (compressive stress-strain) conducted is the measure of an elastomer strain at a given compressive stress (psi) before and after aging. After aging,

elastomers strain increases per given stress. However, a decrease in strain is observed with an increased temperature. This is because of elastomer chain growth, which decreases elongation thus increasing the hardness of the elastomer.

Hardness

Elastomer hardness is defined as the resistance of an elastomer surface to indentation by a Shore A durometer. Adequate knowledge of elastomer hardness is important because O-rings made of harder materials may be required for sealing very high-pressure fluids in oil and gas wells. In addition, when sealing delicate objects - like thin plastics - an elastomer made of a softer material is desired. For this study, the hardness of elastomers was measured on two different spots, for each flat surface of the elastomer. Measurements are taken before and after aging the elastomer. The average of the four reading before aging represented the hardness of the elastomer before aging, whereas the average of the readings after aging represented the new hardness of the elastomer.

Effects of Days

A general observation is that after one, three, and seven days, elastomer hardness tends to drop from its original value. This observation was consistent for the two temperature set points (120 °F and 180 °F). This is because of exposure to temperature, pressure, and corrosive gas conditions. However, from one to three days and from three to seven days, there is a general increase in hardness irrespective of the temperature. This happens because of chain growth or cross-linkage. Jin et al., (2008) showed elastomer hardness increase with temperature. However, from the experiments performed in this study, it is detected that if the temperature is kept constant but the time of exposure is increased, this could compensate for a slow but steady increase in temperature within the elastomer. Thus, resulting to more cross linking and chain growth. This conclusion was drawn

because increase in exposure time of an elastomer to high temperatures, leads to more chain growth within the elastomer. With an increase in chain growth, there is an increase in elastomer hardness and tensile strength.

At 120 °F (Figure 21 (a)), this decrease in hardness is greater than 5% and up to 15% from the original hardness. However, this behavior is not observed in all PTFE (both brine and vapor phase) and all Viton (FKM) in the brine phase. At 180 °F (Figure 21 (b)), there was a 5% to 10% decrease from original hardness excluding PTFE (brine and vapor). In addition, 7-day samples of NBR, EPDM, and Viton aged in brine did not follow this general observation.

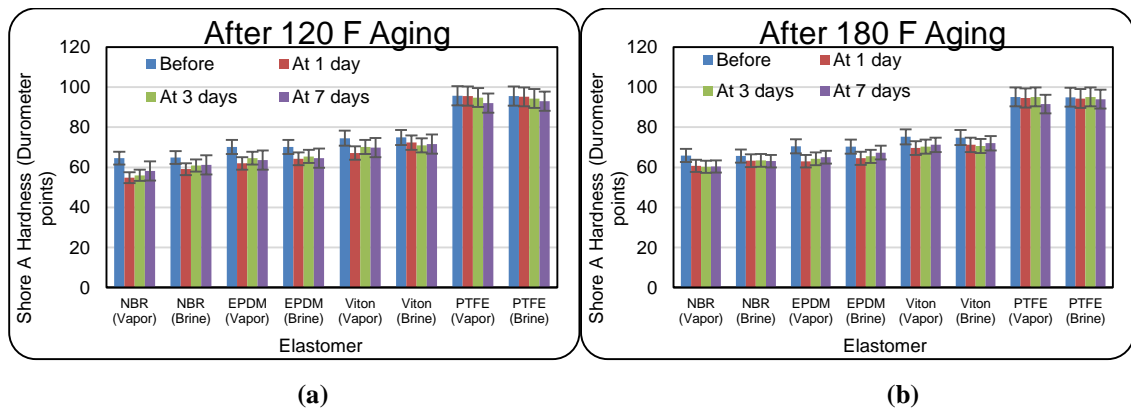


Figure 21: Effects of days on hardness of elastomer samples aged at 1000 psi, and at (a) 120 °F, (b) 180 °F.

Effects of Temperature

Increase in temperature concurrently increases elastomer hardness. The initial exposure of the elastomer to aging conditions (temperature, pressure, and corrosive gas conditions) cause it to soften. Keeping all other conditions in an aging test (1 day or 7 days) constant and altering temperature from 120 °F to 180 °F, results to an increase in hardness. This is due to chain growth or cross-linkage occurring in the elastomer.

Figure 22 (a) shows 1-day aging for 50% CO₂ and 50% H₂S with a CH₄ carrier. A decrease of more than 5% and up to 15% from original hardness is observed. This, however, excludes all PTFE (vapor and brine phase) and all Viton in the brine phase. A slight increase in hardness is observed when shifting from 120 °F to 180 °F. After a 7-day test at the same aging conditions (Figure 22 (b)), a decrease of more than 5% and up to 10% from original hardness is observed. In addition, a slight increase in hardness is observed with an increase in temperature. In the three-day test conducted (Figure 23), results which are like the 1 and 7-day tests were observed. Both Figure 22 and Figure 23 shows that the reduction in elastomer hardness was more severe in the vapor phase (gaseous contaminant) compared to the brine phase (liquid contaminant). This observation is backed by the study carried out by Dajiang et al., (2017).

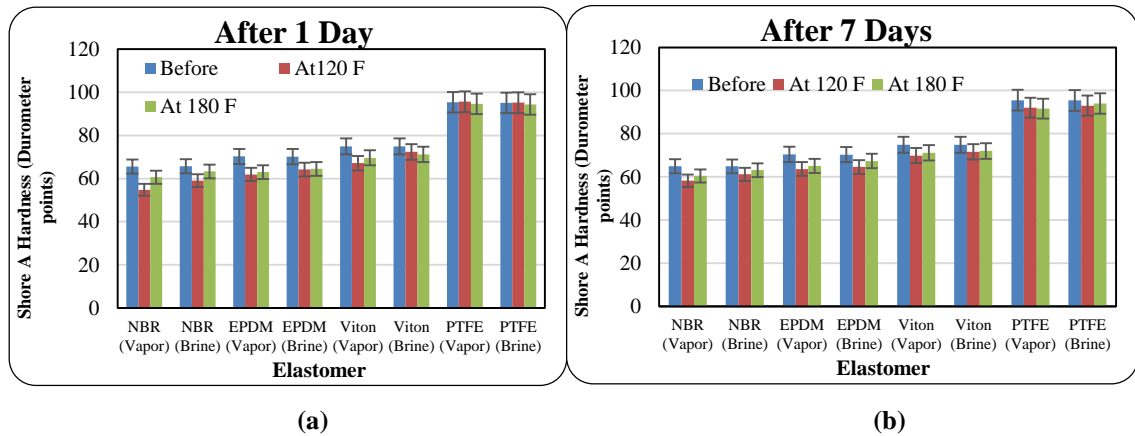


Figure 22: Effects of temperature on hardness of elastomer samples aged at 1000 psi, and after (a) 1 day, (b) 7 days.

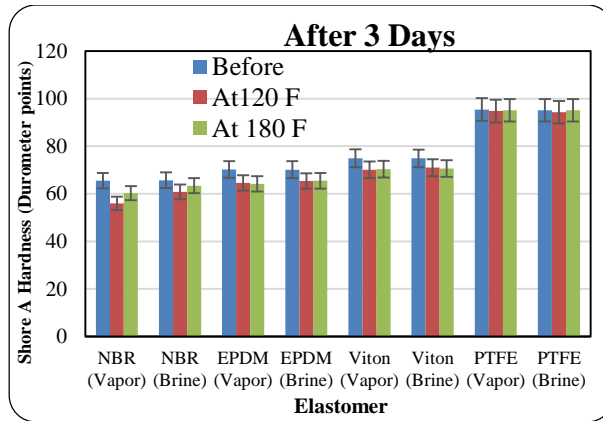


Figure 23: Effects of temperature on hardness of elastomer samples aged at 1000 psi, and after 3 days.

Analysis of Variance (ANOVA) is a statistical tool that was used in analyzing the experimental data. It is a collection of statistical models developed by Ronald Fisher, and used to analyze the variances among group means and their associated procedures. This is done to compare the means between groups, and determine whether any of these means are significantly different from others. Using a 95% confidence interval ANOVA, age, temperature, and fluid medium variation (vapor or brine phase) significantly affect elastomer aging.

However, considering downhole conditions, it is impractical to keep all factors affecting aging constant while varying one at a time. An interaction effect exists when the effect of one factor on the response varies across the levels of another factor. For example, when the effect of days on hardness varies across the various levels of temperature. From the ANOVA, a combination of the effects of days and fluid medium variation presented an insignificant variation for NBR and EPDM. However, there is a significant change in hardness between the Viton in the vapor phase and brine phase, from one to seven days. When fluid medium variation and temperature are combined, the effect was also insignificant for NBR and EPDM. Viton showed a significant change in

hardness with fluid contaminant and temperature interaction. The results showed that the Viton samples immersed in brine had an average drop in hardness of about 3.2 durometer points, while those in the vapor phase dropped by 6.2 durometer points. This implies that the 3.0 durometer points difference is statistically significant. However, Viton does not exhibit a significant change in hardness with aging period and temperature interaction. This is because of its toughness and resistance to temperature. A combination of all three parameters (days, fluid medium variation, and temperature) has an insignificant variation in elastomer aging. It can be inferred that with respect to the hardness of elastomers under corrosive downhole conditions; the time of exposure and the temperature downhole would affect the sealing integrity of the elastomer significantly.

Effects of Gas Variation

For the CO₂ test, 100% CO₂ gas was exposed to the elastomers. For the CH₄ test, 100% CH₄ was exposed to the elastomers. For the H₂S test, 0.05% H₂S in CH₄ carrier was exposed to the elastomers. High bond dissociation energy (410 kJ/mol) and close electronegativity values of carbon and hydrogen in the electronegativity series causes CH₄ to have little to no effect on the aging of elastomers. From Figure 24, CH₄ causes less than 5% decrease from original hardness for all elastomer samples. This decrease is due to physical changes in the elastomer under exposed corrosive conditions. More than 5% and up to 15.6% decrease from original hardness is observed with CO₂. Figure 24 also show H₂S influencing NBR and EPDM. An approximate 5% decrease from original hardness was experienced in NBR and EPDM. However, it is to be noted that a notable change was not seen in the subsequent elastomer samples because the H₂S gas concentration was 500 ppm H₂S with CH₄ carrier. This maps onto 0.05% H₂S in the

presence of CH₄, and CH₄ has little to no reactivity with elastomers. A combined effect of CO₂, H₂S, and CH₄ showed more than 5% and up to 9.6% reduction from original hardness. Finally, for the combined gases test, we have 50% CO₂ and 50% 500 ppm H₂S in CH₄ carrier. In conclusion, gas degradation on elastomers hardness is in the order of CO₂>All gases>H₂S>CH₄.

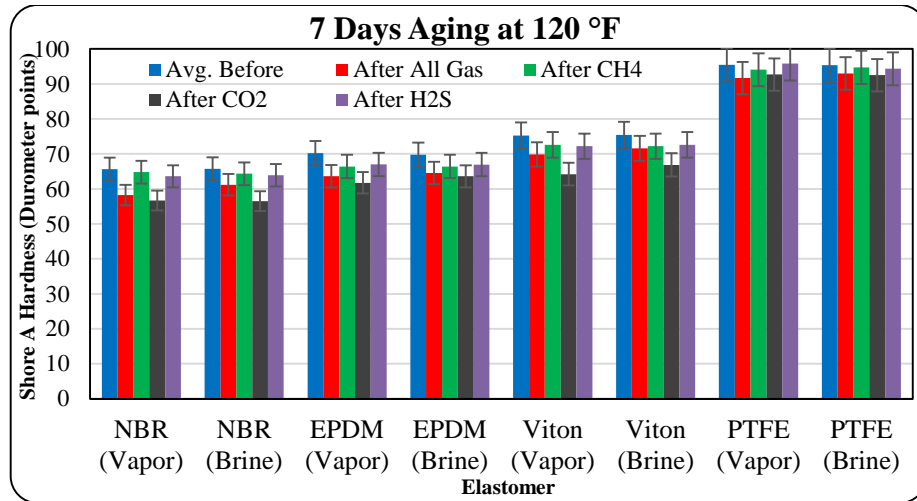


Figure 24: Effects of gas variation on hardness of elastomer samples aged at 1000 psi after 7 days.

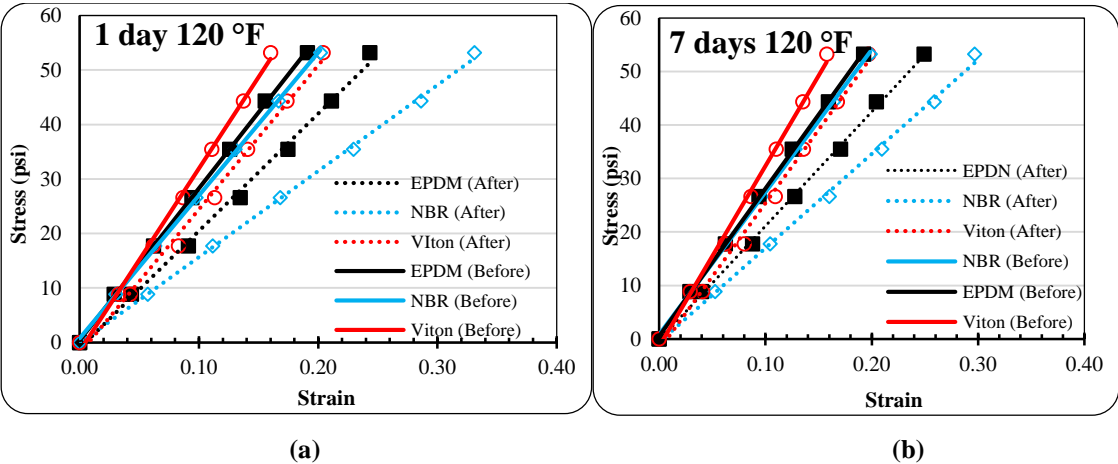
Compression

The compression tests (compressive stress-strain) conducted was to measure the strain of an elastomer at a given compressive stress (psi). “Test Method B - Compression test at Specified Force” in ASTM D575-91 was the compression test procedure followed. Six major forces (15 lbf, 30 lbf, 45 lbf, 60 lbf, 75 lbf, 90 lbf) are applied for three seconds and the deflection on the dial gage recorded. Strain values based on the extension and original thickness of the specimen are calculated, and stress values based on the applied force and areas of the elastomer sample are also calculated. The goal of this is to observe the deformation (strain change) due to aging of the elastomer. This knowledge is important to well sealing integrity because an elastomer in a compressed state under

downhole conditions begins to alter its compression abilities, significantly leading to leakage paths created between the elastomer and the contact surface. This will compromise the sealing integrity of the elastomer thus allowing fluid migration.

Effects of Days

Per Schweitzer P.A., (2000), elastomer chain rupture reverses the effects of cross-linkage or chain growth. This implies that when chain rupture occurs, the elastomer decreases in hardness and tensile strength. Chain rupture also increases elastomer elongation. For the same stress applied on the elastomer before and after aging, Figure 25 (a, b, c, and d) show an increase in strain from original values for each stress. This increase in strain occurs in all elastomers (NBR, EPDM, and FKM) except PTFE. This is because PTFE is a thermoset plastic and thus resistant to heat. PTFE had consistent strain before and after aging, irrespective of the aging conditions (Figure 26). A closer look at the graphs show that 120 °F has the most strain change among the four plots in Figure 25. Comparing Figure 25 (a) with (b) and (c) with (d), it is observed that for the same temperature, an increase in the aging period causes less strain. This is because extended exposure of an elastomer to the same temperature causes chain growth to occur.



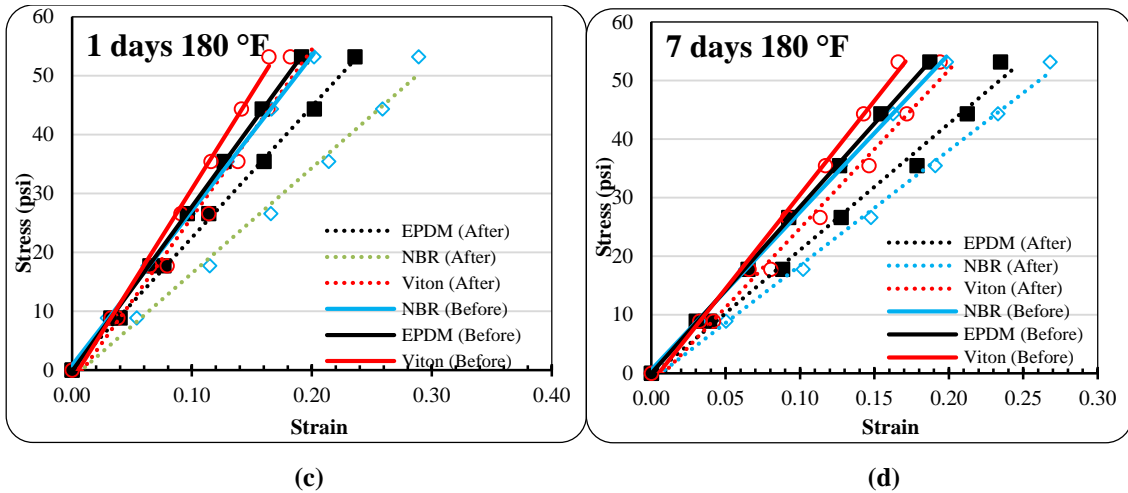


Figure 25: Elastomer compression measurement at: 120 °F (a) after 1 day, (b) after 7 days, and 180 °F (c) 1 day, (d) 7 days.

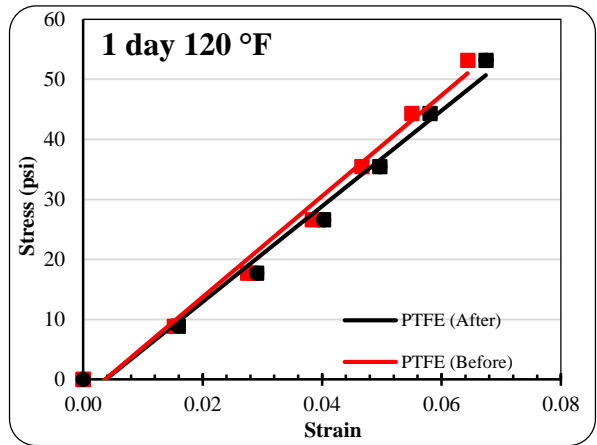


Figure 26: PTFE compression measurement at after 1 day at 120 °F.

Effects of Temperature

Figure 27 shows the results for 3 days aging and the temperature from 120 °F to 180 °F. This rise in temperature cause decrease in strain for the same number of days. These changes are because of chain growth in the elastomer at higher temperatures. Chain growth decreases the elongation of the elastomer, making it stiffer for less strain to occur when it is compressed.

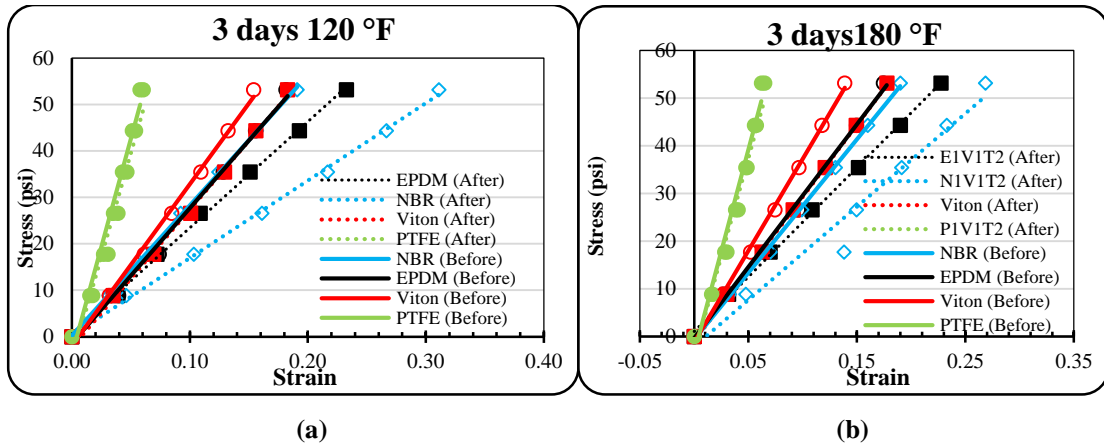


Figure 27: Effects of temperature on compression of elastomer samples after 3 days aging at 1000 psi, and at (a) 120 °F, (b) 180 °F

Compression at maximum stress of 53.2 psi

To understand the effect of aging on the compression of elastomers, the maximum stress (53.2 psi) from the compression machine was selected, and its behavior on each elastomer was investigated. This gave a better understanding of the effect of aging on elastomer sealing integrity.

Effects of Days

At 120 °F, for both one and seven-day tests, there was an increase in strain after aging for a constant 53.2 psi applied stress. This increase was more than 5% and up to 39% from original strain at 53.2 psi (Figure 28) (b)). However, this observation does not include all PTFEs (vapor and brine phases). The initial rise in strain, irrespective of the aging period, is due to an increase in elastomer elongation. Moving from one to seven days, extended exposure of the elastomer samples to corrosive conditions causes chain growth, thereby increasing the hardness of the elastomer and decreasing its strain deviation.

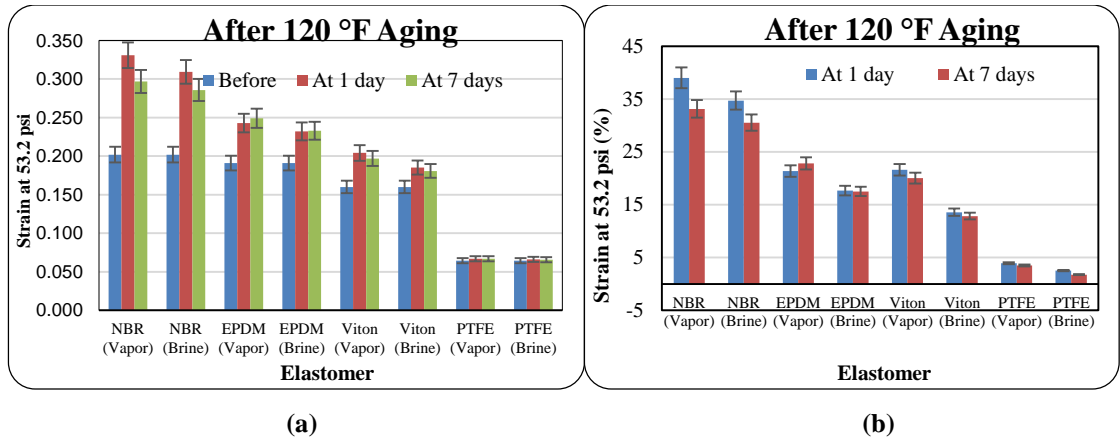


Figure 28: Effects of days on compression of elastomer samples aged at 1000 psi and 120 °F (a) actual strain values, (b) percentage increase in strain values.

Figure 29 shows that at 180 °F, for both one and seven-day tests, there was an increase in strain after aging for a constant 53.2 psi applied stress. This increase was more than 5% and up to 30% from original strain at 53.2 psi, except all PTFEs (vapor and brine phases). This initial rise in compression is due to increase in elastomer elongation. An increase in the number of days, from 1 day to 7 days, causes chain growth. Thereby increasing the hardness of the elastomer and decreasing its strain deviation. The maximum strain increase at 120 °F was 39%, while the maximum strain increase at 180 °F was recorded as 30%. This observation is explained further in the succeeding section.

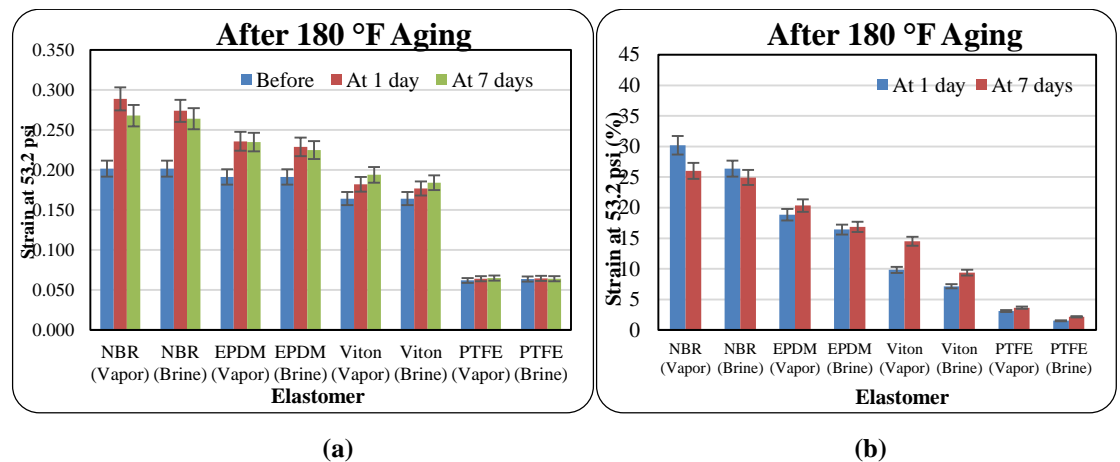


Figure 29: Effects of days on compression (percentage strain) of elastomer samples aged at 1000 psi and 180 °F (a) actual strain values, (b) percentage increase in strain values.

Effects of Temperature

To understand the effects of temperature on elastomer compression, a constant aging period is kept (one or seven days) and the temperature is altered at the selected aging day. After 1 day of aging, aside PTFE in both vapor and brine media, all elastomer samples displayed more than 5% and up to 39% increase from original strain at 53.2 psi. This is shown in Figure 30 (b).

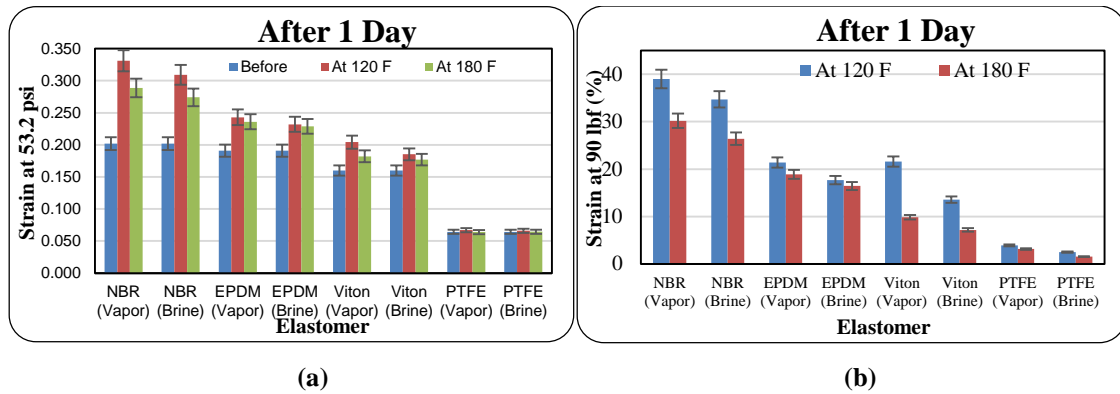


Figure 30: Effects of temperature on compression of elastomer samples aged for 1 day at 1000 psi
(a) actual strain values, (b) percentage increase in strain values.

After 7 days of elastomer aging, all samples except all PTFEs demonstrated more than 5% and up to 33% increase from original strain at 53.2 psi (Figure 31 (b)). From the graphs, it is observed that for both 1 and 7 days, all 180 °F have lower strain increase compared to their 120 °F counterparts. This decrease in percentage strain change at higher temperatures is once again linked to the chain growth that occurs in the elastomers upon exposure to higher temperatures. Irrespective of the length of aging, exposing the elastomer to higher temperatures diminishes its sealing abilities.

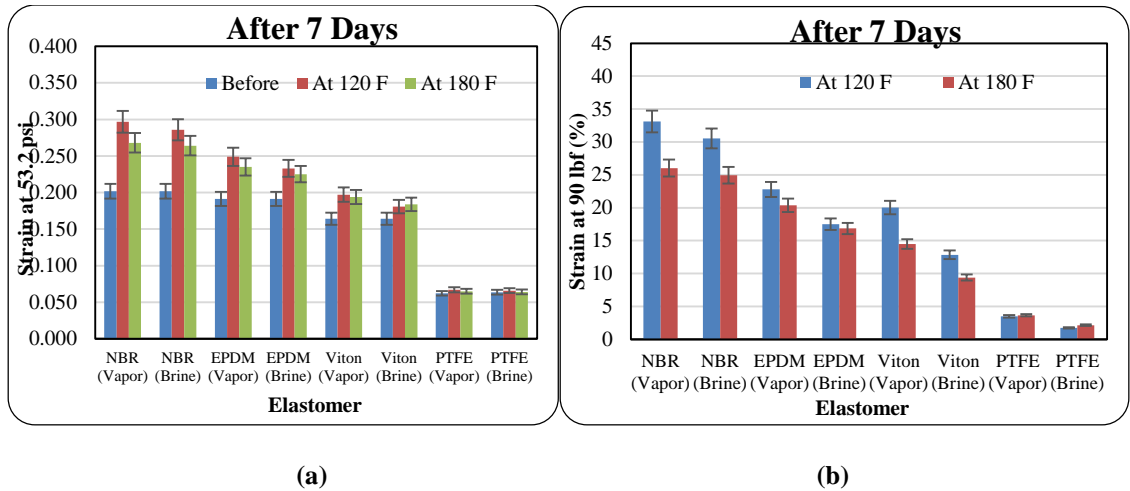


Figure 31: Effects of temperature on compression of elastomer samples aged for 7 days at 1000 psi
(a) actual strain values, (b) percentage increase in strain values.

Using ANOVA with 95% confidence interval, none of the elastomer samples (NBR, EPDM, FKM, and PTFE) showed significant changes shifting from one temperature to another or from one aging medium to another. Considering all three parameters (days, fluid medium variation, and temperature), compression of elastomers is insignificant with a change in any of these parameters. This implies that aging an elastomer for 1 day and for 7 days does not show any significant change. Neither a change in temperature from 120 °F to 180 °F nor a shift from the vapor to the brine phase significantly affects the compression of an elastomer. ANOVA also proves that a combined effect of the mentioned parameters does not affect elastomer compression significantly. With the forgoing, exposing an elastomer to the least corrosive condition (1 day in vapor phase at 120 °F) is enough to cause its sealing integrity to be compromised appreciably. Changing any of these aging conditions afterward is redundant since the elastomer has already been damaged.

Effects of Gas Variation

Compression changes in the elastomers due to gas attack are shown in Figure 32. Figure 32 (a) shows the actual increase in strain values for each elastomer after aging under a particular gas condition, while Figure 32 (b) shows the percentage increase in strain for each elastomer under a particular gas condition. For CH₄, we observed more than 5% and up to 13.8% increase from original strain at 53.2 psi, except for PTFE (vapor and brine). For CO₂, we observed more than 5% and up to 36.3% increase from original strain at 53.2 psi, while an increase of 5% to 17.7% in strain at 53.2 psi was recorded for H₂S. A combination of all gases revealed more than 5% increase but not more than 33.1% increase from original strain at 53.2 psi. This observation excludes all PTFE. As observed in the effect of gas variation on hardness, the order of elastomer degradation with respect to corrosive gases is in order of CO₂>All gases>H₂S>CH₄.

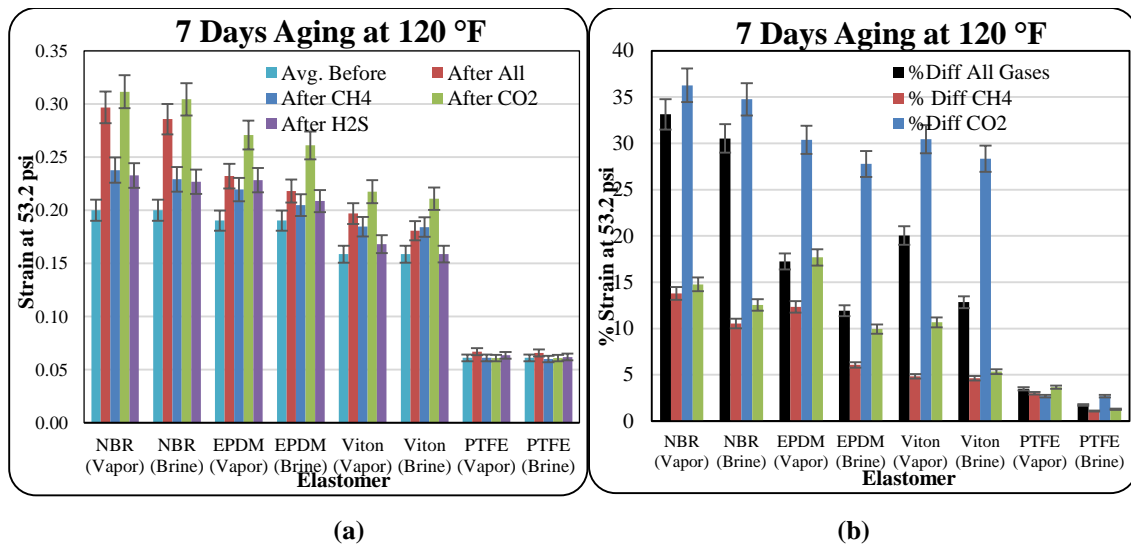


Figure 32: Effects of gas variations on compression of elastomer samples aged at 1000 psi and 120 °F (a) compression measurement (b) percentage difference in compression measurements.

Volumetric Swelling

Volumetric swelling is the volume increase of an elastomer. The volume of the elastomer is calculated before and after aging. The change in these two values is the volumetric swelling. To calculate the volume before aging, one diameter measurement is taken for each elastomer sample along with its length. Using the volumetric calculations, the volume of the elastomer sample is calculated. To calculate the volume after aging, three diameter readings are taken. One at the point of maximum swelling, this is usually the midpoint of the elastomer sample. The other two are taken at the edges of the sample. The average of these three diameter readings and its new length are used to calculate the new volume of the elastomer.

Effects of Days

Figure 33 (a) and (b) shows volumetric swelling at 120 °F. Figure 34 (a) and (b) also show volumetric swelling at 180 °F. These two graphs show a general increase in volumetric swelling after 1 day, a peak in swelling after 3 days of aging, and a gradual decline in swelling after a week of aging. Per Schweitzer P.A., (2000), “some elastomers will continue to harden, and some soften, and some will show an initial hardening followed by softening.” In the volumetric test with the exception of PTFE, the various elastomer samples first softened, reached a maximum point of softening then began to harden. Figure 33 (b) show more than 5% and up to 59% increase from original volume except all PTFEs and 1-day Viton (brine phase). At 180 °F, we see more than 5% and up to 43% increase from original volume except all PTFEs and all Viton (Brine). These changes in elastomeric properties are due to initial chain rupture in the elastomer followed by chain growth within the elastomer. Chain rupture increases the elastomers size (swelling) while chain growth causes the elastomer to shrink.

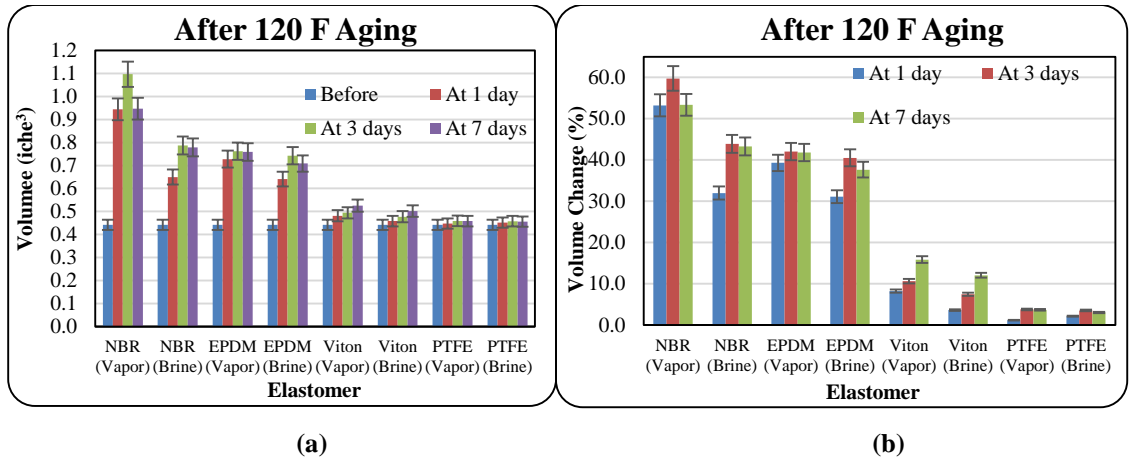


Figure 33: Effects of days on volumetric swelling of elastomer samples aged at 120 °F and 1000 psi, (a) compression measurement (b) percentage difference in compression measurements.

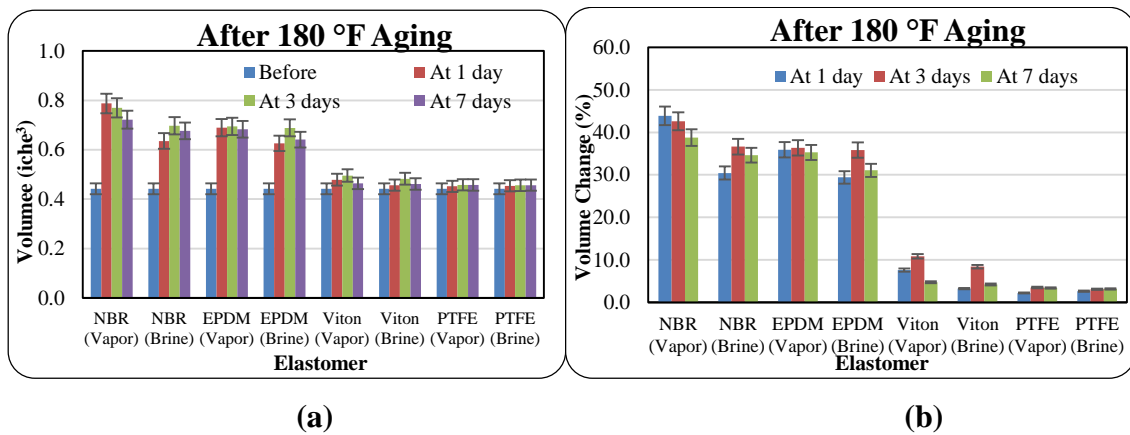


Figure 34: Effects of days on volumetric swelling of elastomer samples aged at 180 °F and 1000 psi, (a) compression measurement (b) percentage difference in compression measurements.

Effects of Temperature

Based on visual observation and measurements shown in Figure 35 (a) and (b), NBR in the vapor phase appears to have shown maximum swelling amongst its counterparts (EPDM and Viton). This observation is made at both 120 °F and 180 °F. For all elastomer samples, the swelling was more predominant in elastomers exposed to the vapor phase compared to those exposed to the brine phase. For example, the NBR samples in Figure

35 (a) clearly shows more swelling at the ends of the elastomer in the vapor phase, compared to NBR exposed to brine. An increase in temperature presents a decrease in swelling. All three samples showed a decrease in swelling from 120 °F and 180 °F. Viton, however, at higher temperatures does not only experience swelling but also blistering.

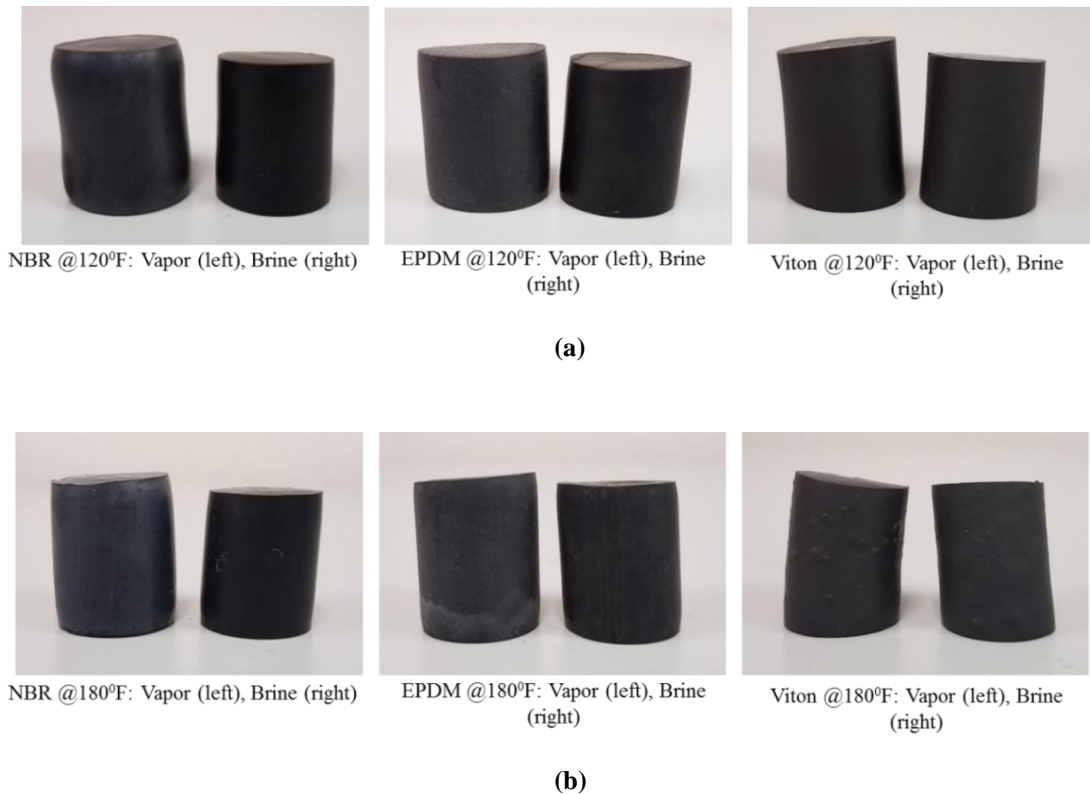


Figure 35: 1 Day aging in CO₂ and H₂S with CH₄ carrier at 1000 psi. (a) 120 °F and (b) 180 °F.

Blisters refer to bubbled or raised defects occurring on the surface of an elastomer which is caused by trapped gases on the elastomer surface. Blistering causes delamination and breakage of the elastomer-lining layer, resulting in a loss of its corrosive protection (Van Dinh and Kubouchi, 2012). Viton's poor decompression resistance causes this blistering at high temperatures. Test samples showed that blistering occurred in one, three, and seven-day tests, and was consistent for only 180 °F. Figure 36 shows visual observations of blistering on the FKM elastomer surface. All images were taken with a

Dino-Lite Digital Microscope. Keeping aging period constant and varying temperature from 120 °F to 180 °F, there is a decrease in volumetric swelling for all elastomer samples. This is because elastomers undergo cross-linkage at elevated temperatures, thus decreasing their elongation.

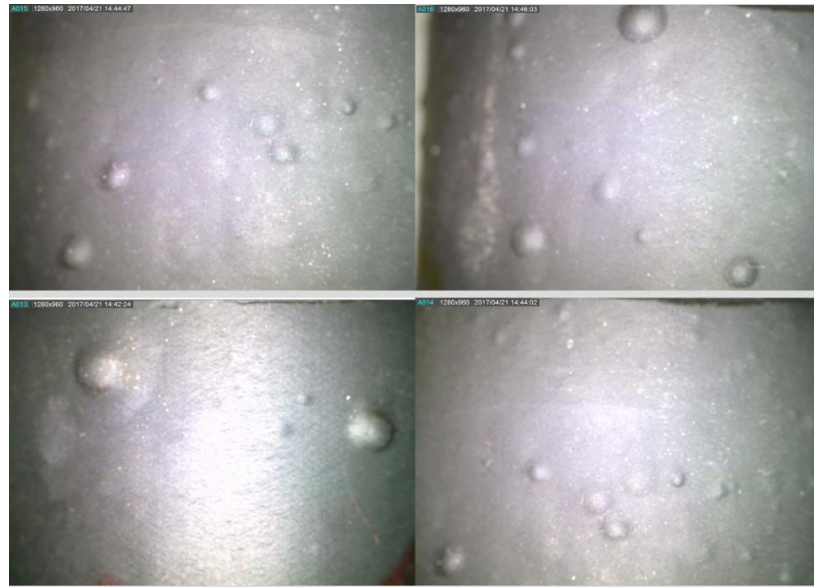


Figure 36: Viton Blistering taken with a Dino-Lite Digital Microscope.

Figure 37 shows the plots of percentage volumetric increase after one, three, and seven days of aging. These aging tests were conducted at 1000 psi and at two temperatures 120 °F and 180 °F. All tests were conducted with 50% CO₂ and 50% 500 ppm H₂S with CH₄ carrier. After 1 day of testing, volumetric swelling of more than 5% and up to 53% increase from original values were recorded. After 7 days, the volumetric swelling was also between 5% and 53% increase from the original volume. These observations exclude PTFE in both vapor and brine phase. Three-day aging tests show the highest recorded volumetric swelling readings - more than 5% and up to 59.7% volumetric swelling. Using these numbers, Figure 37 suggests that irrespective of the aging period and elastomer type

(except PTFE), increase in temperature decreases volumetric swelling, regardless of the aging period.

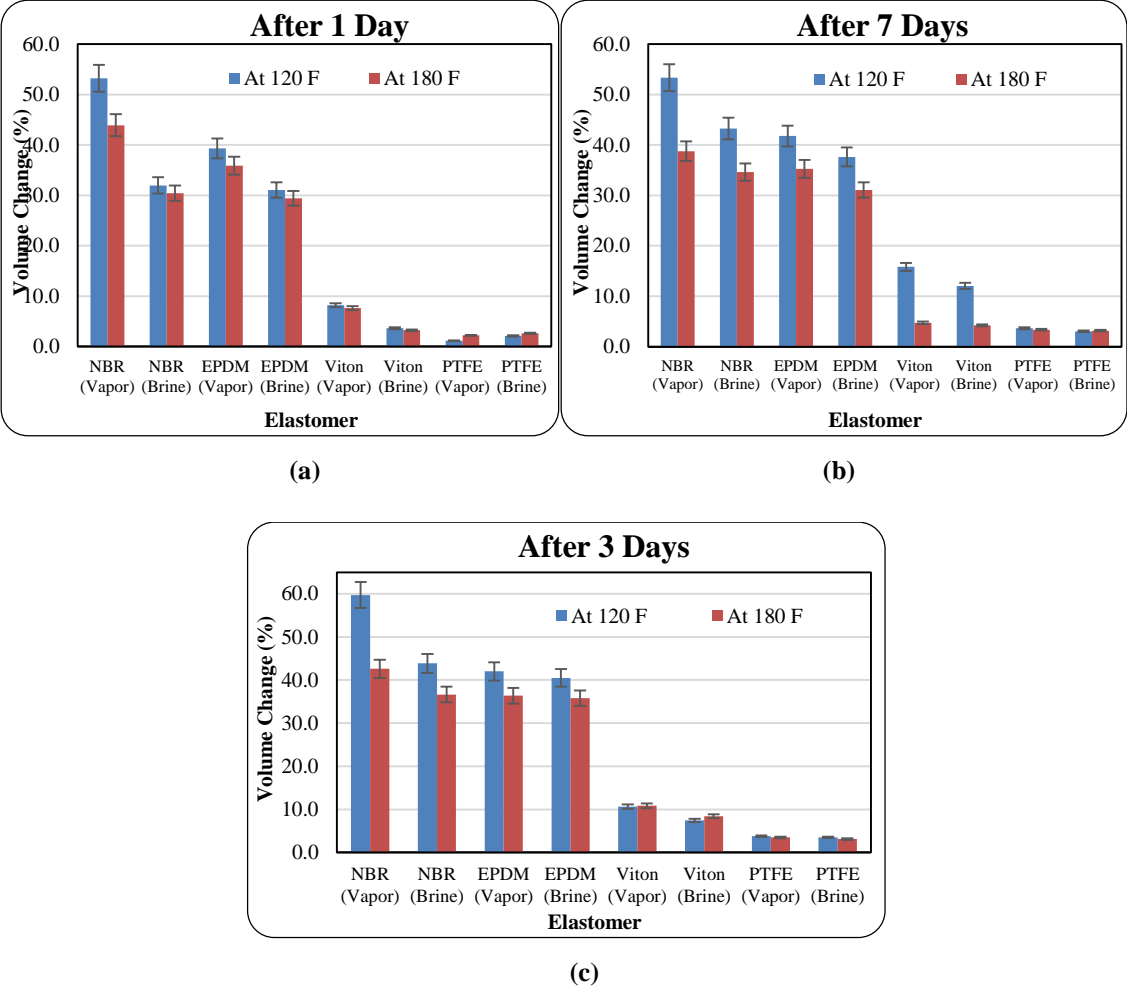


Figure 37: Effects of temperature on percentage volumetric change in elastomer samples aged at 1000 psi, after (a) 1 day (b) 7 days (c) 3 days.

ANOVA results show that volumetric swelling of elastomer samples is not significant with changes in temperature, aging period, or the aging medium. Varying one parameter in the aging test while keeping all others constant, gives an insignificant effect. However, this is impractical given that multiple aging parameters can change simultaneously in real-time downhole conditions. ANOVA results show that the

interaction effect for volumetric swelling was still insignificant. With these results, it can be cautiously concluded that exposing an elastomer to the least corrosive condition (1 day in the vapor phase at 120 °F) is enough to cause its sealing integrity to be compromised. After which, a change in aging conditions is once again considered redundant since the elastomer has already been damaged appreciably.

Effects of Gas Variation

Figure 38 compares the effects of gas variation on volumetric swelling of elastomers. The least effect of volumetric swelling was experienced with CH₄. The chemistry of methane (high bond dissociation energies and close electronegativity) explains its stability and less reactivity. Thus, it is less likely to react with any elastomer sample. Aging in the presence of 100% methane shows volumetric swelling of more than 5% and up to 32.6% from original values. This swelling is mainly because of physical changes of the elastomer rather than a chemical reaction. H₂S caused 5% to 34.2% increase in volume after aging the elastomer. From Figure 38 (b), aging in 100% CO₂ shows more than 5% and up to 53.2% volumetric increase in all elastomers except for some PTFE. PTFE aged in 100% CO₂ had an average swelling of 5.3%. For combined gases, elastomers experienced more than 5% and up to 53.3% increase from the original volume. It is difficult to put all gases in order of corrosion for volumetric swelling. This is because 100% CO₂ showed a more detrimental effect on EPDM compared to NBR, while a combination of CO₂, H₂S, and CH₄ had a more detrimental effect on NBR compared to EPDM. However, CH₄ had the least effect on elastomer volumetric swelling.

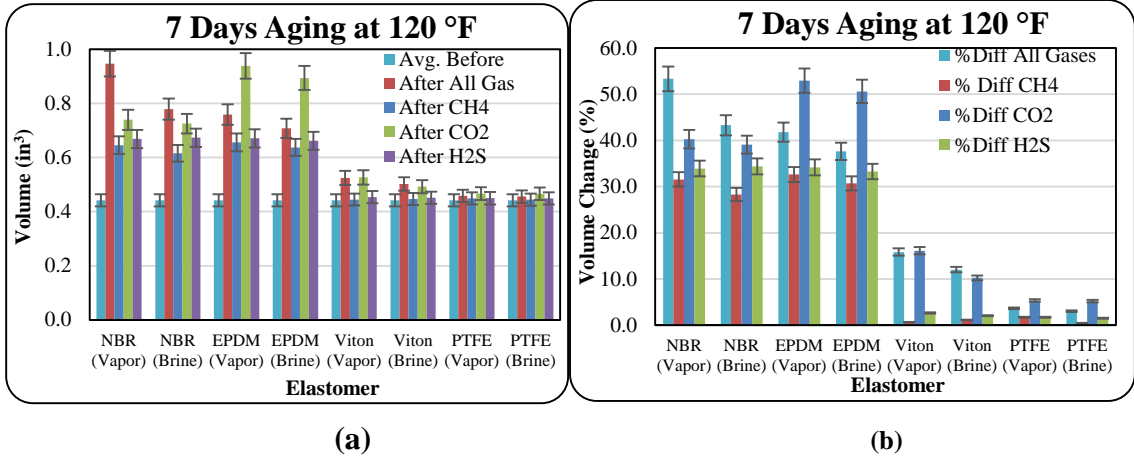


Figure 38: Effects of gas variation on percentage volume measurements of elastomer samples aged at 1000 psi and after 7 days (a) volume measurement (b) percentage volumetric change.

Chapter 4: Cement Experiment and Results

The school of thought as to cement being a primary barrier is still uncertain. In addition, the possible failure of a neat cement to mitigate formation fluid migration makes it imperative to develop a cement slurry that would be able to mitigate flow of formation fluid. Thus, the objectives of this study include:

- Evaluate the cement system integrity as a primary barrier.
- Study the effects of gas migration additives in cement slurry performance.
- Develop a gas tight cement slurry that to mitigate flow of formation fluid.
- Report properties of new cement slurry design.

Research Methodology

In an effort to achieve the aforementioned objectives, both theoretical and experimental approaches have been considered in this study. An extensive literature review has been conducted to assess readily available information on cement properties, slurry designs and additives that can be added to make cement slurries gas tight. The outcomes of reviews and theoretical analysis provided useful information in comprehending the inadequacy of set cement to prevent migration of formation fluids, mainly gas.

Sealability of cement strongly depends on the cement to casing bonds and available pores within the cement. In this study, different slurry designs have been investigated, adding additives like latex, microsilica, and bentonite. We have examined key properties of cement with respect to controlling gas migration, mechanisms for wellbore integrity failure, and the relationship between cement design and its integrity.

In addition to the theoretical analysis, experimental investigations have been conducted to study the behavior of neat oil well cements and oil well cements with

varying percentages of additives. We have successfully designed a physical slurry mixture that has proven to be gas tight. The gas tight cement slurry has the following formulation; Class H, 1.5 liters / 100 kg commercial additive. The formulation was rigorously tested to evaluate the slurry's performance.

Scope of Work

Cement degradation is very sensitive to downhole conditions (temperature, pressure and acid gas concentration) (Ahmed, 2015). However, all experiments aside consistency and rheology were conducted at atmospheric pressure and temperature. This was because experiments were conducted on a large scale and a change in temperature was a daunting task. Pressure was varied from 40 psi to 60 psi using nitrogen gas. Wait on cement (WOC) was varied from 12 to 24 hours and hydraulic ballooning was performed for pressure ranging from 1000 to 2000 psi. Class H cement was considered for the investigate in two phases. One phase involved neat Class H cement while the later phase of the experiments concentrated on Class H cement with additives included.

To quantify the level of improvement, various properties (leakage time, and declining pressures) of set cement were measured and compared. In addition, 1 and 3-day compressive strength tests were conducted to verify the suitability of the new cement mixture. The length of cement column prepared to carry out experiments - cylindrical setups of height 3 feet. A 6 feet was also tested on but for this thesis the pressure data was focused on to give an insight to role cement column height plays in the setup. For the same cement column length, various diameters were experimented on to observe the effect of size.

To develop a gas tight cement formulation, different cement additives were considered in the investigation including, bentonite, latex, microsilica and nanomaterials. Cement slurries with varied formulations of these additives were prepared and tested for their consistency, rheology, density, and sealing ability. Slurries with unacceptable properties were discarded and slurries with acceptable properties (slurries comparable to neat Class H) were cured and tested. The set cement property (compressive strength) was measured and compared to corresponding baseline slurry samples. The final gas tight formulation proved to have comparable mechanical and physical properties to baseline cement, and could seal the annular space to prevent gas migration.

Experimental Investigations

Four major tests and eleven minor tests have been conducted. Seven of these eleven tests contain additives while the other four are neat Class H cement with varying vibration and WOC times. Three test matrices and parameters (Table 11, Table 12 and Table 13) have been established to examine the effect of WOC, additives and vibration on the sealability and setting of cement. There are four independent variables in major tests and three independent variables minor tests. For major tests, the independent variables are: 1) Formulation of cement slurry, 2) Height of cement column, 3) Type of gas injected, 4) Period of gas injection. For minor tests, independent variables include: 1) Formulation of cement slurry, 2) Type of gas injected, 3) Period of gas injection. For each category of tests, leakage time and pressure data were recorded and compared to assess the effect of a changed parameter or the performance of the new formulation.

Table 11: Test matrix 1 and parameters – Studying the effect of WOC and additives on 3ft experiments

Setup 1 -	WOC (hr)	Vibration (mins)	Height (ft)	Additives		Density (ppg)
				Latex (gal/sack)	Bentonite (%)	
Experiment 1	24	15	3	N/A	N/A	16.65
Experiment 2	12	15	3	N/A	N/A	16.65
Experiment 3	24	15	3	3	1	12.5
Experiment 5	24	25	3	Neat Class G		16.65

Table 12: Test matrix 2 and parameters – Studying the effect of additives on 6ft experiments

Setup 1 -	WOC (hr)	Vibration (mins)	Height (ft)	Additives		Density (ppg)
				Latex (gal/sack)	Bentonite (%)	
Experiment 4	24	20	6	N/A	N/A	16.65

For this thesis, only the pressure data of Setup 1 Experiment 4 was analyzed.

Table 13. Test matrix 3 and parameters – Studying the effect of vibration and additives on 3ft experiments.											
Small Setup 1-	WOC (hr)	Vibration (mins)	Material	Height (ft)	Diameter (in.)	Additives					Density (ppg)
						Microsilica (%)	Latex (gal/sack)	Bentonite (%)	Fly ash (%)	Nanomaterial	
Experiment 1	24	12	Steel	3	1	N/A	N/A	N/A	N/A	N/A	16.65
Experiment 2	24	12	Steel	3	2	N/A	N/A	N/A	N/A	N/A	16.65
Experiment 3	24	60	Steel	3	2	N/A	1	0.5	N/A	N/A	16.65
Experiment 4	24	0	Plastic	3	2	N/A	N/A	N/A	N/A	N/A	17.5
Experiment 5	24	120	Steel	3	2	N/A	N/A	N/A	N/A	N/A	17.5
Experiment 6	24	20	Steel	3	2	N/A	1	N/A	30	N/A	14
Experiment 7	24	25	Steel	3	2	5.5	N/A	N/A	N/A	N/A	16.05
Experiment 8	24	25	Steel	3	2	12	N/A	N/A	N/A	N/A	N/A
Experiment 9	24	30	Steel	3	2	N/A	N/A	N/A	N/A	0.5	16.55
Experiment 11	24	25	Steel	3	2	N/A	1	N/A	30	0.5	14.5
Experiment 12	24	25	Steel	3	2	1.5 liters/ 100 kg commercial additive					16.4

Test Materials

In the preparation of baseline cement slurries, standard API cement-water mixing procedures were followed. All dry materials were weighed and mixed thoroughly prior to adding them to the mix fluid. Where latex and other liquid additives were included, the required mass of water and liquid additives were placed in the blender. The motor was turned on to rotate at 4000 rpm for 10 seconds to create a homogenous mixture and then shut down. To add the cement, the mixer is turned on to 4000 rpm, and the cement powder was added to the mix fluid at a uniform rate in not more than 15 secs. In cases where bentonite and other dry additives were included, all dry additives were added to the cement powder and mixed gently into a homogenous mixture before pouring into the mix fluid as stated earlier. After the addition of the dry materials to the mix fluid, the lid of the mixer is put in place and the mixing continues at 12000 rpm for 35 secs.

Accordingly, cement slurries containing cement, water, microsilica, and bentonite were prepared. A brief description of the materials used in the cementing experiment and their specific roles are presented in this section.

Water

For the cement hydration, water is required. Class H cement was used for all experiments and as such a 38% water requirement by weight of cement was used. This was in accordance to API 10A. Distilled water was used for mixing to control contamination and reduce the degree of uncertainty in tests conducted. It is to be noted that with the addition of bentonite and some other solid additives, the total water requirement was increased accordingly.

Bentonite

Bentonite was used in cement slurry preparation to reduce the fluid loss from the cement. With the addition of bentonite, extra mixed water is required since bentonite can absorb water and swell. This decreases the overall density of the slurry and reduces the amount of free water. As a rule, for each 1% added bentonite, mix water should be increased by 5.3%.

Silica and Microsilica

Multiple literature (Lea 1971; Eilers et al., 1983; Grabowski and Gillott 1989) documented that ratio of CaO/SiO_2 (C/S) was crucial to compressive strength. For a C/S ratio greater than 1, the cement developed low compressive strength because of the formation of di-calcium silicate hydrate. However, a lower C/S ratio leads to the formation of tobermorite gel which has low porosity and permeability. With this low C/S ratio a high compressive strength is attained. 30% BWOC silica should thus added to keep the C/S ratio below 1. An addition of silica is followed with an addition of an adequate amount of water. The water requirement is 38.5% (by the weight of the silica).

Microsilica has a particle size range of 0.02 to 0.5 μm , with an average of 0.15 μm . The fine particle size of microsilica allows packing between the cement grains resulting in an improved microstructure of the cement matrix. However, microsilica comes in two major forms – undensified and densified microsilica. Undensified microsilica has bulk density typically 200 – 350 kg/m^3 while densified microsilica has a bulk density typically 500 – 700 kg/m^3 . The microsilica used for Experiments is Silica Fume White and had a bulk density of 400 kg/m^3 . An addition of microsilica into cement without the addition of a water reducer required and addition of a water requirement. The

water requirement ranged from 5% to 12% BWOC based on published articles. However, for these experiments the white silica fume used had manufacturer's requirements of 5% to 20% BWOC replacement.

Gas

To pressurize the base of the cement and cause gas to migrate through the pore in the cement, Nitrogen gas (N_2) is used. N_2 was selected because though not perfectly inert, the triple bond existing makes it difficult to react with any substance until some conditions are met. For our experiments, N_2 would not react with the cement to form any products. It's availability and low cost made it ideal for experiments.

Latex

Latexes are aqueous dispersions of polymer particles such as surfactants which impart stability to dispersion. The mechanism of latex in cementing can be described as an acting impermeable polymer barrier when hit by gas. Latex fills the pores in the cement and reduces the permeability of the cement. The latex used for experiments is Latex Thin Set Mortar Additive. This product comes in liquid form and thus no water requirement is needed.

Fly ash

Fly ash consists of silt-sized particles which are generally spherical, typically ranging in size between 10 μm and 100 μm . Fly ash usually classified as Class C or F consists primarily of silicon oxides, aluminum iron and calcium. They also contain magnesium, potassium, sodium, titanium, and sulfur but to a lesser degree. This small particle size distribution of fly ash and its unique spherical shape makes it a good mineral filler. Fly ash in the presence of water, react with calcium hydroxide at ordinary temperatures to

produce cementitious compounds. A water requirement of 3.6 gal/ 74 lbm is used for the Fly ash.

With the addition of these various test materials – especially additives – the particle size distribution of the solids changes from one slurry design to another. With the use of a Mastersizer 2000 - a laser diffraction particle size analyzer, the particle size distribution of some samples used were measured. Figure 39 shows the particle size distribution of neat Class H, neat Class G, and other slurry designs that are used in this study.

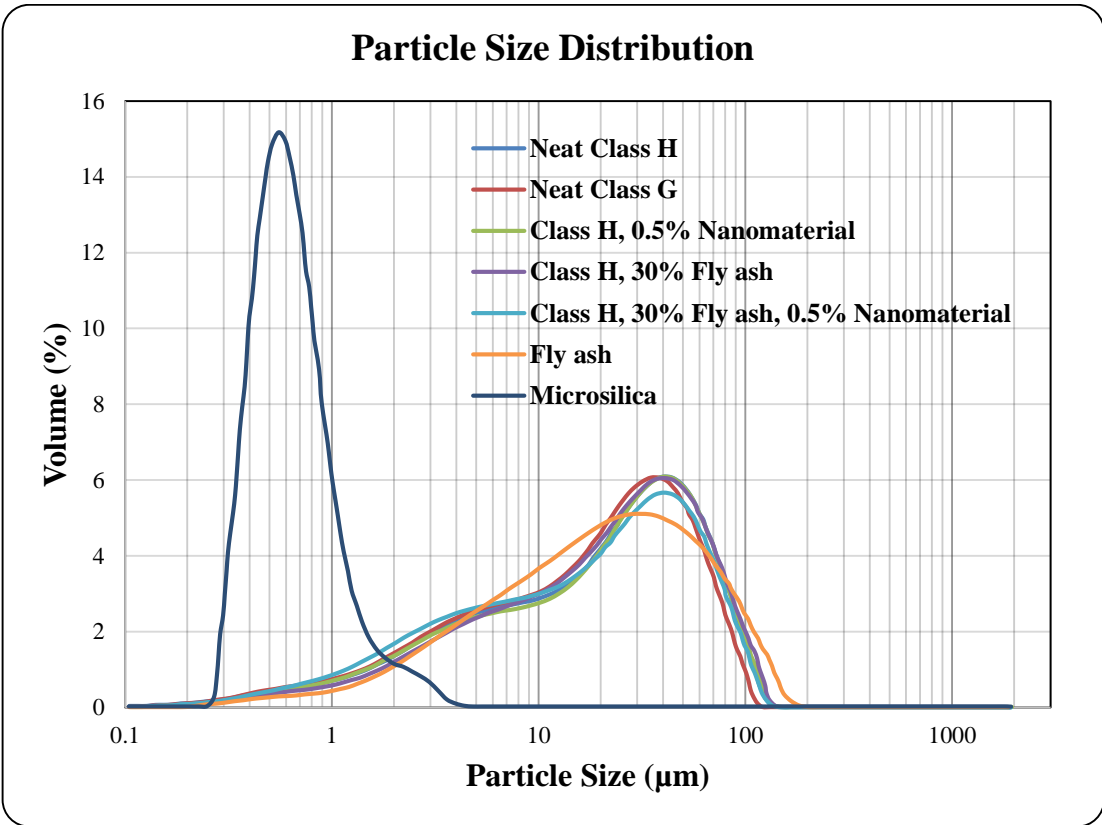


Figure 39: Particle Size Distribution of various samples with Mastersizer 2000.

Cement Slurry Preparation Procedure

Slurry Formulations

This section deals with the mixing procedure, the properties of the mixed slurries, and the test sample preparation procedure. These measures were put in place to ensure consistency in all mixed slurries for experiments. This consistency provides confidence in analyzed data since the slurry formulations were under controlled measures.

Slurry Properties

Following the preparation of cement slurries, vital properties such as density, rheology, static gel strength (SGS) and thickening time were to be measured. The properties of a baseline slurry are presented in Table 14. Since one of the objectives of this study was to investigate the effect of a gas tight cement additive, the physical properties of the new slurry were closely matched to the base slurry.

Table 14: Properties of baseline and gas tight slurries.

Property	Class H base slurry	Class H, 1.5 liters / 100 kg of commercial additive
Density	16.65 ppg	16.40 ppg
Rheological properties (102° F)	Power Law fluid $n = 0.59$ $K = 2.09 \text{ lbf}\cdot\text{s}^n/100\text{ft}^2$	Power law fluid $n = 0.47$ $K = 3.87 \text{ lbf}\cdot\text{s}^n/100\text{ft}^2$
Gas Transit time	1.26 hrs	0.30 hrs
Thickening time	170 mins.	232 mins.

Density: The slurry density was measured with a standard atmospheric mud balance used in the oilfield. As density affects the performance of cement, the additive slurry was formulated to have a density close to the class H base slurry.

Rheology: Following API standards, A Grace viscometer was used to measure the rheological properties of the slurries to verify satisfactory flowability. Table 15 presents the rheological properties of Class H baseline slurry.

Table 15: Rheology of Class H base slurry and gas tight slurry.

	Neat Class H	Class H, 1.5 liters/100 kg commercial additive
Shear Rate (1/s)	Shear Stress (Pa)	
1021.3809	161.32	105.66
510.9969	82.32	70.56
340.6986	53.64	55.84
170.2982	38.64	42.32
10.2138	7.98	12.98
5.1069	6.14	7.64

Gas Transit Time: Cement static gel strength was measured in the lab with a Grace M750 Consitometer. Figure 40 shows the time it takes for the cement slurry to moves from 100 lbf/100 ft² to 500 lbf/100 ft²; this signifies the cement gas transit time. This is discussed more in the section “gas transit time”.

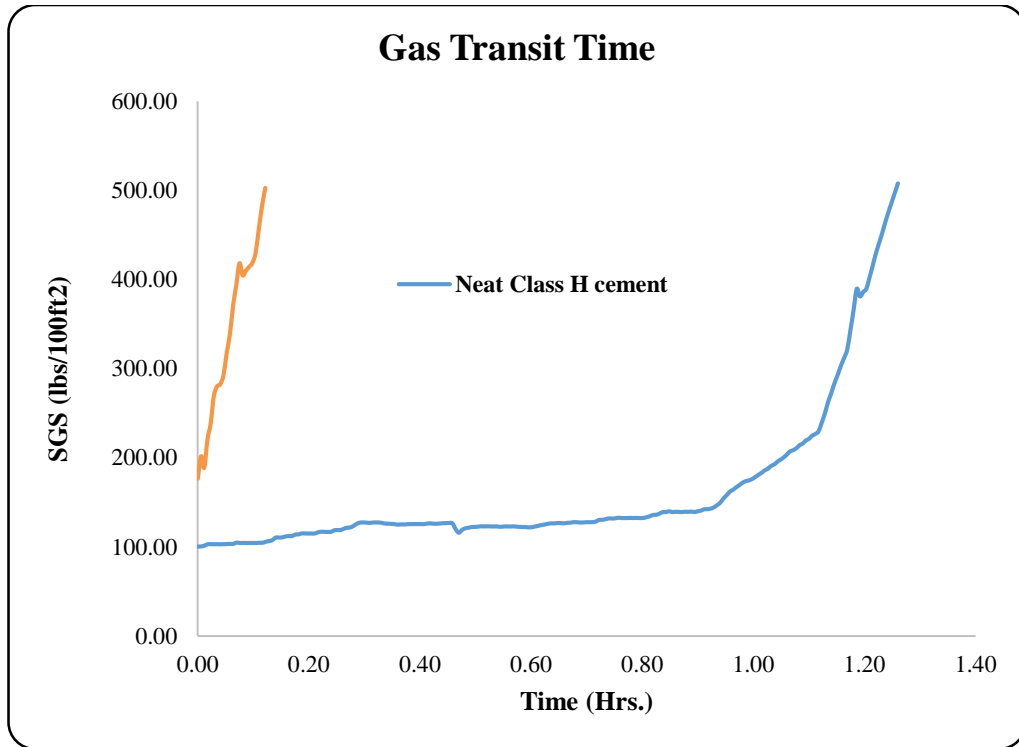


Figure 40: Gas Transit time for Class H base slurry and gas tight slurry.

Thickening Time: It is the time it takes for the cement slurry to attain a predetermined consistency at a given temperature and pressure. It is measured in Bearden units of consistency (Bc), and the end of thickening time is considered to be 50 Bc, 70 Bc or 100 Bc. Thickening time was measured in the lab with a Grace M750 Consistometer. Figure 41 shows the thickening time (time to reach 70 Bc) of the base slurry.

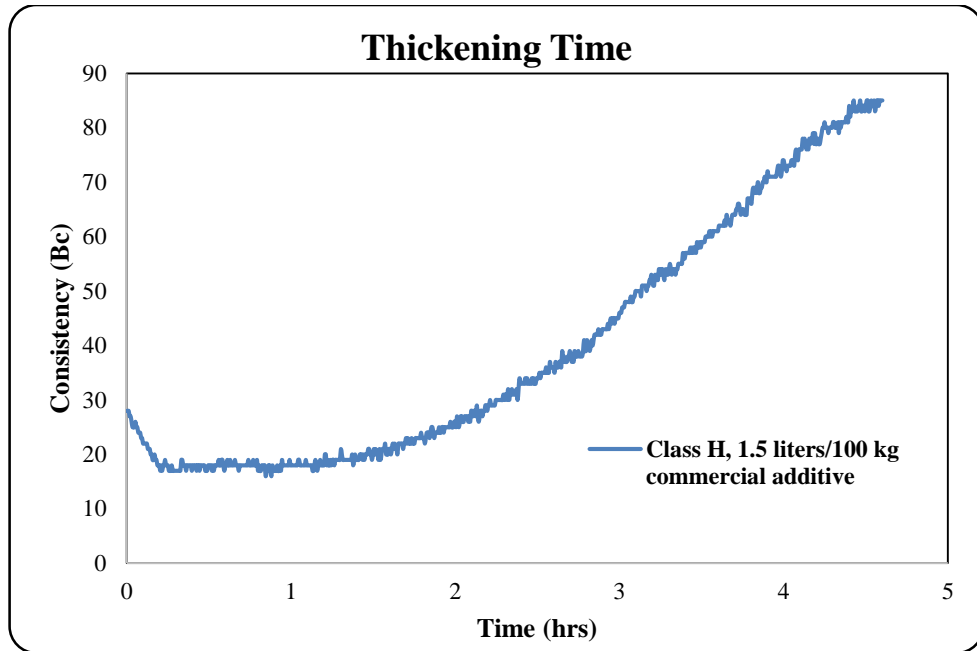


Figure 41: Thickening time for gas tight slurry base slurry.

Cement Gas Migration Experiment

Experimental Setup

Major Test Experimental Setup

To evaluate the cement system integrity as a primary barrier and also simulate gas migration through the liner-casing overlapping length, a test setup was developed. The schematic of the setup is shown in Figure 42. The setup consists of five components. The first component is the liner-casing overlap – represented by an existing annulus between an inner pipe of 4.25" outer diameter (OD) and an outer pipe of 6.5" OD. The second component is the N₂ gas cylinder with a pressure well over 10 times what is needed for each experiment. The third component is the hand pump which is used to balloon the inner pipe to desired pressure of 1000 psi, 1500 psi, and 2000 psi. Component 4 consists of installed cameras, a network video recorder, and a television. These combined are used to observe and record the gas migration that occurs of the surface of the cement sheath.

Recordings are backed up so that they can be viewed whenever necessary to understand what goes on in the cement column. Finally, a data acquisition (DAQ) system and four or six pressure sensors are installed in the setup depending on the length of the pipe being experimented upon. That is to say, when dealing with pipes 3 feet in length – 4 pressure sensors are installed. In 6 feet setup, 6 pressure sensors are installed. For each setup, these number of sensors were selected because they were enough to produce data that can be studied to give a scientific explanation of gas migration in the cement sheath. The pressure sensors used have an error of -0.1%. Figure 77 shows how the pressure sensors were connected to the DAQ system. The DAQ system takes the pressure reading from the setup in an interval of 0.05 seconds, these readings are then stored by the Dasy lab software. Each pressure reading is recorded independent of other sensors; thus, all pressure sensors are recorded simultaneously. The pressure sensors are installed from the bottom of the setup to the top beginning from Sensor 0. Sensor 0 is the first installed sensor which records the gas injection into the setup. It is placed 1" above the threads of the outer pipe as discussed earlier under "Test Equipment and Setup Protocol". Sensors 1 and 3 are placed on the other side of the pipe (directly opposite Sensor 0), each 2" away from the pipe threads. The last sensor - Sensor 2 - is placed in the middle of sensors 1 and 3. This makes sensor 2 to be installed directly in the middle of the pipe. In 6 feet pipes the same procedure is followed, however, 2 extra sensors are placed in the existing gap between sensors 1 and 3 and sensors 3 and 5. Gas injection begins by opening the valve between the injection cylinder and gas migration setup. Gas is injected into the setup in a for a period (usually 30 minutes) depending on the aim of the experiment.



Figure 42: Schematic for gas migration setup (major test)

Minor Test Experimental Setup

In the minor setup, a constant pipe height of 3 feet is maintained. There are no pressure sensors installed and pipe diameters can either be 1" or 2". Minor setups are made up of two components only. The first component is the setup (a hollow pipe with a diameter of 1" or 2") and the second component is the N₂ gas cylinder also with a pressure exceeding 10 times what is needed for each experiment.

Figure 43 shows the schmatic for the gas migration setup (minor tests).

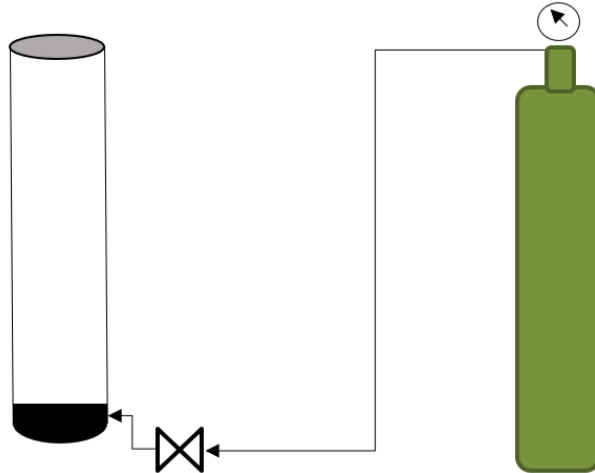


Figure 43: Schematic for gas migration setup (minor test).

Test Procedure

Major Test Procedure

Figure 44 (a) show the setups for gas migration in a three-foot pipe. On the base of the Figure 44 (a), the injection valve is shown while pressure sensors 1 – 3 are opposite this point. Figure 44 (c) shows the DAQ system and the connections made from the power source and sensors to the DAQ system. In the major test, the cement slurry is mixed and poured into the annulus of the setup. After a 12-hour or 24-hour WOC, the cement is drilled through and the pressure sensors installed in place. Distilled water is placed on the top of set cement before the beginning of the experiment as can be seen in Figure 47 and Figure 49. Depending on the cement slurry formulation, pouring water on top of the cement can make it bubble. All bubbling is allowed to cease before proceeding. The N_2 gas is connected to the setup and the gauge is set to 60 psi or 40 psi based on the test being performed. The video cameras are then turned on and recording begins. The valve is opened to allow the set pressure of gas to be pumped into the setup through the installed

sponges and the time the valve is opened is noted down. The gas is pumped into the setup for 30 minutes and during this period the surface of the cement is observed for any gas migration. After the 30-minute window, the gas valve is shut and the gas that was pumped into the cement is allowed to propagate. If gas begins to migrate, before or after the 30 minutes, the positions are marked and the time to see the bubbles are recorded. If multiple positions appear, each position is marked and the time to see the bubbles on the surface of the water is recorded.

A cycle is typically a three-consecutive day testing period at a specified gas pressure. A test is simply the day within a cycle an experiment is being conducted. Cycles are conducted at 60 psi or 40 psi, with a one-week interval between cycles. For each setup typically 3 cycles are performed, two of which are conducted at 60 psi and the last conducted at 40 psi. For example, cycle one – test one (C1T1) would mean the first day testing within the first cycle (three consecutive days of testing) while cycle two – test three (C2T3) would indicate the last day of testing within the second cycle (three consecutive days of testing). Figure 45 shows some positions from tests conducted, Figure 45 (a) shows leak positions from a 3-foot major test.

To understand the effect of ballooning on a cement sheath, a hand pump is installed to communicate with the inner pipe as can be seen in Figure 48. The hand pipe can achieve a pressure of 10,000 psi, but for our experiments a maximum pressure of 2000 psi suffices. The ballooning cycles are conducted in a sequential manner. The pipe is first ballooned to 1000 psi 3 consecutive times, with a 1-minute spacing between two ballooning cycles. In the ballooning phase of the setup, a cycle refers to pressurizing the inner pipe to a predetermined value and holding the pressure in for 5 seconds. After which

a valve on the upper blind plate is used to release the pressure built up in the inner pipe. The next ballooning is conducted at 1500 psi. This consists of 3 cycles of ballooning the inner pipe to 1500 psi, holding the pressure in the pipe for 5 seconds, then releasing the pressure. Once again, a 1-minute interval is kept between two consecutive ballooning cycles. The last ballooning pressure is done at 2000 psi, at this stage the inner pipe is pressured 10 consecutive times, keeping the pressure in the pipe for 5 seconds, releasing the pressure, waiting a minute and then pressurizing the inner pipe again. After each ballooning cycle a 60-psi test is conducted on the setup to see the effects of ballooning on the cement sheath.

Throughout experiments pressure data is constantly collected at a 0.05 second interval from the setup using the DAQ and Daisy Lab software. At the end of each test, the pressure data is exported into a CSV file format for analysis. To analyze the data, the CSV file was taken and converted into excel files. The data points were averaged for every minute and a pressure decline curve was plotted. Graphs were plotted on a semi-log scale with logarithmic trendlines to help obtain an appropriate trend for each experiment.

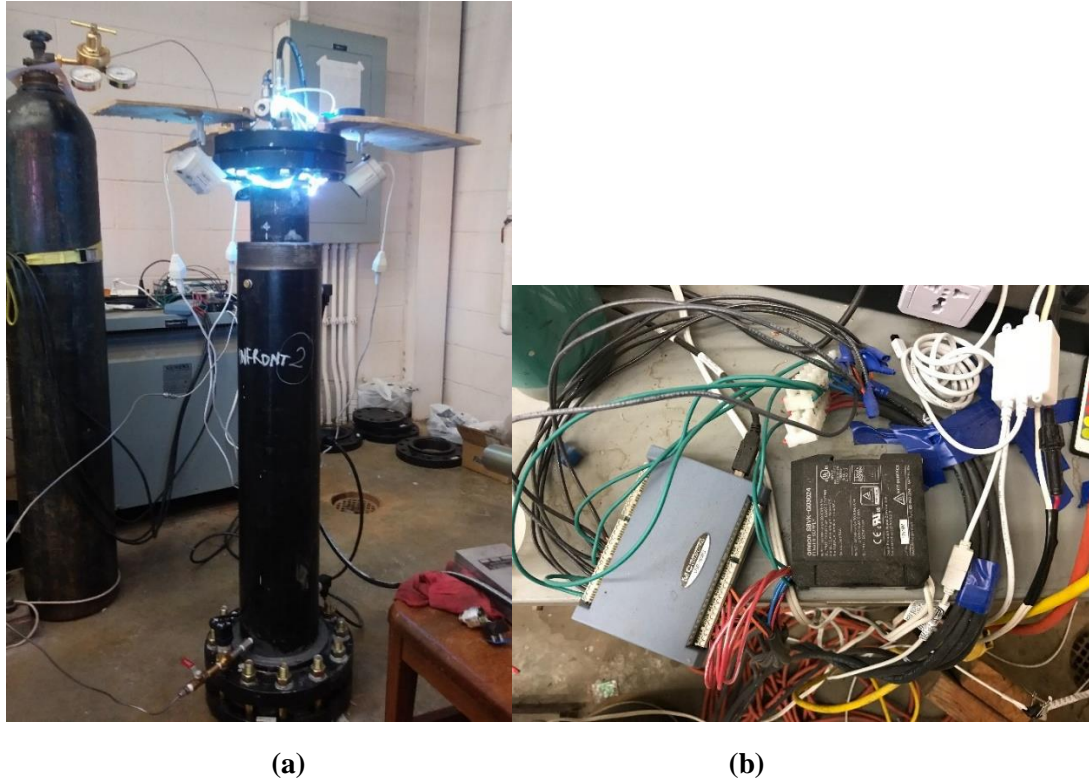


Figure 44: (a) 3-foot whole Setup 1 Experiment 2 (b) Data acquisition card with sensors fitted.

Minor Test Procedure

In the minor testing conducted on the 1" and 2" pipes, the right formulation and volume is mixed to fill the pipe. A 24-hour WOC is considered for all experiments before attaching the N₂ gas to the setup. The gas pressure for minor tests are set at 60 psi. Just as in a major test, the valve is opened to allow the set pressure to be pumped into the setup through the sponges, and the time the valve is opened is noted down. The gas is pumped into the setup for 30 minutes and during this period the surface of the cement is observed for any gas migration. After the 30-minutes window, the gas valve is shut and the gas that was pumped into the cement is allowed to propagate. If gas begins to migrate, before or after the 30 minutes, the positions are marked and the time to see bubbles are recorded. If multiple positions appear, each position is marked and the time to see the bubbles on

the surface of the water is recorded. For minor test 2 cycles of 60 psi are conducted on the setup and there is no ballooning of the pipe. A cycle in the minor test is a three-consecutive day testing period at a specified gas pressure while a test indicates the day within a cycle an experiment is conducted. Cycle two – test two (C2T2) would mean the second day test of the second cycle for a given cement slurry formulation. Figure 45 (b) shows leak positions from a minor test.

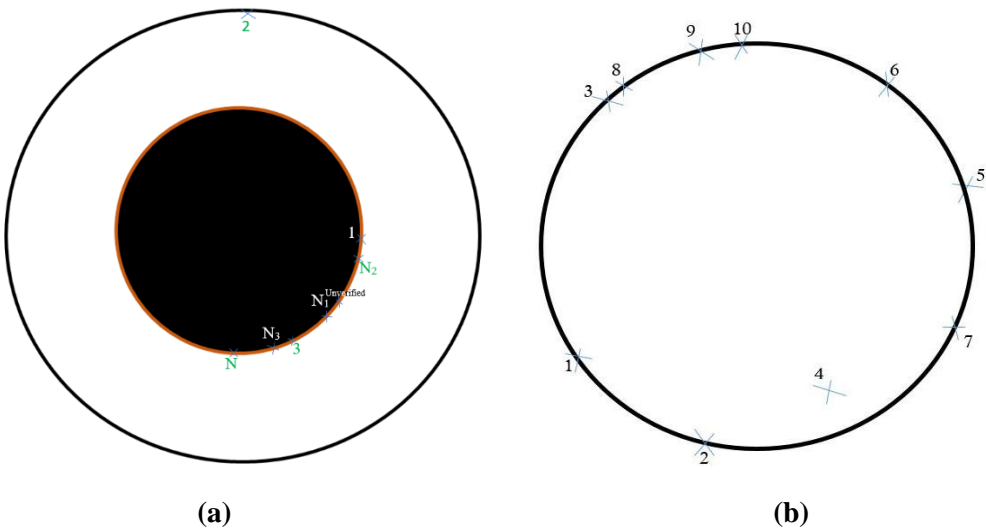


Figure 45: Position of leaks for Setup 1 Experiment 1 (a) and Small Setup 1 Experiment 2 (b).

Cement Experiment Results

Four setups were installed for the experiments; Setup 1 Experiment 1, Setup 1 Experiment 2, Setup 1 Experiment 3, and Setup 1 Experiment 4. In Setup 1 Experiment 1, neat class H cement with no additives was poured into the annulus and cured for 24 hours. N₂ gas was used to pressurize the base of the cement after 24 hours. The first test was conducted with 60 psi of N₂ placed on the setup for 30 minutes and then turned off. A leak was noticed within 11 mins 08 secs of the experiment. Continuous leaks were observed during subsequent days of testing. These leaks were experienced at various locations over time.

A total of 20 tests were conducted on Setup 1 Experiment 1. 17 of them being conducted at 60 psi of N₂ gas pressurization, and the remaining 3 conducted at 40 psi.

In an attempt to help the cement, set well with no or the least amount of created microannuli in Setup 1 Experiment 2, a vibrator was used during the process of pouring the cement. The vibrator was turned on shortly after pouring the cement was initiated. It stayed on throughout the process of pouring the cement and was turned off 20 - 25 minutes after the cement pouring was done. Setup 1 Experiment 2 had a 12-hour wait on cement. 60 psi of N₂ was used to pressurize the base of the cement once again mimicking the tests conducted in Setup 1 Experiment 1. Three leaks positions; Position 1, 2 and 3, were observed after the start of pressurization. The leak at position 1 occurred during 4 mins 28secs of the experiment. Leaks at positions 2 and 3 occurred approximately 32 minutes after the gas was pumped into the setup. The next experiment conducted on the setup was S1E2C1T2. It was observed that a new leakage path was created (Position 4), while previous points of leaks had completely sealed. For S1E2C1T2, the leak at position 4 occurred 14 minutes 35 seconds after the start of the experiment. In S1E2C1T3, a leak was experienced at Position 4, occurring 4 minutes 26 seconds after the gas valve was opened.

Within a cycle, it is interesting to know that the leakage time (time to see the first leak bubble) occurs within a shorter interval as the days go by. That is to say, in each cycle, day 1 has a higher leakage time than day 2, and day 2 has a higher leakage time than day 3.



Figure 46: Left – Positions 2 and 3 as they appear in Setup 1 Experiment 2. Right – Position 4 as it appears in Setup 1 Experiment 2.



Figure 47: Position 4 magnified as it appears in Setup 1 Experiment 2.



Figure 48: Setup for ballooning inner pipe. Left – Connection from hand pump to inner pipe. Right – Hand pump used to pressure the inner pipe of Setup 1.



Figure 49: Left - Gas bubble travelling from cement sheath through water to surface. Right – Travelled gas bubble bursting at surface.

Before discarding Setup 1 Experiment 1, multiple pressurization cycles (ballooning) were conducted on the inner pipe with the aid of a hand pump and a connecting tube (Figure 48). This was done with the aim of studying the effects of casing ballooning on a set cement. In total 5 ballooning tests were conducted. The first set consisted of 3 cycles of pressurizing the inner pipe to 1000 psi. The second set consisted

of 3 cycles of pressurizing the inner pipe to 1500 psi. The third, fourth and final sets involved pressurizing the inner pipe to 2000 psi for 10 cycles. It is to be noted that the pressure placed on the inner pipe in each cycle was kept for 5 seconds and then dissipated via an installed valve. After ballooning, some existing gas migration paths stopped leaking. However, two new leak positions were created in the cement sheath. N₂ gas was allowed to stay on the setup overnight, and multiple leaks were recorded, some from old leak positions and others from new positions. This shows that ballooning is detrimental to cement-sheath integrity. A hypothesis can be drawn stating that ballooning causes multiple paths to be created within a cement sheath that could in turn lead to gas migration. It also has the ability to increase the size of existing fracture and also cause cement-casing debonding.

Setup 1 Experiment 2 was created to mimic Setup 1 Experiment 1 but with a 12 hr wait on cement (WOC) instead of the 24 hr WOC used in Setup 1 Experiment 1. The first test on Setup 1 Experiment 2 (S1E2C1T1) was conducted at 60 psi with the valve opened at 9:08 AM. Three leaks were observed at Positions 1 through 3, with leakage times of 4 minutes 28 seconds, 24 minutes 11 seconds, and 24 minutes 53 seconds respectively. However, Setup 1 Experiment 2 did not exactly mimic Setup 1 Experiment 1 due to some fabrication complications, and time constraints. Only one 60 psi cycle test was conducted in Setup 1 Experiment 2 as compared to two 60 psi cycle tests conducted in its previous counterpart. After the stated 60 psi cycles, both S1E1 and S1E2 has a 40-psi cycle run on them. As done in S1E1, the inner pipe of S1E2 was also pressurized (ballooning). However, the 1000 psi ballooning pressurization was skipped since it had little to no effect on Setup 1 Experiment 2. The first ballooning test was conducted at a

pressure 1500 psi. Once again, the pressure was held in the inner pipe for 5 seconds and then released, keeping a one-minute interval between cycles of ballooning. The cement column was pressurized with N₂ gas and observations were recorded. In the first 2000 psi pressurization test (10 cycles of pressurizing the inner pipe to 2000 psi), the gasket between the upper flange and blind plate of the inner pipe blew on the 7th cycle of pressurization. The gasket was replaced, and the ballooning tests continued as planned mimicking Setup 1 Experiment 1. It is to be noted that the inner pipe in Setup 1 Experiment 1 was not tempered with, while the inner pipe in Setup 1 Experiment 2 was fabricated to reduce the wall thickness of the inner pipe. This was done to ensure effective ballooning of both the cement and inner pipe. Figure 50 and Figure 51 show the graphs of plotted data for Setup 1 Experiment 1 and Setup 1 Experiment 2 before and after ballooning.

Aside the creation of a new position (Position N) after the 1000 psi pressurization sequence conducted in Setup 1 Experiment 1, there was not much difference in leakage times recorded in Setup 1 Experiment 1 (neat class H cement 24hr. WOC) and Setup 1 Experiment 2 (neat class H cement 12hr. WOC), for both 1000 psi and 1500 psi ballooning pressures. Therefore, the 1000 psi ballooning cycle was done away with in S1E2 as already stated. At 2000 psi ballooning pressure, new leak positions were noticed. These included Positions N1, N2, and N3 in Setup 1 Experiment 1 (S1E1) and Position 6 in Setup 1 Experiment 2 (S1E2). Both setups showed that generally cement tends to change leak positions over time. This is because some existing leakage paths may seal due to mobilization and precipitation of minerals along a fracture (Huerta et al., 2012) while expansion and contraction can lead to the formation of micro-annuli (Beharie,

2017). In S1E2, an observation made in S1E1 was confirmed – within a cycle experiment (3 subsequent tests before 1-week fallow period), leakage time decreases with subsequent tests conducted after the initial test. More discussion on this is done in the “Pressure decline curves” section. From the graphs shown in Figure 50 and Figure 51, the leakage time after 2000 psi ballooning pressurization is much lesser than that of 1000 psi, 1500 psi, and no ballooning effect showing the detrimental effect of ballooning on the cement sheath. It is difficult to concluded that it was the detrimental effect of ballooning that reduced the leak time drastically. Since the 2000 psi tests are conducted after 1000 and 1500 psi ballooning tests, and it is already confirmed that within a cycle leakage time decreases with an increase in number of tests, the decrease in leakage time for the 2000 psi pressurization could simply be as a result of it being conducted at a later period in the ballooning cycles. To confirm that the drastic decrease in leakage time was as a result of ballooning, Setup 1 Experiment 2 was left ideal for 1 day to allow all the gas to escape and then a verification test was conducted on the cement at 60 psi. A verification test is a regular 60 psi test conducted on the setup after the 2000 psi ballooning. In verification tests there is no ballooning done on the setup before the experiment. It is performed just as any 60-psi test is conducted in Cycle 1. The results show a shorter leak time verifying the detrimental effect of 2000 psi ballooning pressurization on the cement sheath.

In conclusion, the neat cement (cement with no additives) cannot be considered as a barrier in gas prone formations. Ballooning of the inner casing was also detrimental to the cement sheath integrity and thus may lead to gas migration. 12 hr. WOC was also enough to verify gas migration since the maximum number of leaks in S1E2 were observed after the 12 hr. WOC. It was also determined that cement sheath integrity is

negatively affected by ballooning of the casing and this deterioration was proportional to the degree of ballooning experienced.

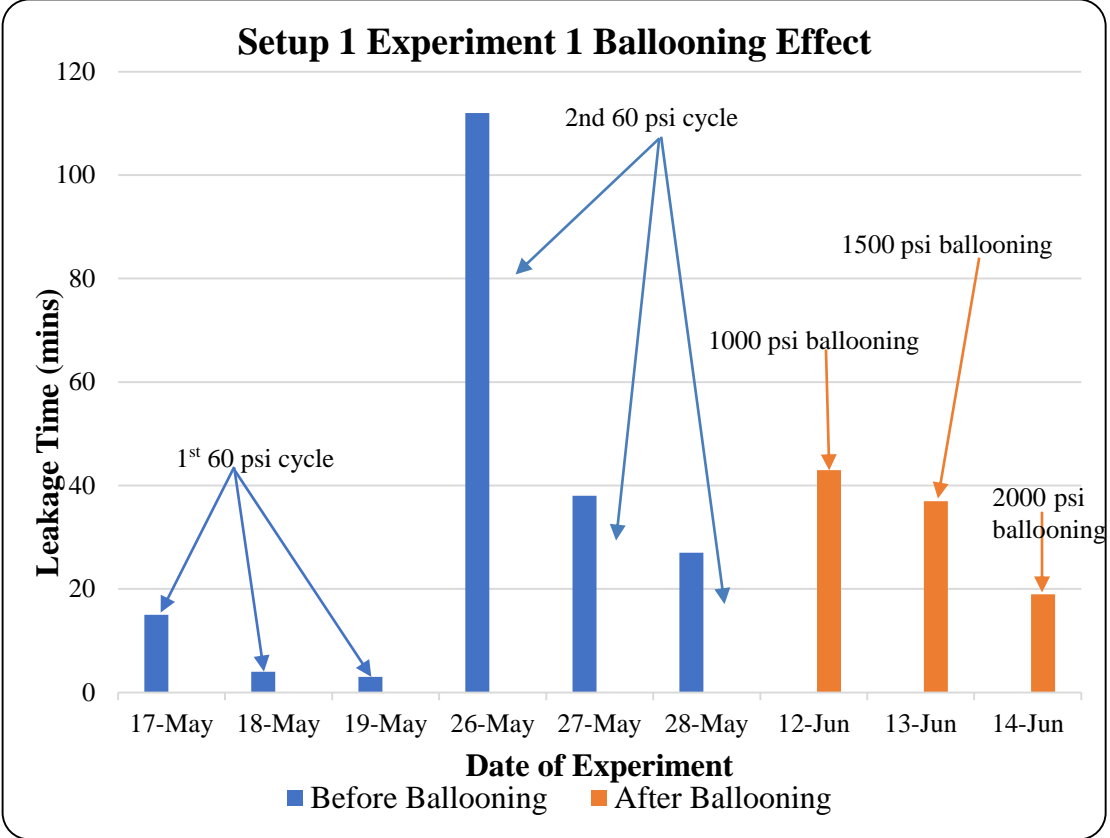


Figure 50: Leakage time of Experiment conducted on Setup 1 Experiment 1 before and after ballooning.

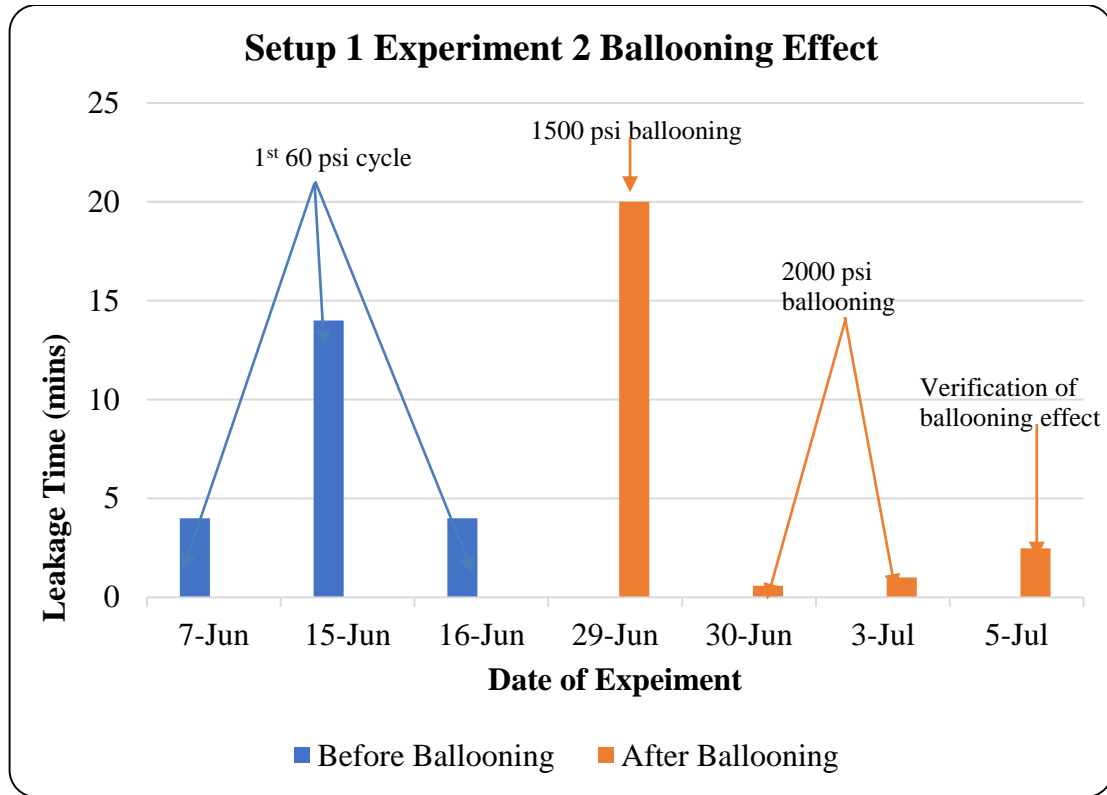


Figure 51: Leakage time of Experiment conducted on Setup 1 Experiment 2 before and after ballooning.

Since it was shown in S1E1 and S1E2 that the cement alone (cement with no additives) cannot be considered as a barrier in gas prone formations. As such a new slurry was designed – S1E3 – with 3 gals/sack latex and 1% BWOC bentonite. The density reported for this slurry was 12.5 ppg which was significantly lower than the base cement slurry (16.65 ppg). S1E3 had a 24 hr. WOC and was experimented on for a period of 27 days. After this period, it was left ideal for over 30 days and the last test was conducted 2 months 9 days from the first day of testing. In its first test, S1E3C1T1, 17+ leak positions were observed with multiple leaks occurring at the same position. With the 3 major experiments conducted, S1E3 proved to have the most number of leak positions within the first 30 minutes of testing.

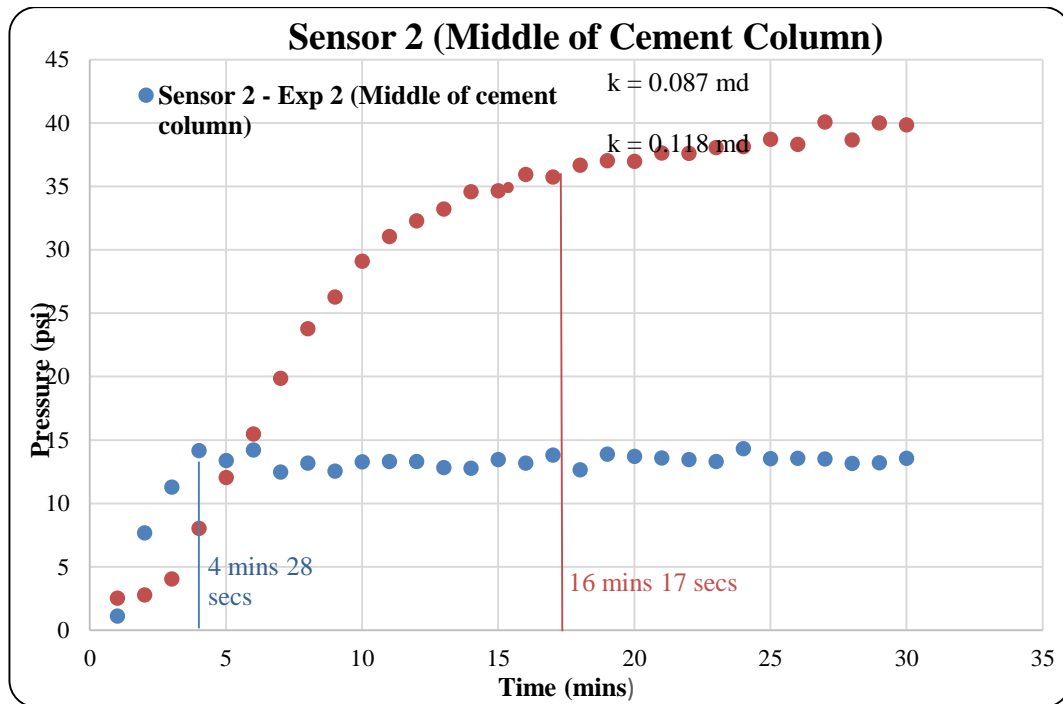
However, Table 16 shows that S1E3 had the ability to hold the pressure in the setup for a period longer before it leaked compared to both S1E1 and S1E2. The pressure sensors placed on the setup recorded a steady increase in the pressure of the cement column in S1E3. At the end of the 30-minute test, there is an approximate 30 psi increase in sensor 2 (middle sensor) and a 10-psi increase in sensor 3 (upmost sensor) between S1E2 and S1E3.

Table 16: Leakage time for Setup 1 Experiment 1, Setup 1 Experiment 2, and Setup 1 Experiment 3.

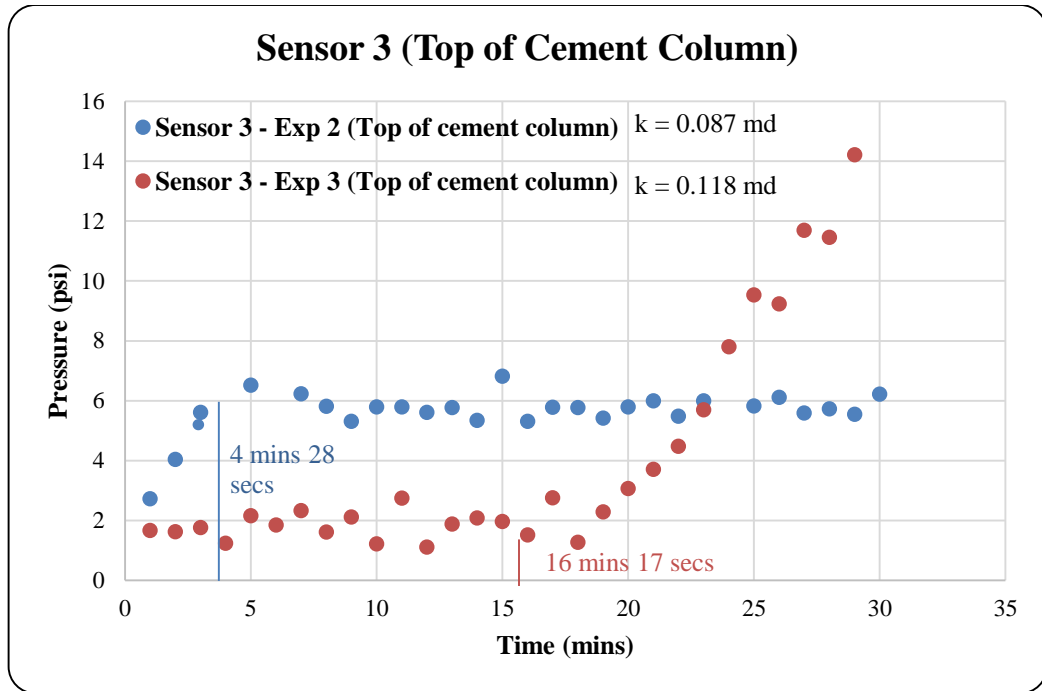
Setup 1 Experiment	Leak time (mins)	Sensor 2 (psi)	Sensor 3 (psi)
S1E1 (24hr. WOC neat class H)	11	N/A	N/A
S1E2 (12hr. WOC neat class H)	4	56.73	13.09
S1E3 (24hr. WOC latex cement - 3 gal per sack latex and 1% BWOC bentonite)	16	60.67	40.25

Figure 52 shows the pressure increase within the first 30 minutes of pressurizing the cement column with N₂ gas. The figure is a plot made for S1E2 (neat class H 12hr. WOC) and S1E3 (latex cement with 3 gals/sack latex and 1% BWOC bentonite, 24hr. WOC) to compare the pressure data before the first leak for a clean class H cement without any additives and the latex formulated cement. Sensor 0 is installed at the inlet of the gas pressure and would always record a constant 60 psi or 40 psi within the initial stages of the test depending on what pressure the test is being conducted. Sensor 1 is also installed close to the inlet pressure thus, might read a pressure similar to the inlet pressure. These two sensors were not adequate in explaining what went on within the cement. So, Sensors 2 and 3 were picked to understand what went on in the cement column in relation to pressure data. It can be observed from the Figure 52 that in Sensor 2 that there is a rise

in the pressure reading followed by a plateau. This steady rise and then plateauing is observed in both S1E2 and S1E3. Overlapping the pressure data with the leakage time, we see that whenever the pressure rise peaks and begins to plateau that is the same point we have our first leak at surface. This leakage time coinciding with the peak in the pressure data occurs in both S1E2 and S1E3 and is independent of the cement slurry formulation or WOC. Sensor 3 also shows a pattern when it comes to overlapping the leak time with pressure data but was not instrumental in explaining what occurred in the cement column, thus, Sensor 2 was considered adequate in analysing the pressure data for gas migration. From the graphs we observed that that latex slurry has capability to hold keep the system gas tight while the gas works its way up the cement column. Immediately the slurry gives way to gas flow a permeability of 0.118 md was observed; one magnitude greater than the neat Class H cement.



(a)



(b)

Figure 52: Pressure data for first 30 minutes of testing for S1E2C1T1 and S1E3C1T1 (a) Sensor 2
(b) Sensor 3.

In Setup 1 Experiment 3, the bubbling begins quite steadily and as the experiment continues to go on, rapid bubbling occurs within a short while after the setup’s steady bubbling. Figure 53 (a) shows S1E3 under rapid bubbling while Figure 53 (b) shows SIE3 under rapid bubbling.



(a)

(b)

Figure 53: (a) Setup 1 Experiment 3 regular bubbling (b) rapid bubbling.

Figure 54 shows the test and ballooning cycles performed on S1E3. In this figure we see that within a cycle, the leakage time decreases with an increase in the test day. This is the same observation made in previous setups. Four ballooning tests were conducted on S1E3 succeeding the 40-psi cycle. The first ballooning test was conducted at 1500 psi while the remaining tests were conducted at 2000 psi. In the 1500 psi test, there were 3 ballooning cycles performed on the inner pipe and then the test was conducted. There 2000 psi tests were conducted, each consisting of 10 cycles of ballooning the inner pipe. The process of ballooning and testing was performed exactly as the ballooning was done in S1E1 and S1E2. At least one new leak position was found after the 2000 psi test. In S1E3, there was also a verification cycle performed one day after all 2000 psi ballooning tests were completed and once again we see that the verification test showed a lesser leak time compared to a regular 60-psi tests conducted before ballooning. This observation confirmed that ballooning is detrimental to the cement sheath integrity.

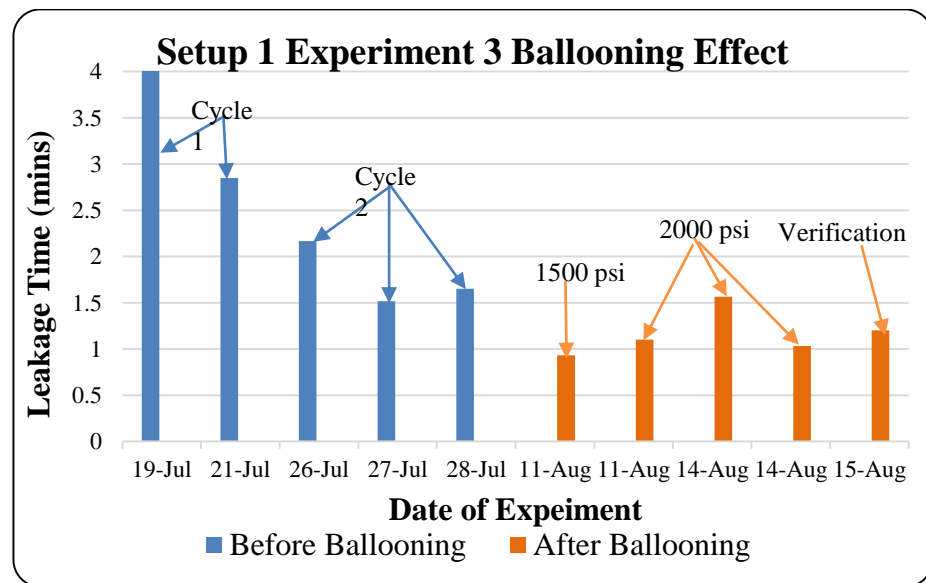


Figure 54: Leakage time for Setup 1 Experiment 3 cycles and ballooning.

Pressure decline curves

With the use of Daisy Lab software and Microsoft Excel, the pressure data was recorded from each individual pressure sensor and then the pressure decline curve was plotted. Daisy Lab stored a pressure data reading every 0.05 secs for a 24-hour period. This data was then retrieved from the Daisy Lab software and was fragmented into smaller chunks of data to be worked on in Excel. In excel the data was averaged out for every one minute for the first 500 minutes of the 24-hour period. The first 30 minutes were used to locate the leakage time but for the pressure decline curves these values were discarded. So, the pressure decline curves started from the 31st minutes to the 500th minute of the test. 500 minutes was selected because after this time the pressure decline would have plateaued, and any extra time does not contribute to the understanding of the pressure decline in the setup. The pressure declines were plotted in two forms, the first being a pressure decline by day and the second being a pressure decline by cycles. A plot of pressure decline curves by day means plotting the pressure decline for various Setup 1 Experiments for a given test. That is to say, Day 1 for Setup 1 Experiment 1, Setup 1 Experiment 2 and Setup 1 Experiment 3 are plotted on the same graph while day 2 for Setup 1 Experiment 1, Day 2 for Setup 1 Experiment 2 and Day 2 for Setup 1 Experiment 3 are all plotted together on a separate graph. This is done to understand what happens to the same test when conducted on different cement samples. In a plot of pressure decline by cycles, the Setup Experiment is chosen, and all tests conducted within a particular cycle (3 consecutive days of testing) are plotted on the same graph. For example, in Setup 1 Experiment 3, a cycle is selected (Cycle 1) and all tests conducted in Cycle 1 are plotted

on the same graph to understand what happens in the cement column with consecutive tests. The results from these pressure decline graphs are discussed in this section.

Pressure decline curves by days

This section involves a discussion of the pressure declines when a similar test is performed but on different cement samples. In essence we compared the pressure declines for Day 1 of say Setup 1 Experiment 1, Setup 1 Experiment 2 and Setup 1 Experiment 3. Then compare them for Day 2, to see what changes go on in the Setup for the same test conditions but varying slurry composition or WOC. The pressure decline curves were mainly in three folds. Two were conducted at 60 psi – Cycle 1 and Cycle 2, while the last was conducted at 40 psi.

Pressure decline curves by days – 60 psi

All major experiments begun with a 60-psi test. In Cycle 1 three consecutive tests were conducted – Day 1, Day 2, and Day 3. In Cycle 2, three consecutive tests were conducted – Day 1, Day 2, and Day 3 succeeding Cycle 1. For pressure decline curves by days for 60 psi cycles. All comparisons on the three feet pipes were performed on Sensors 2 since this sensor had the ability to record the gas migration through the cement column accurately. The cement samples included – Setup 1 Experiment 1 (S1E1 – neat class H cement; 24 hr. WOC), Setup 1 Experiment 2 (S1E2 - neat class H cement; 12 hr. WOC), and Setup 1 Experiment 3 (S1E3 – class H with 3 gals. / sack latex and 1% BWOC bentonite). Figure 55 show that irrespective of the Setup Experiment, the same test conducted in two separate cycles would have the pressure data in the later cycle (Cycle 2) being lower than the pressure data in the earlier cycle (Cycle 1). This observation is independent of the type of cement slurry used for testing. However, the degree of

deviation between two tests from different cycles (for the same setup) is highly dependent on the age of the cement sheath (days of hydration). The older the cement sheath the lesser the degree of deviation. The age of the set cement also affects system permeability. Using S1E3 as an example, S1E3C1T2 had a permeability of 0.2461 md, S1E3C2T2 had of 0.2291. Keeping all factors constant and the system fully vented, an increase in cement age corresponds to a decrease in system permeability.

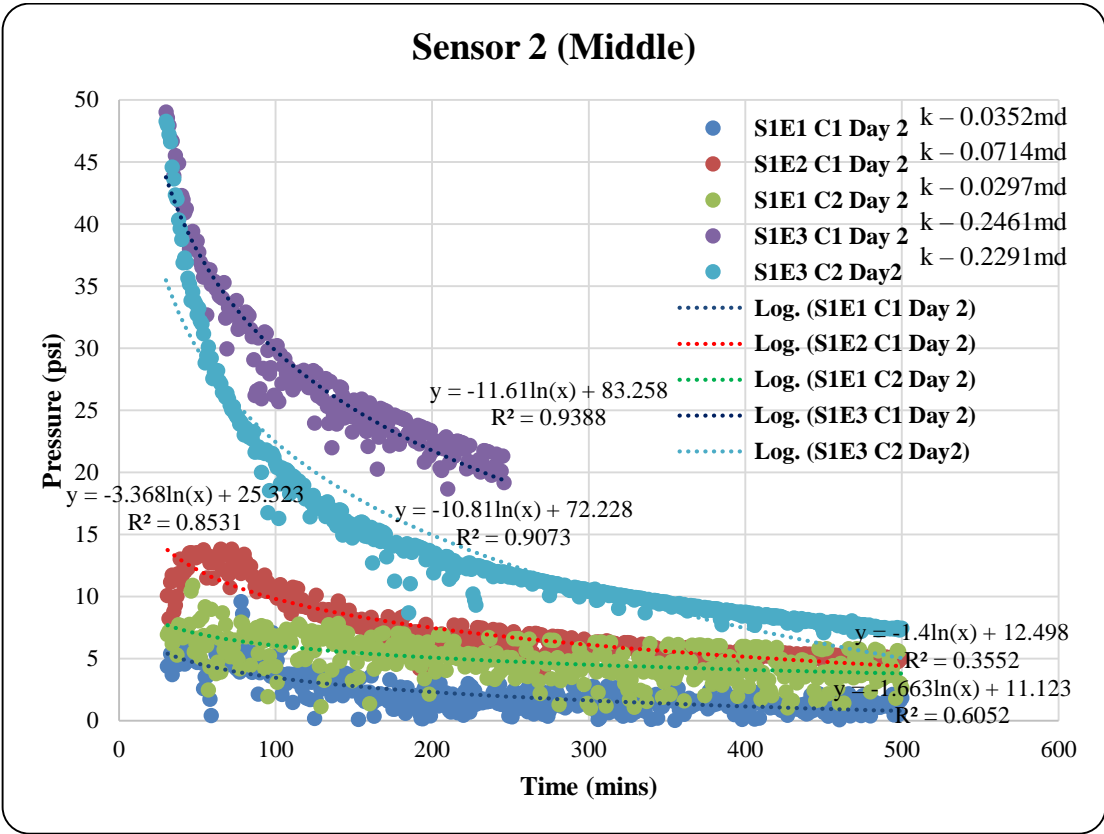


Figure 55: Day 2 Setup 1 Experiment 1, Setup 1 Experiment 2 and Setup 1 Experiment 3 (Cycle 1 and Cycle 2 – 60 psi) – Sensor 2

Pressure decline curves by cycle

This section involves a brief discussion of the pressure declines when 3 consecutive tests are performed in one cycle. These consecutive experiments are conducted on the same

setup and the cycle can be a 60-psi or 40-psi cycle. The pressure declines for Day 1, Day 2 and Day 3 of Setup 1 Experiment 3 and a comparison of Day 1, Day 2 and Day 3 of Setup 1 Experiment 4 are reported. This type of graphing was done to understand the changes that ensued within one specific cycle. The effect of ballooning on pressure data was also discussed.

Setup 1 Experiment 3

A three-day consecutive test was conducted in Cycle 2 (60 psi). Analyzing the pressure data from the sensors, a similar behavior like that in S1E2 was observed. With an increase in days for a consecutive test the pressure decline curves increase as well (Figure 56). That is to say, S1E3C2T1 has lesser pressure readings compared to subsequent tests. Although S1E3C3T1 had lower pressure readings, it had the highest permeability values of 0.3644 mD. As the cement hydrates, we see an improvement in the system permeability (S1E3C2T2 = 0.2266 mD, S1E3C2T3 = 0.2722 mD). Comparing C2T2 to C2T3 for S1E3, we observe an increase in both permeability values and pressure readings. This behavior is attributed to a rising existence of residual gas pressure in the cement sheath from one test to the next test within the cycle.

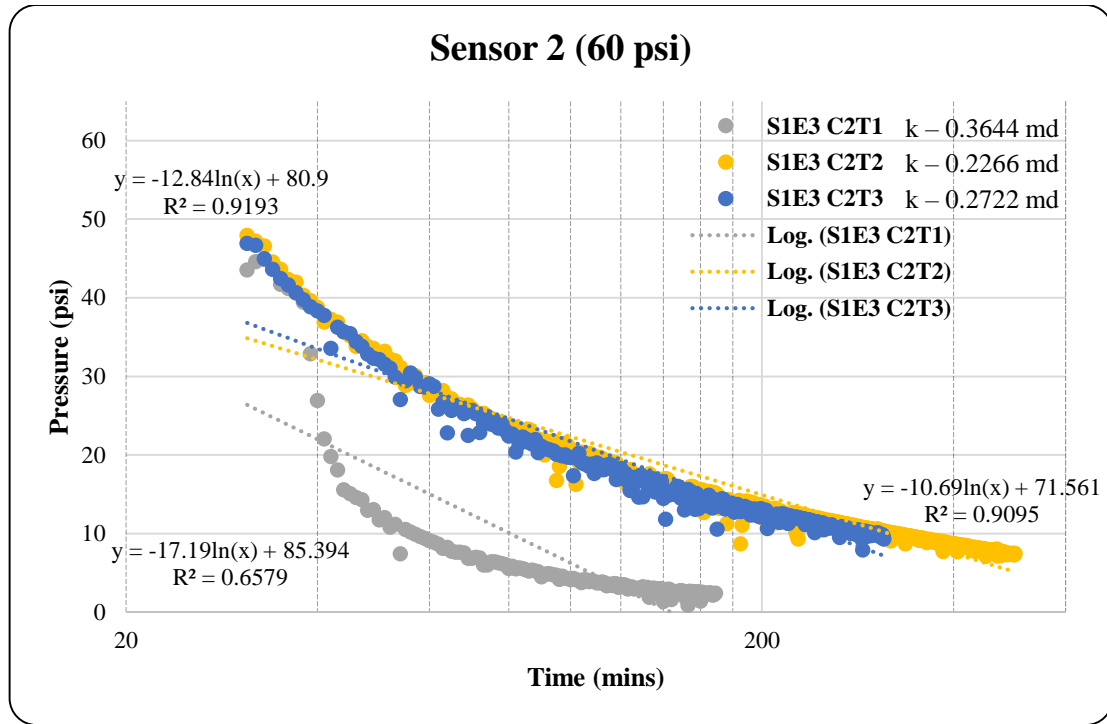


Figure 56: Day 1, Day 2, Day 3 for Setup 1 Experiment 3 (Cycle 1 – 60 psi) – Sensor 2

Setup 1 Experiment 4

In an effort to keep consistency between previous Setups and Setup 1 Experiment 4, Sensors 3 was chosen to be studied since Sensor 3 was the middle sensor. With this approach Sensor 2 of Setup 1 Experiment 1 can directly be compared to Sensor 3 of Setup 1 Experiment 4 since both these sensors are located directly in the middle of their respective setups.

Analyzing the pressure data obtained in the 6-foot setup, some similarities were noted between S1E2, S1E3 and S1E4. From Cycle 1 Day 1 to Cycle 1 Day 2, a decrease in annulus gas pressure is observed. This is because the cement builds more compressive strength with an increase in hydration time. From 24 hrs. to 48 hrs. hydration period an improvement in cement compressive strength is observed (“Unconfined Compressive Strength and Ultrasonic Testing”). However, from Day 2 to Day 3, the pressure sensors

indicate an increase in pressure data (Figure 57). Calculations also show an increase in effective permeability from 0.1122 md to 0.13 md. This increase in pressure readings and system permeability is due to residual or saturated gas pressure in the cement. The residual gas pressure allows for faster gas migration; which is confirmed by a shorter leak time. With this observation, we conclude that irrespective of the height of the cement column (3-ft or 6-ft), the cement behavior does not change. Aging improves compressive strength and decreases permeability, while residual gas in the cement column increases pressure readings and permeability simultaneously.

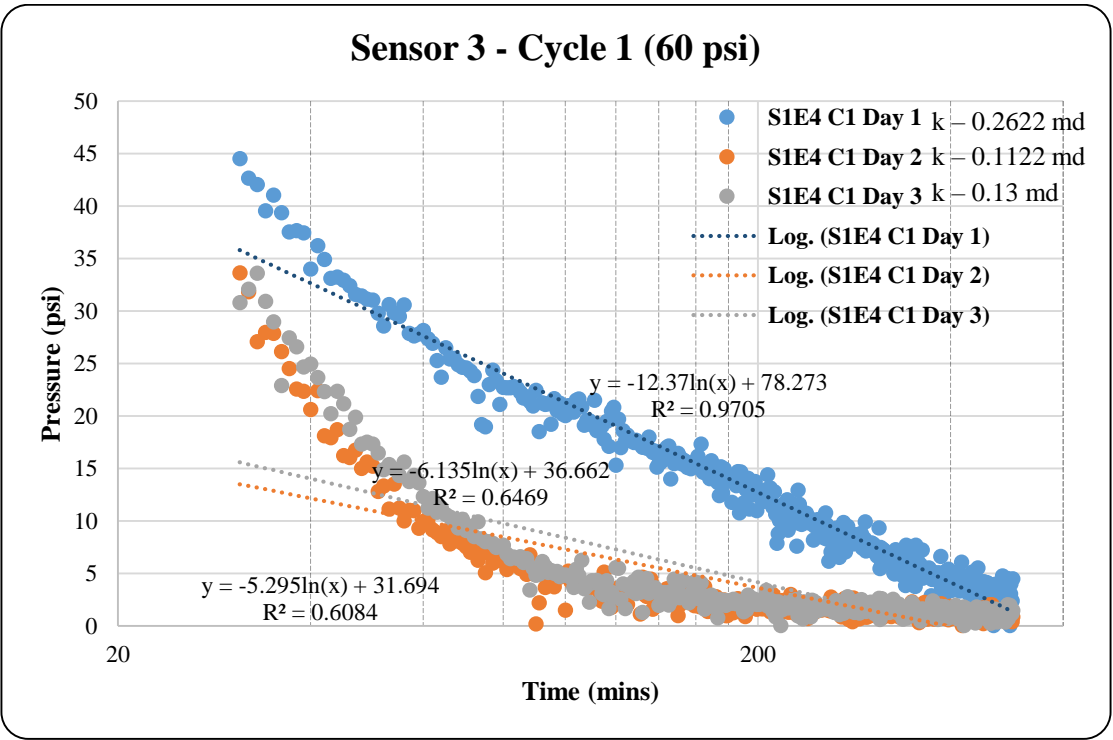


Figure 57: Day 1, Day 2, Day 3 for Setup 1 Experiment 4 (Cycle 1 – 60 psi) – Sensor 3

Pressure decline curves by ballooning

For every built setup, ballooning was conducted to access the effect of gas expansion in the inner pipe on the set cement sheath. The ballooning was performed at varied pressures as mentioned earlier. To understand the visual results better, the pressure values obtained

from ballooning tests were plotted with regular tests conducted at the same gas injection pressure. In Figure 58, it is observed that the ballooning cycles have pressure data similar to Day 3 and Day 2 of testing. Since ballooning is conducted 5-weeks into the age of the cement, the data is expected to deliver a lower permeability. However, performing a calculation on the ballooning data, a higher permeability (0.1416 md) is observed. This rise in permeability coupled with verification tests were ample in indicating the detrimental effects of ballooning on the set cement, as discussed early on in the “cement experiment results” section.

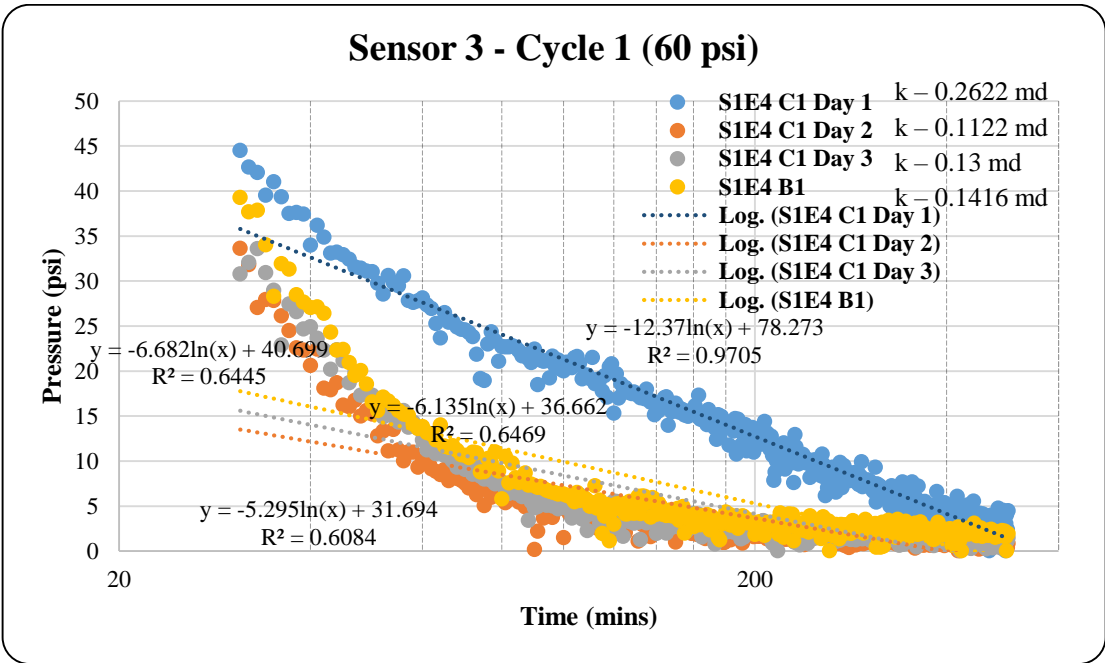


Figure 58: S1E4 Sensor 3 ballooning vs. Day 1, Day 2, Day 3 for Setup 1 Experiment 4

Predicting Effective or System Permeability (K) from decline curves

To predict the effective permeability of the entire system, an approach used by Brace et al. (1968) was adopted. The volume (V1) was estimated as a fourth of the volume where the sponge is placed in Major setups. Volume (V2) was estimated with a correlation given

in their literature. To obtain the final permeability, the graph had to be replotted by changing the semi-log axes. The y-axis (Pressure) was made log while the x-axis (Time) was converted into a linear axis. This was done in an effort to attain the slope needed to satisfy the equation. All nitrogen gas (N₂) properties were used obtained from published articles. A MATLAB code was then written to predict 3 permeability values in millidarcy (md or mD) for side by side comparisons. Thus from a plot, all three permeability values can be obtained for each cycle or for experiments conducted by day. The MATLAB code is found in Appendix B.

Small Setup 1

Major experiments were conducted on 3-foot pipes with a 6.5" OD, mimicking field case scenarios. These large setups are energy intensive, time consuming and use a lot of raw material. To minimize waste, small setups were fabricated to test the cement slurry before using them for major setups. These small setups were used to verify appropriate cement slurry mixture and see the effect of size on the experiments. For all small setups a maximum of two 60 psi cycles was performed on the setup before discarding them. There were no 40 psi tests conducted and no form of ballooning was done of the cement. In Small Setup 1 Experiment 1 and Small Setup 1 Experiment 2, similar observations to major tests (S1E1, S1E2, S1E3) were made. One of these observations was that leakage time decreased with a cycle as time went on. Another observation was that positions disappeared, and some appeared as time passed with the Setup. In Small Setup 1 Experiment 1, some positioned that disappeared in the first cycle included Positions 2, 3, 4, and 5. In cycle 2, Position 6 disappeared. In Small Setup 1 Experiment 2, some positions that disappeared included Positions 3 and 4. Both these positions disappeared

in the first cycle of testing. Figure 59 shows the leak positions on Small Setup 1 Experiment 1 (a) and Experiment 2 (b). Figure 60 shows the full design for Small Setup 1 Experiment 2. All Small Setups followed the same design pattern for consistency in experimental work.

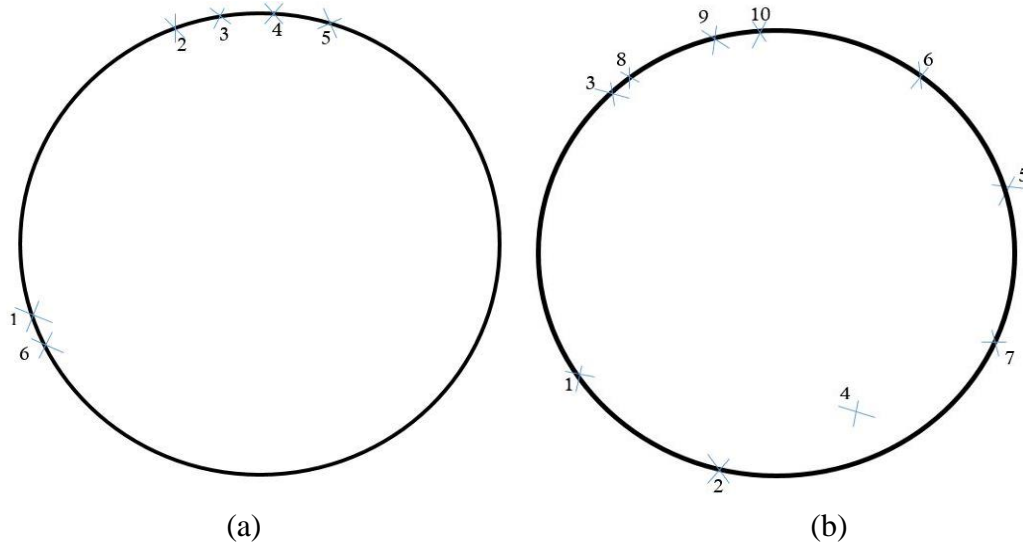


Figure 59: Small Setup 1 Experiment 1 (a) Experiment 2 (b)



Figure 60: Small Setup 1 Experiment 2.

As one of its objectives; Small Setup 1 was also to investigate the effect of size. Looking at Table 17 and comparing the leakage time of Small Setup 1 Experiment 1 and 2 to Setup 1 Experiment 1, a significant deviation in leak times are observed with the smaller setups having a faster leak time than the bigger major setups. An explanation for this would be the total volume to be filled with 60 psi gas. The 3-foot major experiments have a volume of 8303 ml to be filled by the 60 psi N₂ gas while the Small Setup 1 has a volume of ranging from 463.33 ml (1-inch) to 1853.3 ml (2-inch) to be filled with N₂ gas.

For both major and minor tests, the gas pressure was a constant 60 psi, this volume difference allows the gas to migrate faster in the smaller setups thus the shorter leak time recorded. In Table 17, a higher leak time is observed in Small Setup Experiment 2 compared to Small Setup 1 Experiment 1. This is because Experiment 2 had a 2-inch diameter, while Experiment 1 had a 1-inch diameter. The volume difference – Small Setup 1 Experiment 1 (463.33 ml) and Small Setup 1 Experiment 2 (1853.3 ml) – accounts for this change in time since the pressure is kept at a constant 60 psi though out all experiments.

Table 17:Leakage time for Setup 1 Experiment 1, Small Setup 1 Experiment 1 and Small Setup 1 Experiment 2.

	Leakage Time (mins)
Setup 1 Experiment 1	11
Small Setup 1 Experiment 1	1
Small Setup 1 Experiment 2	5

In Small Setup 1 Experiment 3, the slurry mixture was cement with 1 gal / sack Thin Mortar Additive Latex and 0.5% bentonite. The vibration time was over 1 hour. The experiment was performed after 24 hours WOC. Before the experiment, water was poured on the cement surface to help track the bubbling. Before the gas is connected there were bubbles already migrating from the surface of the cement. This migration is normal since a similar experience was encountered in Setup 1 Experiment 3. There is however an abnormal observation; there was a major hole observed on the side of the cement sheath and this position also had some bubbling.

The cement surface bubbled for over $\frac{3}{4}$ of an hour thus delaying the beginning of the experiment. After most bubbling was done the setup was connected to the gas line

and 60 psi N₂ gas was pumped through the base of the cement. 21 minutes after the beginning of the experiment, the first bubble was recorded. Position 2 started bubbling 1 hour 32 minutes after the experiment has started. Position 2, however, was not consistent bubbles. It was mainly gushes of bubbles coming out intermittently. The second test was performed the following day, there was a single bubble from Position 2 and Position 3 (the observed hole). There were also 3 random bubbles observed from different sections of the cement. These were not classified as leaks. After 9 minutes 53 seconds, Position 2 experienced its first gush of bubbles. After 1 hour, there were random bubbles that appeared from time to time but no consistent bubbles were observed.

A third test (72 WOC) was conducted on Small Setup 1 Experiment 3. After 9 minutes 31 seconds of starting the experiment the first random bubble was observed. After this, other random bubbles were observed with one of them being from Position 3. However, none of these were recorded as the leak time because no constant leak was observed. The leak time was recorded as 20 minutes 9 seconds because this is when the Position 3's bubbling became more pronounced and consistent. It would be good to define what consistent at this point is: a 7-20 seconds delay between one bubble and the next at the same leak position.

Since there was not much consistent bubbling in Small Setup 1 Experiment 3, an extended experiment was carried on the setup. The valve was opened at 3:42 pm on September 26, 2017(8 days WOC). The first leak occurred after 8 hours of testing. After 20 hours of testing two constant leak positions were observed.

Class H and Fly Ash Cement Sample

To achieve gas tight cement fly ash was used. Fly ash is typically finer than Portland cement and lime. Fly ash consists of silt-sized particles which are generally spherical, typically ranging in size between 10 μm and 100 μm . Fly ash usually classified as Class C or F consists primarily of silicon oxides, aluminum iron and calcium. They also contain magnesium, potassium, sodium, titanium, and sulfur but to a lesser degree. This small particle size distribution of fly ash and its unique spherical shape makes it a good mineral filler. Fly ash in the presence of water, react with calcium hydroxide at ordinary temperatures to produce cementitious compounds (Federal Highway Administration, 2017). For our experiment, 30% Fly ash BWOC and 1 gal/sack Latex was used. A water requirement of 3.6 gal/ 74 lbm was used for the Fly ash. This setup was dubbed Small Setup 1 Experiment 6; and was a 2-inch, 3 feet pipe.

It was conducted on November 10, 2017. The setup was pressurized with gas for 30 minutes. During the experiment, a visual rise of the water level was observed and shortly afterwards there was a leak. The leak occurred at Position 1, 21 minutes 26 seconds after the commence of the experiment. After bubbling continuously for a while, the experiment stopped bubbling but continues almost immediately afterwards. This was approximately 1 hour 18 minutes from the beginning of the experiment. Two other tests were conducted on the experiment, one on November 11, 2017 (48 WOC) and the last on November 14, 2017. The leak time for these experiments were recorded as 14 minutes 25 seconds and 20 minutes 48 seconds respectively. Less bubbling was observed in the second experiment compared to the first indicating an improvement in the cement compressive strength and a decrease in cement permeability with hydration. The shorter

leak time is attributed to residual gas in the cement from the experiment the day before. The 2-day fallow period allows all gas to escape the setup and we observe an increase in leakage time once again. This observation directly corresponds to previous setups. It is to be noted that throughout all experiment only one leak position – Position 1 was observed.

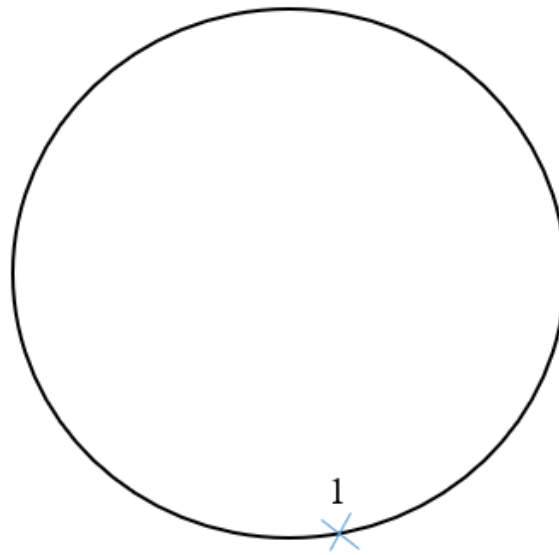


Figure 61: Leak Positions for Small Setup 1 Experiment 6.

Figure 61 above shows the leak position of Small Setup 1 Experiment 6. Figure 62 gives a pictorial view of the leak during the experiment, while Figure 63 shows the position in the set fly ash cement where leaks occurred.



Figure 62: Fly ash cement showing leak position (Small Setup 1 Experiment 6).



Figure 63: Fly ash cement showing leak position (Small Setup 1 Experiment 6).

Microsilica Cement Sample

Small Setup 1 Experiment 7 was 2 inches in diameter and 3 feet in height. The vibration period was limited to 25 minutes to be consistent with previous setups. For the mixing procedure, the already outlined mixing procedure was used. Since the gas migration additive being added was solid, it was homogenized with the cement manually in a big container before the mixing began. The cement slurry was formulated as such; Portland cement with 38% water, 5.5% Microsilica (silica fume white) BWOC and a 5% water requirement for the microsilica. A 5% water requirement was selected because no water reducers were used during the mixing.

The first test was run after 24 hr. WOC, the first leak was observed 15 seconds after the start of the experiment. This indicated a poor bonding between the microsilica cement the casing since the leak occurred at the wall (Position 1). The experiment continued for the full 30 minutes, and no subsequent leaks were recorded. The second test was conducted the following day. Two new leak positions were recorded making a

total of 3 leaks. The second and 3rd leaks occurred 57 seconds and 2 minutes 11 seconds respectively, after the start of the experiment. In test 3, after 72 hours WOC, the first leak occurred 11 seconds after the beginning of the experiment. The leak in Position 2 was recorded as 35 seconds after the start of the experiment. It is to be noted that the water was not topped on the cement to observe the change in leak time.

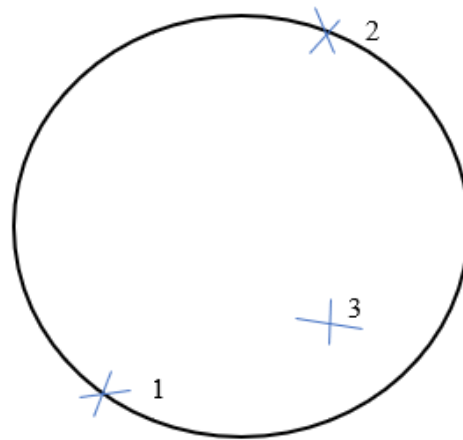


Figure 64: Leak Positions of Small Setup 1 Experiment 7

Figure 64 shows the various leak positions in Small Setup 1 Experiment 7. It is observed that not all the leaks occur at the walls, Position 3 occurs directly in the cement indicating a faulty cement since the cement does not bond to itself properly. An image of the leaking region was taken with a Dino-Lite Digital Microscope and shown Figure 65 . To verify the inadequacy of silica fume white, Small Setup 1 Experiment 8 was conducted. This was an exact mimic of Small Setup 1 Experiment 7. However, 12% cement replacement of microsilica was used. Thus, for Small Setup 1 Experiment 8, no water requirement was needed. The microsilica concentration was increased in a bid to create an improved cement slurry. A 24-hour curing period was kept before the first experiment was conducted. A leak was observed within the first 7 to 10 seconds of testing. The second test (48 hrs. WOC) conducted on this setup had the first leak within 10

seconds of testing. Both tests had the gas leaking through the same position – between the cement and the steel wall – due to poor bonding between the cement and the metal surface. The almost instantaneous leak time indicate poor bonding through the whole length of the cement column. The failure of the cement could be as a result of its densification. As stated in literature microsilica has a particle size range of 0.02 to 0.5 μm , with an average of 0.15 μm . Cement on the other hand has a particle size range of 1 μm to 90 μm with 10 wt% of the cement being made of particles larger than 50 μm , and only a few wt% consists of particles larger than 90 μm . On the fine end, less than 10% of the cement is particles smaller than 2 μm .

Figure 18 shows the particle size distribution of cement, undensified, and densified microsilica on the same plot. The fine particle size of microsilica allows packing between the cement grains resulting in an improved microstructure of the cement matrix. Undensified microsilica has bulk density typically 200 – 350 kg/m^3 while densified microsilica has a bulk density typically 500 – 700 kg/m^3 . The microsilica used for our experiment had an approximate density of 400 kg/m^3 . Per Daou and Piot (2009) “only microsilica with a bulk density of approximately 300 kg/m^3 is the adequate compromise between proper handling characteristics and good slurry performance”.



Figure 65: Cement after leak

Nanomaterial Cement Sample

Nanomaterial was used as an additive in mitigating gas migration. A 0.5% BWOC concentration of nanomaterial was used in combination with Class H cement to create a new slurry sample. Due to the fine nature of the nanomaterial, the mixing procedure was slightly altered to accommodate the nanomaterial. After regular API mixing was completed, an extra 15 seconds of shear at 4000 rpm followed by an extra 15 seconds of mixing at 12000 rpm was included. This modification allowed the nanomaterial to disperse appropriately in the new slurry. This slurry sample was then poured in a 2 inch, 3 feet steel pipe as in previous experiments. The cement slurry was cured for 24 hours after which the first test was conducted on the sample. The inlet gas pressure was kept at a constant 60 psi. A leak was detected at the base of the setup and the experiment had to be halted and this leak fixed with the inclusion of Teflon tape at the base of the setup. The 60-psi gas was maintained for 30 minutes after which the valve was closed. The first leak

was detected 9 minutes 54 seconds after the onset of testing. The bubbles recorded were extremely tiny. Position 2 was recorded 11 minutes after Position 1 was marked. The bubbles at Position 2 were also miniscule and had an average 1 min 28 seconds delay between one bubble and the next. This delay was recorded by an average of the time between 4 consecutive bubbles. Two other tests were conducted after 48 hr. WOC and 72 hr. WOC. Both 2nd and 3rd day of testing was conducted at 60 psi. No bubbles were recorded on the 2nd day of testing. However, on the third day of testing continuous bubbling was recorded 2 hours 4 minutes and 35 seconds after the beginning of the experiment. This leak was at a completely different location which was marked Position 3, Position 3 was a small in the surface of the set cement. Figure 66 shows the surface of the set cement after a leak at Position 1 was detected.



Figure 66: Nanomaterial Cement Sample with leak position highlighted in red.

After leaving the nanomaterial cement fallow for 5 days, another test was conducted on the sample. The water had dried from the surface of the set cement. Before the beginning of the experiment the water was topped up and the experiment commenced. The first leak was detected at position 3, occurring 1 minute 11 seconds into the start of

the experiment. Five new positions were noticed after the first leak, some being in the center of the set cement while others were between the cement and casing. Figure 67 indicates all the leak positions on Small Setup 1 Experiment 9.

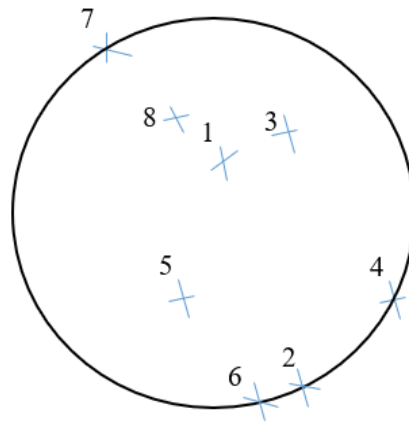


Figure 67: Leak positions in Small Setup 1 Experiment 9

Class H, Flyash, Latex and Nanomaterial Cement Sample

To try and improve upon the Class H cement slurry a combination of additives was tried. Table 21 shows the improvement brought about by the addition of fly ash and latex, and the addition of nanomaterial – 21 mins 26 secs and 9 mins 54 secs respectively. So, in SS1E11, a Class H cement slurry with 30% fly ash, 1 gal/sack latex, and 0.5% nanomaterial was formulated. The water requirement for fly ash was kept at 3.6 gal/ 74 lbm. A gas pressure of 60 psi was placed at the base of the setup and the experiment was started. The first leak was recorded 1 min 14 secs into the experiment, while the second position's leak time was recorded as 1 min 20 secs. There was rapid bubbling recorded in the first day of testing and this was from multiple locations in the pipe (Figure 68).

A 3-day consecutive testing was performed on the set cement. With the passing of time, the set cement experiences some improvement thus less bubbling occurs with an increase in the number of days. By the end the 3-day testing period, a total of eight locations were recorded, five of which were in the set cement itself while the other 3 were located at the interface between the set cement and the steel pipe. Figure 69 shows the locations of all recorded leaks in SS1E11.



Figure 68: Bubbling in Small Setup 1 Experiment 11

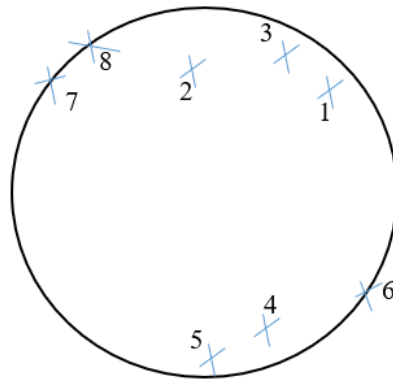


Figure 69: Leak positions for Small Setup 1 Experiment 11

Class H, 1.5 liters / 100 kg commercial additive Cement Sample

To mitigate gas flow completely, a commercial additive from a service company was used to design a new slurry. A recommendation from the service company required us to use a range of 4.5 - 9 liters of commercial additive per 100 kg of cement. A concentration

of 6 liters / 100 kg and 3 liters / 100 kg were tried. However, both of these two concentrations made the cement slurry too thick to be used in the lab due to the unavailability of the required equipment. As such, a concentration of 1.5 liters / 100 kg was used to make the cement design workable in the lab. The new slurry comes with a high static gel strength but regular thickening time. The cement slurry was mixed and poured in a 2-inch, 3-foot pipe, keeping consistent with other tests. The cement slurry was cured properly for 24 hours and the first test was conducted on SS1E12. The first day of testing had 30 minutes of gas pressure applied to the setup and no leak was recorded. After 48 hours WOC, the set cement was pressurized with gas for 6 hours – 4 hours followed by a 2-hour session. No leaks were noticed the system remained gas tight. In C1T3, 60 psi N₂ gas pressure was placed on the setup for 2 hours and the system still proved to be gas tight even after 72 hours of consistent tests being carried out on the cement.



Figure 70: No bubbling in SS1E12.

Properties of Cement Samples

Rheology

From the Figure 78 (Appendix B), all cement slurries are non-Newtonian shear thinning fluids. From the plots we observe that although neat Class G cement is naturally more viscous to neat Class H cement, the addition of some additives like fly ash and nanomaterial make the formulated slurries develop higher viscosity. This can be seen from the equations by the rise in K values. A combination of nanomaterial and fly ash in the same slurry increases the viscosity of the designed more. Although cement slurries with additives included tend to be more viscous, they also proved to be much more shear thinning than the base slurry. This is indicated by the reduction in the flow behavior index for slurries with additives included. The addition of 0.5% nanomaterial to the base slurry made the slurry design more shear thinning. The addition of 30% fly ash and 1 gal/sack of latex also proved to make the cement slurry more shear thinning. However, an addition of 0.5% nanomaterial to the slurry design with 30% fly ash and 1 gal/sack of latex increased the 'n' value drawing it closer to Newtonian properties.

The rheology of these two samples are shown in Figure 78 (Appendix B). From the apparent viscosity graph – Figure 79 (Appendix B), the new slurry designs with fly ash inclusive shows the ability to withstand temperature. With an increase in temperature the neat Class H, neat Class G begun to decline steadily while all samples with fly ash and latex was able to withstand a rise in temperature. Figure 78 (Appendix B) also show that all slurry designs are thixotropic except samples with fly ash included. The addition of fly ash to the cement slurry makes it slightly Rheopectic in nature. Table 18 shows the rheological properties of the various tested cement slurries.

Table 18. Rheological Properties of Tested Cement Slurries						
	Neat Class H	Class H cement, 30% Flyash and 1% latex	Class H, 0.5% nanomaterial	Neat Class G	Class H, 30% fly ash, 1 gal/sack latex 0.5% nanomaterial	Class H, 1.5 liters/100 kg commercial additive
Shear Stress (Pa)						
Shear Rate (1/s)						
1021.3809	161.32	107.60	131.58	58.32	120.34	105.66
510.9969	82.32	71.44	76.38	40.40	70.28	70.56
340.6986	53.64	57.50	58.14	34.24	53.74	55.84
170.2982	38.64	44.58	44.22	27.10	38.90	42.32
10.2138	7.98	14.26	9.840	8.68	13.36	12.98
5.1069	6.14	10.94	6.90	4.14	10.30	7.64
Apparent Viscosity Profile (255.4 s-1) from Room Temperature to 102°F						

Gas Transit time

Static gel strength (SGS) is measured using a cement consistometer. It is calculated by the geometry and slow motion of the consistometer paddle (10°). This slow movement allows SGS to be measured but does not inhibit gel strength development. Sabins (1982) estimated that transition time ends when the cement slurry has developed SGS exceeding 250 Pa (522 lbf/100 ft²). Generally, gas transit time is the time it takes for a cement slurry to move from 100 lbf/100 ft² to 500 lbf/100 ft².

From the Table 26, Neat class H takes 1.05 hours to reach 100 lbf/100 ft² and 2.3228 hours to reach 500 lbf/100ft². The slurry with a combination of Class H cement, 30% flyash and 1 gal/sack latex takes 0.2689 hours to reach 100 lbf/100 ft². It also takes the same slurry 0.7228 hours to attain 500 lbf/100 ft². The gas transit time of these two slurries as displayed in the Figure 71. The shorter gas transit time in the new slurry mixture provides better properties in mitigating gas flow through the cement slurry. With the addition of 30% flyash and 1 gal/sack latex, we were able to reduce the gas transit time by almost 1 hour, making the new slurry design desirable. The new slurry design with 30% flyash and 1 gal/sack latex proved to be a better substitute to neat Class H. It had a leak time of 21 minutes 26 secs in a 2-inch pipe while neat Class H proved to prevent gas flow for only 5 minutes.

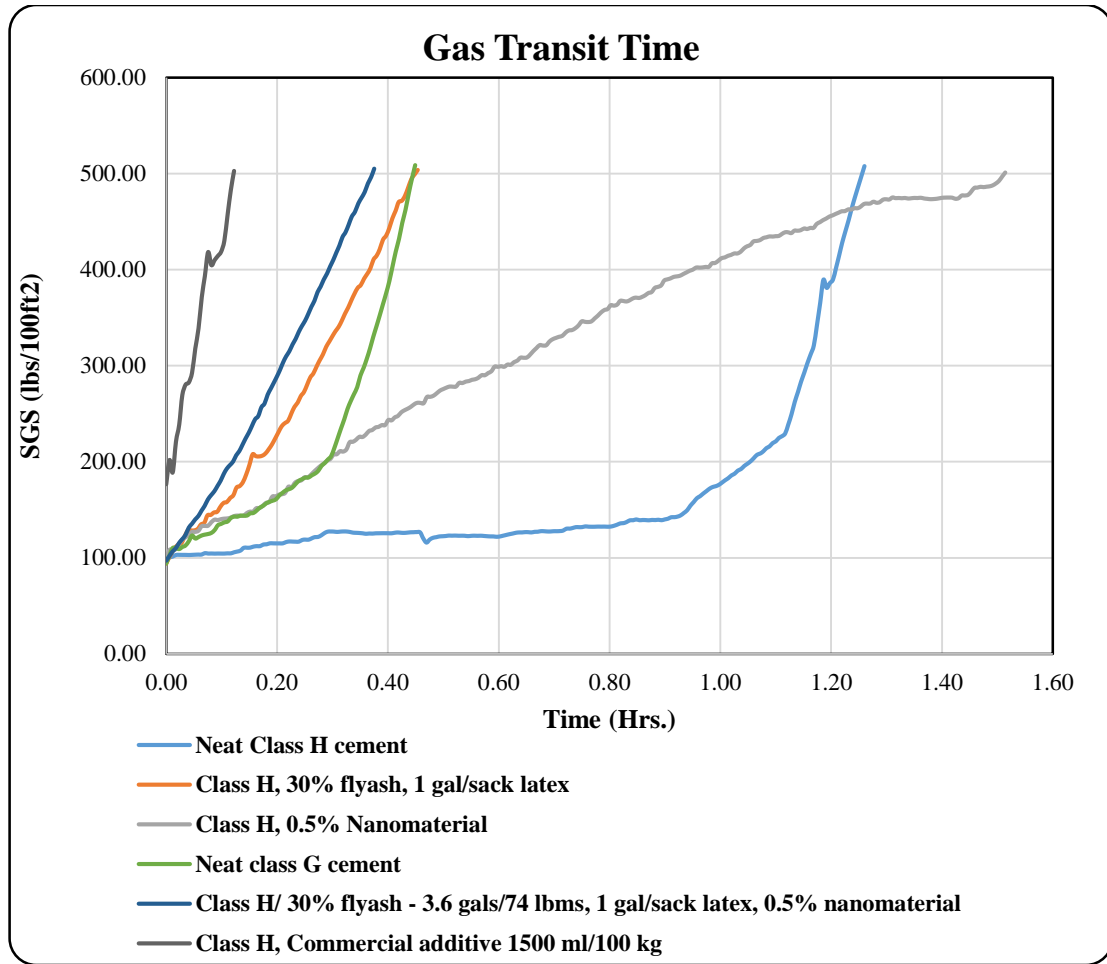


Figure 71: Gas Transit time for various slurry samples.

The Figure 71 also shows that Class H with 0.5% nanomaterial inclusive has a better gas transit time compared to neat Class H. Once again, we see this slurry design show better performance with an improved leak time of 9 minutes 54 secs. From the Table 26 it is observed that these two new slurries also attain a static gel strength (SGS) of 100 lbf/100 ft² and 500 lbf/100 ft² earlier than neat Class H.

At this point, we can conclude that a slurry with a shorter gas transit time, a shorter time to reach 100 lbf/100 ft², and a shorter time to attain 500 lbf/100 ft² has a better ability to mitigate gas migration. However, we are unable to stop here. The final slurry tried was a combination of neat Class H, 30% (BWOC) flyash, 1 gal/sack latex and 0.5% (BWOC)

nanomaterial. It takes this slurry design 12.5 minutes (0.2089 hrs.) to attain an SGS of 100 lbf/100 ft² and 35 minutes to attain an SGS of 500 lbf/100 ft². We also see the gas transit time (time to move from 100 lbf/100 ft² to 500 lbf/100 ft²) to be 22 minutes 30 seconds. However, we see a negative performance of this slurry design from the experiments conducted. The leak time for this slurry design was recorded as 1 min 14 secs. With the addition of 1.5 liters/ 100 kg of commercial additive, it is observed that the gas transit time or transition time is reduced to 7 minutes 19 seconds. This has been the least recorded time. From the experiments we observe

Unconfined Compressive Strength and Ultrasonic Testing

The unconfined compressive strength (UCS) is the maximum axial compressive stress that a right-cylindrical or cubic sample of material can withstand under unconfined conditions (zero confining stress). For this study all materials were set cement samples. UCS is also known as the uniaxial compressive strength of the material (cement cubes) because the application of compressive stress is only along one axis — the longitudinal axis—of the sample. In an ultrasonic compressive-strength test, a high-frequency sound pulses to a cement slurry sample and measures the length of time required for the sound wave to travel completely across the lateral dimension of the sample. This generates an ultrasonic pulse velocity (UPV). With the hardening or setting of cement, the wave travels faster, thus taking a shorter time to reach the other end of the sample. This transit time data helps to plan a cementing schedule for a well.

In this thesis, an ultrasonic cement test and unconfined compressive strength were carried out for 1 and 3 days on varied samples that have been used in Setup 1 and Small

Setup. This was done to provide a holistic picture of the performance of cement slurries used for testing. Using procedures according to API 10B, cubical cement samples were prepared for both UPV and UCS testing. The cylinders were cored out of the 2" × 2" cubes, using a 1-inch diamond impregnated coring bit. Figure 80 (Appendix B) displays samples being cured for UCS and Ultrasonic testing while Figure 81 (Appendix B) shows a UPV test being carried out on an experiment sample. Table 19 shows the Ultrasonic Pulse Velocity (UPV) readings obtained from the ultrasonic cement tests.

Table 19: Ultrasonic Pulse Velocity (UPV) and Unconfined Compressive Strength (UCS) test results reported.

	Day	UPV	UCS
Neat Class H	1	2191.69	4.00
	3	2972.17	15.36
Neat Class G	1	2915.39	15.34
	3	3406.41	28.36
Class H, Nanomaterial	1	2369.56	6.09
	3	3123.44	19.66
Class H, Flyash, latex Nanomaterial	1	1888.46	1.69
	3	2686.24	6.41

For the unconfined compressive strength (UCS) tests, a Test Mark Compressive Strength machine is used. A uniaxial force is applied to the cement matrix till it fails in shear. The point where a maximum stress is applied on the body is termed as the UCS of the sample. UCS testing is performed of all three samples for the same day of testing and the average of these values if the strength of the set cement at the day of testing. For an example, if a 1-day test is being conducted on a neat Class H sample, three different cubes

cured for one day are selected. A UCS test is performed on each sample and the average of these three values represents the day-1 unconfined compressive strength of the set cement. The 1-day and 3-day compressive strengths of various samples are reported in Table 19. From Table 19 we observed an increase in UCS for all Class H base slurry designs. This increase was in the range of 220% to 285% for a period of 1 day to 3 days of testing. The addition of additives like nanomaterial and flyash reduces the compressive strength increase in these slurries.

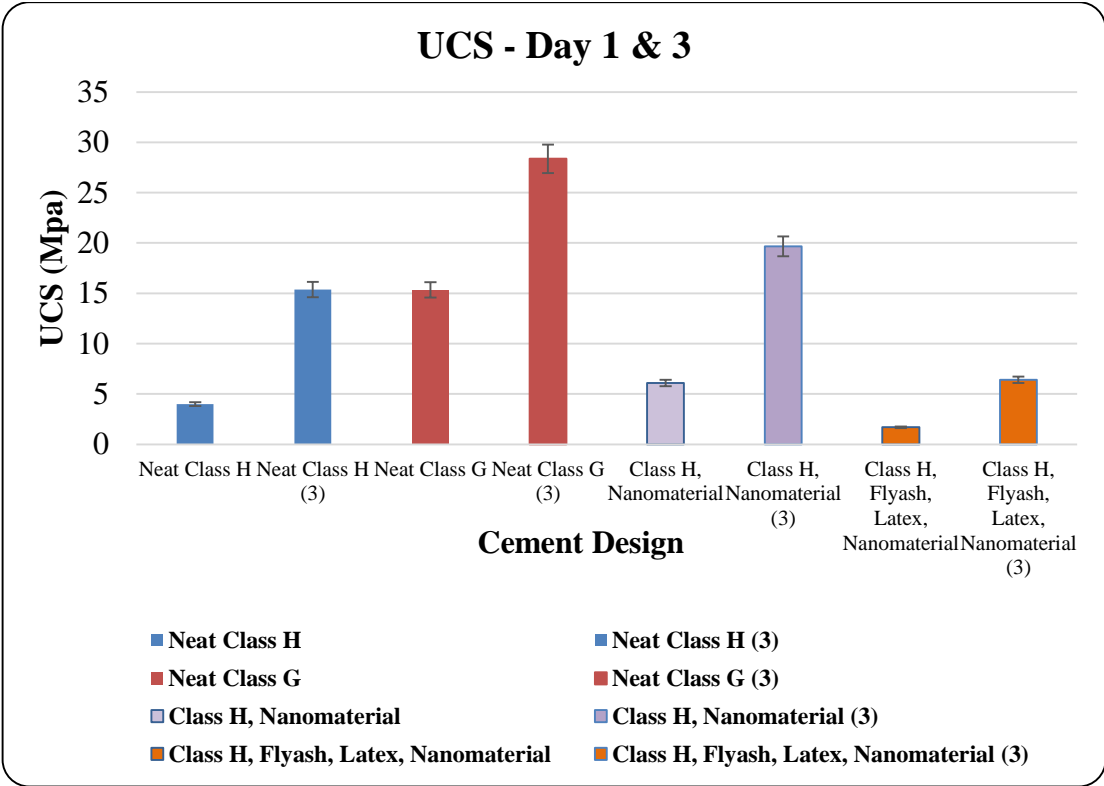


Figure 72: Days 1 and 3 results for Unconfined Compressive Strength (UCS) tests.

From Figure 72 we observe that the addition of 0.5% nanomaterial to the slurry design improves the initial compressive strength of the new slurry. A 52.3% increase in Day 1 compressive strength is recorded with an addition of 0.5% nanomaterial. However, the late time effect of nanomaterial is not as significant as the early time improvement.

An increase in 28% is recorded in the Nanomaterial cement slurry design for Day 3 UCS testing. This increase is in relation to the base Class H cement slurry after the third day of UCS testing. The addition of latex, nanomaterial, and fly ash does not improve the UCS test values. The light weight of the fly ash and the latex negatively affects the compressive strength of the cement slurry. Aside the recorded decrease in density the new slurry design decreases the compressive strength by 57.75% in the first day of testing and 58.27% by the third day of testing. Comparing Class H and Class G cement slurries; Class G proves to provide better compressive strength in both first and third days of UCS testing. A 283.5% increase in UCS strength is recorded in the first day of testing, proving Class G cement to be superior to class H in compressive strength performance.

Chapter 5: Summary and Conclusions

The following conclusions and proposed recommendations are drawn from the experimental investigations and obtained results:

Elastomer Experiment Conclusions and Summary

Some conclusions drawn from the elastomer aging experiments include:

- Physical and chemical degradation of elastomers occur when exposed to testing conditions.
- The degree of chain growth and chain rupture depends on temperature and degree of chemical exposure.
- NBR exhibited the most significant deterioration.
- Viton showed the least amount of degradation but has poor decompression resistance.
- CO₂ showed the most damaging effect of all corrosive gases.
- Hardness is inversely proportional to volumetric swelling and compression.
- For all samples, the general order of corrosive gas effect on elastomer degradation is CO₂>All gases>H₂S>CH₄.
- Statistical analysis indicates that exposing an elastomer to the least corrosive condition (1 day in vapor phase at 120 °F) is enough to cause its sealing integrity to be compromised appreciably. However, this cannot be extended to higher temperature conditions (greater than 180 °F) due to unavailability of experimental data.

Cement Experiment Summary and Conclusions

Some conclusions drawn from the cement gas migration section include:

- Cement sheath alone (without anti-gas migration additives) is inadequate as a primary well barrier.
- Effective permeability decreases by the hundredth ($0.CX$ md) with an increase in cement hydration (C – constant value, X – varying value based on cement age).
- Within a cycle, both the migrating gas pressure and cement permeability increases. This behavior is attributed to a rising existence of residual gas pressure in the cement sheath from one test to the next test within the cycle.
- Keeping all factors constant and the system fully vented, an increase in cement age corresponds to a decrease in system permeability.
- A 12-hour wait on cement (WOC) is inadequate for cement to develop enough gas mitigation abilities since Setup 1 Experiment 2 (S1E2 - 12 hr. WOC) showed the maximum number of leak paths for S1E2.
- Cement sheath deterioration is proportional to the degree of ballooning.
- After cement is damaged it remains damaged.
- Partially densified and densified microsilica behave as inert materials in the cement formulation thus, they do not provide the performance required for adequate zonal isolation as is expected of microsilica cement.
- Vibration period may be a key factor in cement – casing bonding.
- 30% BWOC fly ash and 1 gal/sack latex proved to mitigate gas flow significantly.
- The inclusion of nanomaterial improves the gas mitigation abilities of set cement.
- Cement with 30% fly ash and 1 gal/sack latex proves to be a slurry design that mitigates gas percolation, its low density may also make it desirable in shallow wells, however, it has a low compressive strength even after 3 days of curing.

- Nanomaterial even at low concentrations of 0.5% BWOC improved 1-day compressive strength significantly.
- A slurry with a shorter gas transit time has a better ability to mitigate gas migration.
- 1.5 liters / 100 kg of commercial additive is adequate in mitigating gas migration completely.

Recommendations

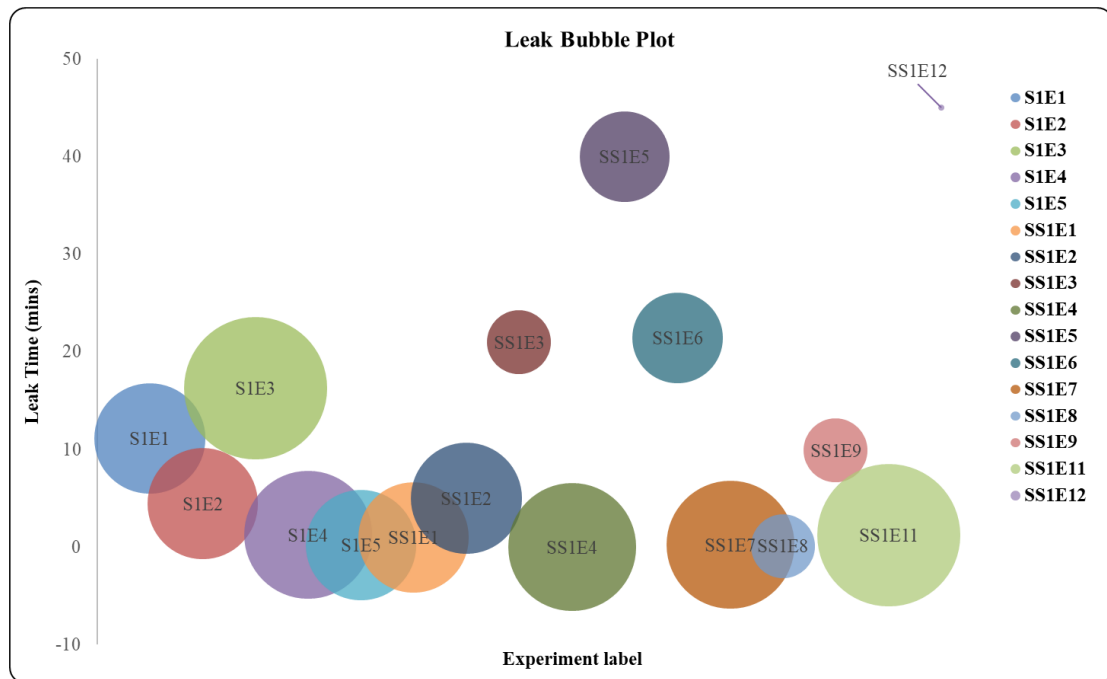
- It is recommended to test sealing systems for exposed downhole condition (gas/liquid, temperature, and pressure) before using them and considering them “fit for service”.
- All the tests in this study are limited to 180 °F. To have a better understanding of elastomer behavior in HPHT conditions, it is recommended to conduct some tests at higher temperature.
- In gas prone regions, a gas tight cement is binding since neat cement cannot mitigate gas flow.
- More studies should be made in relation to cement curing since this plays a major role in cement hydration and future performance.
- More slurry formulations should be experimented upon for a suitably cost-effective gas tight slurry.
- Additives like carbon black should be experimented on.

Table 20. Leak time for Major and Minor Setups

Leak time for Major Setups						
Setup Experiment	WOC (hrs.)	Density (ppg)	Composition	Leak time (mins:secs)	Bubbling description	
S1E1	24	16.65	Neat Class H	11 mins 08 secs	3	
S1E2	12	16.65	Neat Class H	4 mins 28 secs	3	
S1E3	24	12.5	3 gals/sack latex, 1% bentonite	16 mins 17 secs	5	
S1E4	24	16.65	Neat Class H	1 mins 14 secs	4	
Leak time for Minor Setups						
Setup Experiment	WOC (hrs.)	Density (ppg)	Composition	Leak time (mins:secs)	Bubbling description	
SS1E1	24	16.65	Neat Class H	1 min	3	
SS1E2	24	16.65	Neat Class H	5 mins	3	
SS1E3	24	16.65	1 gal/sack latex, 0.5% bentonite	21 mins	1	
SS1E4	24	17.5	Neat Class H	1 sec	4	
SS1E5	24	17.5	Neat Class H	6 days +	2	
SS1E6	24	14	1 gal/sack latex, 30% flyash	21 mins 26 secs	2	
SS1E7	24	16.05	5.5% microsilica	15 secs	4	
SS1E8	24		12% microsilica	7 secs	1	
SS1E9	24	16.55	0.5% nanomaterial	9 mins 54 secs	1	
SS1E11	24	14.5	1 gal/sack latex, 30% fly ash, 0.5% nanomaterial	1 min 14 secs	5	
SS1E12	24	16.4	1.5 liters/ 100 kg commercial additive from a service company	N/A	0	

1 - Tiny inconsistent bubbling, 2 - Tiny consistent bubbling, 3 - Regular bubbling, 4 - Intense bubbling with multiple locations.

Figure 73 depicts the bubble graph for Table 20. The level at which the center of the bubble stands represents the leak time of that particular experiment. The size of the bubble stands represents the leak time of that particular experiment. The size of the bubble in the bubble graphs indicates the degree of bubbling. The bubbling degree is on a scale of 1 to 5. '1' indicating tiny consistent bubbling, whereas '5' indicates intense bubbling with multiple locations. The bubble graph just provides a pictorial view of the experiments conducted in this Thesis.



S – Small, S – Setup number, E – Experiment number

Figure 73: Bubble graph to depict leak time for major and minor tests

Abbreviation

ACN	–	Acrylonitrile
atm	–	atmosphere
Bc	–	Bearden units of consistency
BOP	–	Blow out preventer
BSEE	–	Bureau of Safety and Environmental Enforcement
BWOC	–	By weight of cement
BWOW	–	By weight of water
CSR	–	Compression stress relaxation
EDS	–	Energy dispersive spectroscopy
ELES	–	Ethoxylated lauryl ether
ENP	–	Ethoxylated nonyl phenols
EPDM	–	Neoprene ethylene propylene diene monomer
°F	–	Degree Fahrenheit
FEPM	–	Fluorocarbon/ Tetrafluoro ethylene/ Propylene rubber
FFKM	–	Perfluoroelastomer
FKM	–	Fluoroelastomer
ft ²	–	squared feet
GoM	–	Gulf of Mexico
HFA	–	Hydraulic fluid
HNBR	–	Hydrogenated Nitrile Butadiene Rubber
hrs.	–	hours
IIR	–	Butyl rubber
in	–	inch
ITZ	–	Interfacial-transition zone
lbm	–	pound mass
lbf	–	pound force
LFC	–	Lightweight foamed cement
LOWC	–	Loss of well control
MCSA	–	Mud cake solidification agent
min	–	minute
ml	–	milliliter
MMS	–	Mineral Management Service
MWD	–	Measurement while drilling
NAF	–	Non-aqueous fluid
NBR	–	Nitrile Butadiene Rubber
NCS	–	Norwegian Continental Shelf
NR	–	Natural rubber
OBM	–	Oil based mud

OCS	–	Outer Continental Shelf
PDM	–	Positive displacement motor
ppm	–	parts per million
PSA	–	Petroleum Safety Authority
PSD	–	Particle size distribution
psi	–	pounds per square inch
QC-FIT	–	Quality Control – Failure Incident Team
RGD	–	Rapid gas decompression
ROP	–	Rate of penetration
SAP	–	Super absorbent polymer
SBC	–	Styrenic block copolymer
SBR	–	Styrene butadiene rubber
SEM	–	Scanning electron microscope
SWF	–	Shallow Water Flow
T _g	–	Glass transition temperature
TPO	–	Thermoplastic elastomer
WOC	–	Wait on cement

References

- Abbas, G., Irawan, S., Kumar, S., Khan, M. N., & Memon, S. (2013, November 26). Gas Migration Prevention Using Hydroxypropylmethylcellulose as a Multifunctional Additive in Oil Well Cement Slurry. Society of Petroleum Engineers. <https://doi.org/10.2118/169643-MS>.
- Adams, N. J., Kuhlman, L. G. 1990. Case History Analyses of Shallow Gas Blowouts. Presented at the IADC/SPE Drilling Conference, Houston, Texas, February 27 - March 2. IADC/SPE 19917. *Society of Petroleum Engineers*. <http://dx.doi.org/10.2118/19917-MS>
- Ahmed R., Shah S., Osisanya S., Hassami S., Omosebi O., Elgaddafi R., Maheshwari H., Srivastava A., Hwang J., Sharma M., Tale S., Jeon J. 2015. Effects of H₂S and CO₂ in HPHT Wells on Tubulars and Cement. BSEE Project #E12PC00035, The University of Oklahoma.
- Al-Buraik, K., Al-Abdulqader, K., Bsaiibes, R. 1998. Prevention of Shallow Gas Migration through Cement. *Society of Petroleum Engineers*. <https://doi.org/10.2118/47775-MS>.
- Al-Yami, A. S., Nasr-El-Din, H. A., & Al-Humaidi, A. S. (2009, January 1). An Innovative Cement Formula to Prevent Gas-Migration Problems in HT/HP Wells. Society of Petroleum Engineers. <https://doi.org/10.2118/120885-MS>.
- API Standard 65 – Part 2. 2010. Second Edition. Isolating Potential Flow Zones During Well Construction. December 2010.
- Badrak, R. P. 1994. Effects of New Generation Drilling Fluids on Drilling Equipment Elastomers. Presented at SPE/ASDC Drilling Conference, 15-18 February, Dallas, Texas. *Society of Petroleum Engineers*. SPE-27452-MS <http://dx.doi.org/10.2118/27452-MS>
- Bannister, C. E., Shuster, G. E., Wooldridge, L. A., Jones, M. J., and Brich, A. G. 1983. Critical Design Parameters to Prevent Invasion During Cementing Operations. *Society of Petroleum Engineers*. <https://www.onepetro.org/download/conference-paper/SPE-11982-MS?id=conference-paper%2FSPE-11982-MS>.
- Beirute, R. M., Cheung, P. R. 1990. Method for Selection of Cement Recipes to Control Fluid Invasion after Cementing. *Society of Petroleum Engineers*. <https://doi.org/10.2118/19522-PA>.
- Bogaerts, M., De Bruijn, G. G., Khalilova, P. R., Moretti, F., and Voon, E. 2012. Identifying and Mitigating the Risks of Shallow Flow in Deepwater Cementing Operations. Society of Petroleum Engineers. <https://doi.org/10.2118/155733-MS>
- Bois, A., Vu, M., Galidiolo G., Badalamenti, A. 2017. Use of Advanced Gas Migration Model to Optimize Zonal Isolation. AADE-17-NTCE-104. <http://www.aade.org/technical-papers/2017-national-technical-conference-papers/>.

- Bortsov VP, Baluev AA, Bastrikov SN. 1997a. Plugging solution for oil and gas wells – contains portland cement, aluminium powder, fish scale, anionic and nonionic surfactant, plasticiser and water, RU patent 2 078 906, assigned to Sibe Oil Ind. Res. Inst.; 1997.
- Bortsov VP, Baluev AA, Bastrikov SN. 1997b. Plugging solution for oil and gas wells – contains portland cement, expanding additive, water and additionally aluminium powder, surfactants and plasticiser, RU patent 2 082 872, assigned to Sibe Oil Ind. Res. Inst.; 1997.
- Bosma, Martin Genrard Rene, Cornelissen, Erik Kerst, Cuijpers, Juul, Picchioni, Francesco, Rastogi, Sanjay. 2006. *System for sealing a space in a wellbore*. EP 1 649 136 B1. <https://data.epo.org/publicationserver/rest/v1.0/publicationdates/20061018/patents/E P1649136NWB1/document.pdf>
- Bour, D. L. and Wilkinson, J. G. 1992. Combating Gas Migration in the Michigan Basin. *Society of Petroleum Engineers*. <https://doi.org/10.2118/19324-PA>.
- Bourgoyne A. T., Rocha L., Bender C., Bourgoyne D. 1995. Analysis of Platform Vulnerability to Cratering Induced by a Shallow Gas Flow. *Petroleum Engineering Department. Louisiana State University*.
- Brace, W. F., Walsh, J. B., Frangos, W. T. 1968. Permeability of granite under high pressure. *Journal of Geophysical Research*. <http://dx.doi.org/10.1029/JB073i006p02225>.
- BSEE 2015a, Investigation into the January 30, 2014 Loss of Well Control Lease OCS-G 17921, Vermilion Block 356, Well A-007. OCS report BSEE 2015-01. U.S. Department of the Interior, Bureau of Safety and Environmental Enforcement.
- BSEE 2015b, Investigation of Loss of Well Control and Fire South Timbalier Area Block 220, Well No. A-3, OCS-G 24980, July 2013. OCS report BSEE 2015-02. U.S. Department of the Interior, Bureau of Safety and Environmental Enforcement.
- BSEE. Bureau of Safety and Environmental Enforcement. 2014. QC-FIT evaluation of fastener failures addendum. https://www.bsee.gov/sites/bsee_prod.opengov.ibmcloud.com/files/memos/public-engagement/qc-fit-bp-bolts-report-final.pdf.
- Calloni, G., Moroni, N., & Miano, F. (1995, January 1). Carbon Black: A Low Cost Colloidal Additive for Controlling Gas-Migration in Cement Slurries. *Society of Petroleum Engineers*. <https://doi.org/10.2118/28959-MS>.
- Carter, L. G., Cook, C., Snelson, L. 1973. Cementing Research in Directional Gas Well Completions. *Society of Petroleum Engineers*. <https://doi.org/10.2118/4313-MS>.
- Carter, L. G., Waggoner, H. F., and George, C. 1966. Expanding Cements for Primary Cementing. *Society of Petroleum Engineers*. <http://dx.doi.org/10.2118/1235-PA>.

- Chen, X., Bartos, J., Salem, H., and Zonoz, R. 2016. Elastomers for High Pressure Low Temperature HPLT Sealing. Presented at Offshore Technology Conference held in Houston, USA, 2-5 May 2016. OTC-27227-MS. <http://dx.doi.org/10.4043/27227-MS>
- Cheung, P. R., and Beirute, R. M. 1985. Gas Flow in Cements. *Society of Petroleum Engineers*. <http://dx.doi.org/10.2118/11207-PA>.
- Cheung, P. R., and Myrick, B. D. 1983. Field Evaluation of an impermeable Cement System for Controlling Gas Migration. *Society of Petroleum Engineers*. <http://dx.doi.org/10.2118/11983-MS>.
- Christian, W. W., Chatterji, J., Ostroot, G. W. 1976. Gas Leakage in Primary Cementing – A Field Study and Laboratory Investigation. *Journal of Petroleum Technology*. V. 28, No. 11. 1361-1369.
- Cong C. B., Cui C. C., Meng X. Y. 2013. Degradation of hydrogenated nitrile-butadiene rubber in aqueous solutions of H₂S or HCl, Chem. Res. Chin. Univ. 29 (2013) 806-810. <http://dx.doi.org/10.1007/s40242-013-2401-7>
- Cook, C., Cunningham, W. C. 1977. Filtrate Control - A Key in Successful Cementing Practices. Society of Petroleum Engineers. <https://doi.org/10.2118/5898-PA>.
- Cooke, C. E., Kluck, M. P., Medrano, R. 1983. Field Measurements of Annular Pressure and Temperature during Primary Cementing. *Society of Petroleum Engineers*. <https://doi.org/10.2118/11206-PA>.
- Cowan, K. M., & Eoff, L. (1993, January 1). Surfactants: Additives To Improve the Performance Properties of Cements. Society of Petroleum Engineers. <http://dx.doi.org/10.2118/25181-MS>
- Dajiang, K., Yuanhua, L., Huali, Z., Yufei, L., Lin, Z., Kuanhai, D. 2017. Experimental studies on CO₂ corrosion of rubber materials for packer under compressive stress in gas wells, (2017), doi:10.1016/j.engfailanal.2017.01
- Danenberger, E. P. 1993. Outer Continental Shelf Drilling Blowouts, 1971-1991. *Offshore Technology Conference*. <http://dx.doi.org/10.4043/7248-MS>.
- Daou, F., & Piot, B. M. (2009, December 1). Cement-Slurry Performance and Set-Cement Properties vs. Microsilica Densification. Society of Petroleum Engineers. <http://dx.doi.org/10.2118/112701-PA>.
- Davies, O. M., Arnold, J.C., Sulley, S. 1999. The mechanical properties of elastomers in high-pressure CO₂. *Journal of materials Science*, 34, 417-422. <http://dx.doi.org/10.1023/A:1004442614090>
- Davis, T. W., and McCrady, D. D. 2008. Using Swellable Packers to Provide Annular Isolation for Multistage Fracture Treatments. Society of Petroleum Engineers. doi:10.2118/115775-MS <http://dx.doi.org/10.2118/115775-MS>

- Dean, G. D., and Brennen, M. A. 1992. A Unique Laboratory Gas Flow Model Reveals Insight To Predict Gas Migration in Cement. *Society of Petroleum Engineers*. <http://dx.doi.org/10.2118/24049-MS>.
- DeBruijn, G.; Skeates, C. et al. 2008. High pressure, high temperature technologies, *Oil Review* 20 (03): 46-60. Elliott, J. 2014. Diffusion in Polymers, Course M6-Lecture 6. http://people.ds.cam.ac.uk/jae1001/cus/teaching/materials/M6_lecture_6.pdf
- Drecq, P., and Parcevaux, P. A. 1988. A Single Technique Solves Gas Migration Problems Across a Wide Range of Conditions. *Society of Petroleum Engineers*. <http://dx.doi.org/10.2118/17629-MS>.
- Drobny, J.G., 2014. Handbook of thermoplastic elastomers. Elsevier.
- Dylan Moore. 2015. http://www.cementkilns.co.uk/images/cem_psd.png.
- Eaton, L. F. 1999. Drilling Through Deepwater Shallow Water Flow Zones at Ursa. *Society of Petroleum Engineers*. <https://doi.org/10.2118/52780-MS>.
- Eilers, L.H., Nelson, E.B. and Moran, L.K. 1983. High Temperature Cement Compositions – Pectolite, Scawtite, Truscotite or Xonoloite: Which Do You Want? *Journal of Petroleum Technology* 35 (7): 1373-1377.
- Encyclopaedia Britannica, 2009. Neoprene (CR) Chemical Compound. <https://www.britannica.com/science/neoprene>. Published July 20, 1998. Article revised and updated July 22, 2009. (Accessed June 3, 2017).
- Eriks Seals and Plastics (2017), Eriks O-ring Technical Handbook
- Evans, H. P. 1984. La tecnica efectiva para cementacion primaria en pozos de gas. Cuarto Congreso Latinoamericano de Perforacion, Caracas, Venezuela (October 1-5, 1984)
- Faul, R., Reddy, B. R., Griffith, J., Fitzgerald, R., and Waugh, B. 2000. Next-Generation Cementing Systems to Control Shallow Water Flow. Offshore Technology Conference. <https://doi.org/10.4043/11977-MS>
- Fernández, C., and Castaño, P. 2016. Compatibility Behavior of Elastomers for PCP Applications. *NACEI international*. NACE-2016-7106. <https://www.onepetro.org/conference-paper/NACE-2016-7106>
- Garcia, J. A., and Clark, C. R. 1976. An Investigation of Annular Gas Flow Following Cementing Operations. *Society of Petroleum Engineers*. <http://dx.doi.org/10.2118/5701-MS>.
- Garcia, J. A., Clark, C. R. 1976. An Investigation of Annular Gas Flow Following Cementing Operations. *Society of Petroleum Engineers*. <https://doi.org/10.2118/5701-MS>.

- Gavioli, P., Vicario, R. 2012. The Evolution of the Role of Openhole Packers in Advanced Horizontal Completions: From Novel Technology to a Critical Key to Success. *Society of Petroleum Engineers*. <http://dx.doi.org/10.2118/132846-PA>
- Grabowski, E. and Gillott, J. E. 1989. Effect of Replacement of Silica Flour with Silica Fume on Engineering Properties of Oil Well Cements at Normal and Elevated Temperatures and Pressures, *Cement and Concrete Research*, Vol. 19, pp 333-344.
- Grinrod, M., Vassoy, B., & Dingsoyr, E. O. (1988, January 1). Development and Use of a Gas-Tight Cement. *Society of Petroleum Engineers*. <http://dx.doi.org/10.2118/17258-MS>.
- Guidroz, B. C., Barton, S. P., and Hussain, M. 2011, January 1. Can You Protect Your Motor Without Sacrificing Performance? *Society of Petroleum Engineers*. SPE-146575-MS. <http://dx.doi.org/10.2118/146575-MS>
- Harder, C., Carpenter, R., Wilson, W., Freeman, E., and Payne, H. 1992. Surfactant/Cement Blends Improve Plugging Operations in Oil-Base Muds. *Society of Petroleum Engineers*. <http://dx.doi.org/10.2118/23928-MS>
- Hartoni, A., Hobson, B., Huizenga, R., and Helmana, M. 2000. A Single Slurry System for Cementing Surface Casing in a Low Fracture Gradient Shallow Gas Area Off Shore Kalimantan. *Society of Petroleum Engineers*. <https://doi.org/10.2118/62747-MS>
- Hibbeler, J. C., DiLullo, G., and Thay, M. 1993. Cost-Effective Gas Control: A Case Study of Surfactant Cement. *Society of Petroleum Engineers*. <http://dx.doi.org/10.2118/25323-MS>.
[http://dx.doi.org/10.1016/0008-8846\(83\)90064-9](http://dx.doi.org/10.1016/0008-8846(83)90064-9).
- Huerta J. N., Hesse A. M., Bryant S. L., Strazisar B. R., Christina L. L. 2012. Experimental Evidence for Self-Limiting Reactive Flow through a Fractured Cement Core: Implications for Time-Dependent Wellbore Leakage. *Environmental Science & Technology*. <https://doi.org/10.1021/es3013003>.
- James Walker, 2012. Elastomeric Seals and Components for the Oil and Gas Industry Issue 10.1
- Jin Hyun-Ho, Hong Chang-Kook, Cho Dong-Lyun, and Kaang Shin-Young; (2008) Effects of Temperature on Hardness of Rubber Materials with Different Curing System. *Elastomers and Composites* vol. 43 (4), 213-220.
- Kelessidis, V. C., Fraim, M., Fardis, M., Karakosta, E., Diamantopoulos, G., Arkoudeas, P., Elhardalo, S., Lagkaditi, L., Papavassiliou, G. 2014. Comprehensive Assessment of Additive and Class G Cement Properties Affecting Rheology, Fluid Loss, Setting Time and Long Term Characteristics of Elastic Cements. *Society of Petroleum Engineers*. <http://dx.doi.org/10.2118/167731-MS>

- Killian Paul. 2014. Understanding TPEs- RTP Company. 9 March 2014. <https://www.rtpcompany.com/wp-content/uploads/2014/03/Understanding-TPEs.pdf>
- Kubena, E., Ross, K. C., Pugh, T., and Huycke, J. 1991. Performance Characteristics of Drilling Equipment Elastomers Evaluated in Various Drilling Fluids. *Society of Petroleum Engineers*. SPE-21960-MS. <http://dx.doi.org/10.2118/21960-MS>
- Kucyn, P. V. et al. 1997. Prevention des manifestations du gaz entre le tubage et les parois du puits et de l'eruption incontrolee au cours du forage. *Gazovaja Promyshlennost*. Translated from Russian.
- Kuksov AK, Krezub AP, Mariampolskij NA, Ryabova LI, Lyshko GN, Loskutov DA, et al. Oil and gas borehole plugging solution reagent – contains brown coal treated with alkali, organic silicon compound and lignosulphonate. SU patent 1 719 618, assigned to Borehole Consolidation Mu.; 1992.
- Lea, F.M. 1971. *The Chemistry of Cement and Concrete*, third edition, Chemical Publishing Co., New York City, 177-202.
- Levine, D. C., Thomas, E. W., Bezner, H. P., and Tolle, G. C. 1979. Annular Gas Flow after Cementing: A Look at Practical Solutions. *Society of Petroleum Engineers*. <http://dx.doi.org/10.2118/8255-MS>.
- Martinez J., and McDonal J. M. 1980. Study of Cementing Practices Applied to the Shallow Casing in Offshore Wells. National Energy Technology Laboratory. <http://www.netl.doe.gov/kmd/CDs/Disk17/C%20-%20Drilling%20Completion%20Stimulation/DOE%20BETC%202273%201.pdf>
- Matthew, S. M., and Copeland, J. C. 1986. Control of Annular Gas Flow in the Deep Anadarko Basin. *Society of Petroleum Engineers*. <http://dx.doi.org/10.2118/14980-MS>.
- MMS Safety Alert. U.S. Department of the Interior Minerals Management Service, Gulf of Mexico OCS Region. Safety Alert No. 216. October 22 2003. <https://www.bsee.gov/sites/bsee.gov/files/safety-alerts/safety/safety-alert-no-216.pdf>
- Morgan, G.; Clarke, P. et al. 2014. Challenges of temperature extremes for elastomers materials. Presented at High Performance Polymers for Oil and Gas 2014, Edinburgh, Scotland, 15-16 April.
- Nelson B. E., Guillot D. 2006. *Well Cementing*. Second Edition. Schlumberger, Sugar Land, Texas 77478.
- NORSOK Standard D-010. 2014. Well integrity in drilling and well operations. (Rev. August 3, 2014) <http://www.standard.no/pagefiles/1315/d-010r3.pdf>.
- O'Leary, J., Flores, J. C., Rubinstein, P., and Garrison, G. 2004. Cementing Deepwater, Low-Temperature Gulf of Mexico Formations Prone to Shallow Flows. *Society of Petroleum Engineers*. <https://doi.org/10.2118/87161-MS>

- Overney R. M., Buenviaje C., R. Luginbuhk and F. Dinelli. 2000. Glass and Structural Transitions Measured at Polymer Surfaces on the Nanoscale. *Journal of Thermal Analysis and Calorimetry*, Vol. 59 (2000) 205-225. <http://citeseerx.ist.psu.edu/viewdoc/download?doi=10.1.1.530.124&rep=rep1&type=pdf>
- Parcevaux, P. A., and Sault, P. H. 1984. Cement Shrinkage and Elasticity: A New Approach for a Good Zonal Isolation. *Society of Petroleum Engineers*. <http://dx.doi.org/10.2118/13176-MS>.
- Parcevaux, P. A., Sault, P. H. 1984. Cement Shrinkage and Elasticity: A New Approach for a Good Zonal Isolation. *Society of Petroleum Engineers*. <http://dx.doi.org/10.2118/13176-MS>.
- Pervez T, Qamar SZ, van de Velden M. 2012. Comparison between Fresh and Exposed Swelling Elastomer *Journal of Elastomers and Plastics*, Vol. 44, No. 3, May 2012, p 237–250 <http://dx.doi.org/10.1177/0095244311420530>
- Petroleum Engineer's Guide - Chapter 10 - Cement additives, In Petroleum Engineer's Guide to Oil Field Chemicals and Fluids (Second Edition), edited by Johannes Fink,, Gulf Professional Publishing, Boston, 2015, Pages 317-367, ISBN 9780128037348, <https://doi.org/10.1016/B978-0-12-803734-8.00010-2>.
- Pinto H. V. P. Gustavo, Rocha Marcelo S. José, Martins L. André, Petrobras. 2012. New Methodology for Gas Migration Prediction after Oilwell Cementing. AADE-12-FTCE-40. Presented in Houston, Texas, April 10-11 2012.
- Prince, P. K. 1990. Current Drilling Practice and the Occurrence of Shallow Gas. Society of Underwater Technology. SUT-AUTOE-v25-003. <https://www.onepetro.org/conference-paper/SUT-AUTOE-v25-003>
- PSA. Petroleum Safety Authority Norway. 2011. Annual Report. http://www.nsd.uib.no/polsys/data/filer/aarsmeldinger/AE_2011_29603.pdf.
- Qamar SZ, Hiddabi SA, Pervez T, Marketz F. 2009. Mechanical Testing and Characterization of a Swelling Elastomer, *Journal of Elastomers and Plastics*, Vol. 41, No. 5, September 2009, p 415-431 <http://dx.doi.org/10.1177/0095244309105248>
- Qamar SZ, Pervez T, van de Velden M., Sanchez FJ. 2012. Design and Fabrication of Test Facility for Longevity Testing of Elastomer Seals. *AME 2012 International Mechanical Engineering Congress and Exposition in Houston, Texas, USA*, 9-15 November 2012. IMECE2012-93145. <http://dx.doi.org/10.1115/IMECE2012-93145>
- Rae, P. 1987. Cementing: Preventing Gas Migration during Setting. *Noroil* (March 1987) No. 3, 31.
- Rae, P., Wilkins, D., and Free, D. 1989. A New Approach to the Prediction of Gas Flow after Cementing. Society of Petroleum Engineers. <http://dx.doi.org/10.2118/18622-MS>.

- Roylance David. 2000. Atomistic Basis of Elasticity. Published 27 January 2000. *Massachusetts Institute of Technology*. http://web.mit.edu/course/3/3.11/www/modules/elas_2.pdf
- Rupak K. Khandka. 2007. *Leakage behind Casing*. Norwegian University of Science and Technology, Trondheim, Norway. (June 11, 2007).
- Sabins, F. L., and Sutton, D. L. 1986. The Relationship of Thickening Time, Gel Strength, and Compressive Strength of Oilwell Cements. Society of Petroleum Engineers. *Society of Petroleum Engineers*. <http://dx.doi.org/doi:10.2118/11205-PA>.
- Sabins, F. L., Tinsley, J. M., and Sutton, D. L. (1982, December 1). Transition Time of Cement Slurries between the Fluid and Set States. Society of Petroleum Engineers. <http://dx.doi.org/10.2118/9285-PA>.
- Salehi, S. 2013. Modelling Near Wellbore Leakage Pathways in Shale Gas Wells: Investigating Short and Long Terms Wellbore Integrity. Presented at US EPA Technical Workshop on Well Construction/Operation and Subsurface Modelling, April 16-17, US EPA Research Triangle Park, North Carolina
- Schweitzer P.A, 2000. Mechanical and Corrosion-Resistant properties of Plastics and Elastomers.
- Severine, A. E. B. and Grolier, J.P. E. 2005. Modification of the glass transition of polymers by high-pressure gas solubility, *Pure Appl. Chem.*, 77(7), 593-603. <http://dx.doi.org/10.1351/pac200577030593>
- Shakirah, S. (2008, January 1). A New Approach for Optimizing Cement Design to Eliminate Microannulus in Steam Injection Wells. International Petroleum Technology Conference. <https://doi.org/10.2523/IPTC-12407-MS>.
- Shiflet Ned, Dion O. Michael, Flores P. David. 2005. A practical Solution to Control Gas Migration. AADE-05-NTCE-71. Presented in Wyndam Greenspoint, Houston, Texas, April 5-7, 2005. <http://www.aade.org/technical-papers/2005national-technical-papers/>.
- Skalle, P., & Sveen, J. (1991, January 1). Emulsion Cement. Society of Petroleum Engineers. <http://dx.doi.org/10.2118/23075-MS>.
- Stiles, D. A., & Baret, J. F. (1993, January 1). Sedimentation and Free Water of Cement Slurries: Mathematical Models and Practical Solutions. Society of Petroleum Engineers. <https://doi.org/10.2118/25866-MS>.
- Stone, W. H., and Christian, W. W. 1974. "The Inability of Unset Cement to Control Formation Pressure" paper SPE 4783 presented at the SPE Symposium of Formation Damage Control, New Orleans, Louisiana, USA (February 7-8, 1974). <http://dx.doi.org/10.2118/4783-MS>.
- Sutton, D. L., Sabins, F. L., and Paul, R. 1984. New Evaluation for Annular Gas-Flow Potential. *Oil Gas Journal* (December 17 1984) No. 51, 109-112.

- Talabani, S., Hareland, G., and Islam, M. R. 1997. Gas Migration Eliminated Through Correct Cement Design Including Elastomers. *Society of Petroleum Engineers*. <http://dx.doi.org/10.2118/39279-MS>
- Tanaka, N. 2007. *World Energy Outlook 2007, China and India Insights* Chapter 1. International Energy Agency.
- Technology Assessment and Research Study Number 195: “Analysis of Platform Vulnerability to Cratering Induced by a Shallow Gas Flow.”
- Technology Assessment and Research Study Number 27: “Study of Cementing Practices Applied to the Shallow Casing in Offshore Wells.”
- Teodoriu C., Asamba P. 2015. Experimental study of salt content effect on class G cement properties with application to well integrity, *Journal of Natural Gas Science and Engineering*, Volume 24, May 2015, Pages 324-329, ISSN 1875-5100. <http://dx.doi.org/10.1016/j.jngse.2015.03.039>.
- Tinsley, J. M., Miller, E. C., Sabins, F. L., and Sutton, D. L. (1980, August 1). Study of Factors Causing Annular Gas Flow Following Primary Cementing. Society of Petroleum Engineers. <http://dx.doi.org/10.2118/8257-PA>.
- Tripathy, B. and Smith, K. 1998. The Myth about Low Temperature Performance of Fluoroelastomers in Oil Seal Applications *SAE Technical Paper 980850*, 1998, <http://dx.doi.org/10.4271/980850>
- Tuckner, P. F. 2005. Considerations and comparison for compression set Vs. Compression stress relaxation (CSR). Presented at Fall 168th Technical meeting, Pittsburg, PA, ACS rubber division, 1-3 Nov.
- Tynan Carroll. 2016. Successful selection of oil and gas seals, *World Pumps*, Volume 2016, Issue 9, September 2016, Pages 28-30, ISSN 0262-1762, [http://dx.doi.org/10.1016/S0262-1762\(16\)30235-8](http://dx.doi.org/10.1016/S0262-1762(16)30235-8)
- Visakh P.M., Sabu Thomas, Arup K. Chandra, Aji. P. Mathew. 2013. *Advances in Elastomers I, Blends and Interpenetrating Networks*. Volume 11. Springer-Verlag.
- Walker James. 2011. *Elastomer Engineering Guide*. 10 November 2011. https://www.jameswalker.biz/de/pdf_docs/148-elastomer-engineering-guide
- Wang WJ. 1996. The development and applications of cx-18 antichannelling agent. *J Xi'an Pet Inst* 1996;11(5):6-7,50-53.
- Wang Zhengjin, Chen Chao, Qihan Liu, Yucun Lou, Zhigang Suo. 2017. Extrusion, slide, and rupture of an elastomeric seal. *Journal of the Mechanics and Physics of Solids*, Volume 99, February 2017, Pages 289-303, ISSN 0022-5096, <http://dx.doi.org/10.1016/j.jmps.2016.12.007>.

Wang, X., Sadana, A. K., and Mathur, V. 2015. Water-Swellable Elastomers for Heavy Brine Environments. *Society of Petroleum Engineers*. SPE-174825-MS. <http://dx.doi.org/10.2118/174825-MS>

Watters, L. T., and Sabins, F. L. 1980. Field Evaluation of Method to Control Gas Flow Following Cementing. *Society of Petroleum Engineers*. <http://dx.doi.org/10.2118/9287-MS>.

Webster, W. W., Eikerts, J. V. 1979. Flow After Cementing: A Field and Laboratory Study. *Society of Petroleum Engineers*. <https://doi.org/10.2118/8259-MS>.

Appendix A: Elastomers

Test Equipment and Testing Protocol

Degradation of elastomers can significantly change its properties and performance. To assess the extent of elastomer degradation after exposure to an acidic environment, different tests were conducted to measure the changes in their physical properties. Measurements included hardness, volumetric swelling, and compression.

Hardness

To measure the hardness of the elastomer, each elastomer was placed on a firm, flat surface. The hardness readings are taken with a Shore 'A' durometer (Figure 74). Shore A durometer measures how much a material indents when a standardized amount of pressure is applied. The indentation hardness is inversely related to the indenter's penetration and is dependent on the material's viscoelastic behavior and elastic modulus (PennCoat Inc., 2014).

The durometer is tuned to zero before using it for any reading. The needle at the bottom of the durometer is pressed onto the surface of the elastomer until the round bottom part of the durometer touches the elastomer surface. The durometer reading decreases gradually, and observed until a constant value is reached for three to five seconds. This reading is recorded and documented. The hardness is measured on two different spots on one flat surface, and repeated at two other different spots on the second flat surface. The average of these four readings is then taken to be a representation of the hardness of the elastomer sample. After the aging test, the hardness measurement is conducted immediately after removing the elastomer samples from the aging cell. The same procedure is followed. Table 21 shows the hardness measurements.

Table 21: Durometer readings for three days aging test.

Sample	Before					After				
	Duro 1	Duro 2	Duro 3	Duro 4	Avg. Duro	Duro 1	Duro 2	Duro 3	Duro 4	Avg. Duro
T1	76.2	75.5	76.1	75.8	75.9	67.5	67.9	69.1	69.6	68.5
T2	76.5	76.1	75.3	75.5	75.9	69	68.7	68	68.8	68.6
T3	75.8	75.3	76.4	76	75.9	68.7	68.1	68.4	68.6	68.5
T4	76	74.8	76.2	75.4	75.6	68.6	67.3	67.3	69.5	68.2
T5	75.6	75.8	75.1	76.2	75.7	68.5	68.2	69	69.2	68.7
T6	76.5	75.2	75.5	76	75.8	68.3	69.6	67.7	69.2	68.7



Figure 74: Digital Durometer Model DD-4.

Volumetric Swelling

The diameter and length of each elastomer sample are measured before and after the aging test. A Vernier caliper (Figure 75) is used in taking the readings. Before aging, one diameter reading is taken and recorded. After aging, three diameter readings are taken for each sample. The first reading is obtained from the point where the elastomer sample reveals the most diameter swelling. This will be the midpoint for most samples, except a few. The second and third readings are obtained from the edges of the sample. They may vary but are usually the same. The average of these three readings represent the diameter

reading of the sample after aging. All readings are taken immediately after removing the elastomer from the aging cell. Table 22 shows the diameter and length measurements.

Table 22: Diameter and length readings for three days test.

Sample	Before			After					
	Length	Diameter	Volume	Length	Dia. M	Dia. E1	Dia. E2	Avg. Dia.	Volume
T1	0.515	0.759	0.233	0.59	0.886	0.875	0.874	0.878	0.358
T2	1.033	0.759	0.467	1.167	0.883	0.874	0.874	0.877	0.705
T3	1.504	0.759	0.681	1.7	0.875	0.876	0.876	0.876	1.024
T4	0.505	0.759	0.229	0.571	0.89	0.875	0.877	0.881	0.348
T5	0.985	0.759	0.446	1.128	0.885	0.879	0.879	0.881	0.688
T6	1.503	0.759	0.68	1.719	0.88	0.8766	0.875	0.877	1.039



Figure 75: Digital Vernier Caliper.

Compression Test

The compression test was conducted using the compression machine in Figure 76, before and immediately after the aging test. The ASTM D575-91 specimen standard was followed, and the ratio of specimen diameter to thickness (2.3) was kept constant. To maintain this ratio, the specimen diameter was maintained at 0.75 inches, while the specimen thickness was 0.33 inches. “Test Method B - Compression test at Specified Force” in ASTM D575-91 was the compression test procedure followed. A specified

minor mass is applied for a period long enough to adjust the deflection gauge. After this, major forces (15lbf, 30lbf, 45lbf, 60lbf, 75lbf, 90lbf) are applied for three seconds. The deflection on the dial gauge at the end of the three-second period is read. This reading does not include any deflection caused by the minor force. The percent deflection or strain based on the extension and original thickness of the specimen is calculated. The stress based on the applied force and area of the elastomer sample is also calculated. The median of the values taken from three specimens of one elastomer type or aging condition is reported. The six major forces were selected based on preliminary tests conducted and machine limitation. Table 23 shows an example of compression test values.



Figure 76: Compression machine setup.

Table 23: Stress vs. strain relationship of NBR before and after three days aging.

NBR 1						NBR 1 After (Vapor)		
Force (Lb)	Area (in ²)	Exten. (in)	Length (in)	Stress (psi)	Strain	Exten. (in)	Length (in)	Strain
15	1.692	0.038	0.34	8.87	0.112	0.035	0.339	0.103
30	1.692	0.047	0.34	17.73	0.138	0.045	0.339	0.133
45	1.692	0.051	0.34	36.6	0.15	0.06	0.339	0.177
60	1.692	0.06	0.34	35.46	0.176	0.067	0.339	0.198
75	1.692	0.066	0.34	44.33	0.194	0.076	0.339	0.225
90	1.692	0.074	0.34	53.19	0.218	0.085	0.339	0.251

Appendix B: Cementing

Calculations

In this section, a few calculations that were needed for the successful mixture of the cement slurries are shown. Some additive calculations included latex given in gals/sack, bentonite – by weight of cement, fly ash – by weight of cement, and barite. Some of these additives had water requirements to keep the viscosity, rheology and pumpability of the cement slurry desirable. The calculations presented vary based on the slurry component mixture. The calculations below are an example of calculations used during cement slurry mixing.

$$M_{cement} = 1290.4 \text{ g}$$

$$M_{water} = 490.35 \text{ g}$$

Latex (1 gal per sack)

$$1 \text{ sack} = 94 \text{ lbs}$$

$$1290.49 \text{ g} = 2.844845 \text{ lbs}$$

$$X \text{ gals} = 2.844845 \text{ lbs}$$

$$X = \frac{2.844845}{94} \times 1 = 0.030264 \text{ gals}$$

$$\rho_{latex} = 8.33 \text{ ppg}$$

$$8.33 = \frac{m(\text{lbs})}{0.030264}$$

$$m_{latex} = 0.2521 \text{ lbs}$$

$$m_{latex} = 114.35 \text{ g}$$

Bentonite (2% BWOC)

$$\frac{2}{100} \times 1290.4 = 25.808$$

Fly ash (30% BWOC)

$$M_F = \frac{30}{100} \times 1290.49 = 387.147 \text{ g}$$

$$M_{wF} = 3.6 \text{ gals} / 74 \text{ lbm} = 13627.5 \text{ ml} / 33563.8 \text{ g}$$

$$\frac{387.147}{33563.8} \times 13627.5 \text{ ml} = 157.18 \text{ ml}$$

Changing Density of cement from ρ_1 to ρ_2

$$\rho_1 = 15.15 \text{ ppg}$$

$$\rho_2 = 16.6 \text{ ppg}$$

$$V_{wB} = 0.015$$

$$V_1 = V_2 \left[\frac{\rho_B \left(\frac{1 + \rho_w V_{wB}}{1 + \rho_B V_{wB}} \right) - \rho_2}{\rho_B \left(\frac{1 + \rho_w V_{wB}}{1 + \rho_B V_{wB}} \right) - \rho_1} \right]$$

$$V_1 = 900 \left[\frac{35 \left(\frac{1 + (8.33 \times 0.015)}{1 + (35 \times 0.015)} \right) - 16.6}{35 \left(\frac{1 + (8.33 \times 0.015)}{1 + (35 \times 0.015)} \right) - 15.15} \right]$$

$$V_1 = 777.67756 \text{ ml}$$

$$m_{\text{Barite}} = \frac{\rho_B (V_2 - V_1)}{1 + \rho_B V_{wB}}$$

$$m_{\text{Barite}} = \frac{4.1944(900 - 777.67756)}{1 + 35(0.015)} = 336.4388 \text{ g}$$

$$V_{wB} = \frac{0.015 \times 3785 \text{ ml}}{453.392} = 0.125167 \text{ ml/g}$$

$$V_{wB} = 0.125167 \frac{\text{ml}}{\text{g}} \times 336.4388 = 42111 \text{ g}$$

Permeability prediction matlab code

```
clear all
clc
% Three permeability values are predicted here
% Equation used is a slightly modified version of Brace et
Al. (1968)
for i = (1:3)
slope(i) = input ('What is the slope of the pressure
decline curve?\n');
alpha(i) = slope(i); % SLOPE FROM DECLINE GRAPH - SEMILOG
R1 = 15.24; % OUTER RADIUS OF PIPE
R2 = 10.16; % INNER RADIUS OF PIPE
height = 5.08; % HEIGHT OF SPONGE AREA
A = pi*((R1^2)-(R2^2)); % CROSSSECTIONAL AREA IN cm2
u = 0.0001747; % VISCOSITY OF N2 GAS IN dynesec/cm2
B = 2.41729E-7; % N2 FLUID COMPRESSIBILITY IN cm2/dyne
L = 91.44; % LENGHT OF PIPE
alphan(i) = alpha(i)*10^7;
V1 = (pi*((R1^2)-(R2^2))*height)/3.085;
V2 = 0.25*V1;
% permeability prediction
Permeability_in_md(i) = (alphan(i)/((1/V1) -
(1/V2))) * ((u*B*L)/A)
end
```

Test Sample Preparation Procedure

The volume of the annulus the cement was to be poured into was calculated. The cement with the required concentration of additives was mixed and kept agitated. The mixed cement slurry was then poured into the annulus and allowed to cure for 12 or 24 hours at ambient pressure and temperature. After the required WOC time has elapsed, N₂ gas was injected into the cement column to study gas migration in the cement column.

Pressure measurements were taken with DASyLab while the time it takes for the gas to bubble and position at which it bubbles is captured by a Zomodo camera. Microsoft Excel was used in analyzing the pressure to develop a regression analysis in the cement column while MATLAB was used to predict system permeability from the excel graphs. Test nomenclature or the test identification code follows a pattern to indicate the type of

setup being used; the cement slurry mixture composition, the cycle within which a test is carried out, and finally the day the test is carried out. Table 24 describes the nomenclature for identifying both the cement sample and the test conducted.

Table 24: Nomenclature for major experiment

S1E1C1T1				
S1	E	1	C1	T1/Day 1
Setup 1	Experiment	First experiment being conducted	Cycle	Test
-		(3 feet, neat class H cement)	Number	Number

As an example, S1E1C1T1 or S1E1C1 Day1 means Setup 1 Experiment 1 Day 1. In the nomenclature Day 1 or Test 1 represent the same thing – the day of testing. This nomenclature is documented for each test prior to the running of the test. After all necessary tests are conducted on a setup, it is discarded. A total of 4 setups have been put together, and a total of 54 major tests have been conducted. Out of these 54 major tests, 42 of them were conducted at 60 psi while remaining tests were conducted at 40 psi.

For minor tests Table 25 describes the nomenclature for identifying both the slurry mixture and the test conducted. Just like in major tests, every nomenclature is

Table 25: Nomenclature for minor experiment

S. Experiment 1 C1 T1		
S. Experiment 1	C1	T1
First slurry mixture in test matrix	Cycle Number	Test Number

documented for each test prior to the running of the test. After all necessary tests are conducted on a setup, it is discarded. A total of 11 setups have been put together, and a total of 30 minor tests have been conducted. All tests have been conducted at 60 psi.

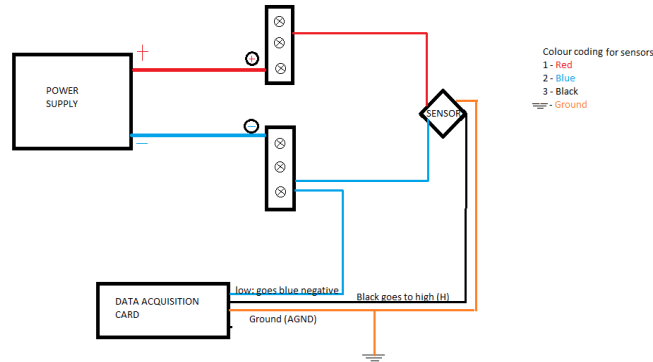


Figure 77: Schematic of sensor connection to data acquisition system.

Gas Transit Time

Table 26: Recorded time for slurries to attain 100 lbf/100 ft² and 500 lbf/100 ft².

Sample	Time (hrs) to 100 lbf/100 ft ²	Time (hrs) to 500 lbf/100 ft ²
Neat Class H	1.0569	2.3228
Neat Class G	0.0369	0.4869
Class H, 30% Flyash - 3.6 gals/74lbm, 1 gal/sack latex.	0.2689	0.7228
Class H, 0.5% Nanomaterial; no water requirement	0.3361	1.8505
Class H, 30% Flyash - 3.6 gals/74lbm, 1 gal/sack latex, 0.5% Nanomaterial; no water requirement	0.2089	0.5834
Class H, 1.5 liters/ 100 kg commercial additive from a service company	0.0072	0.1292

Rheology

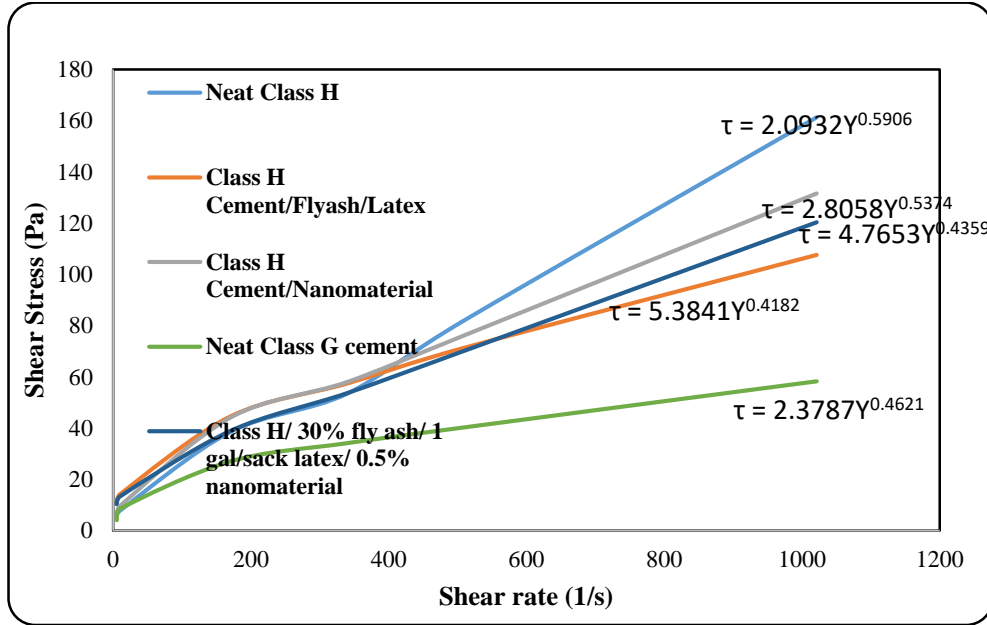


Figure 78: Shear rate vs. Shear rate of various slurry samples.

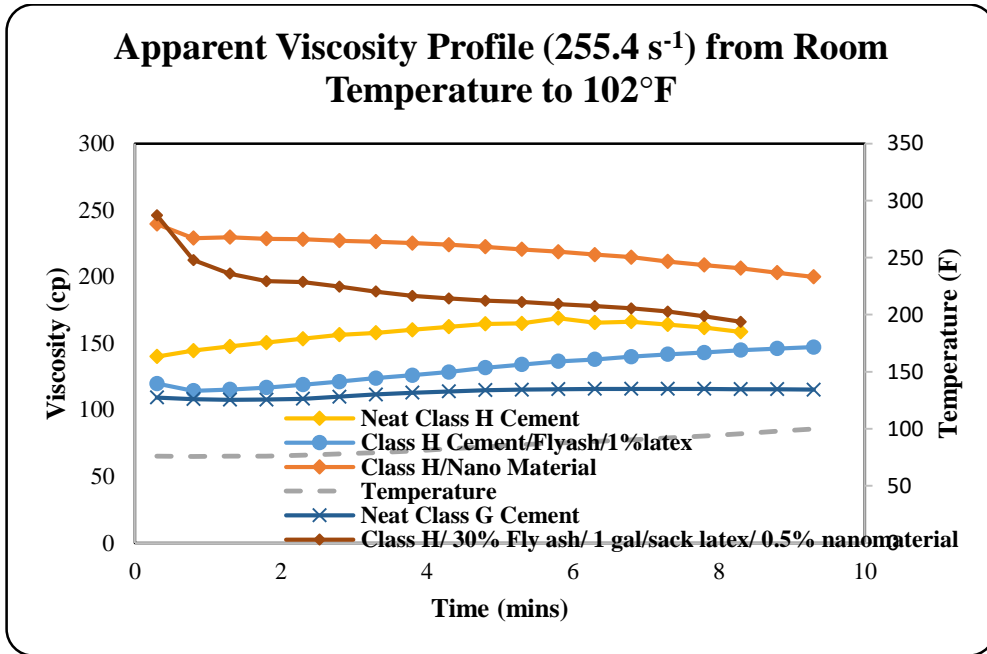


Figure 79: Apparent viscosity graph for various slurry samples at 255.4 s⁻¹.

Unconfined Compressive St Strength and Ultrasonic Testing



Figure 80: Prepared samples for Unconfined Compressive Strength and Ultrasonic Cement Testing.

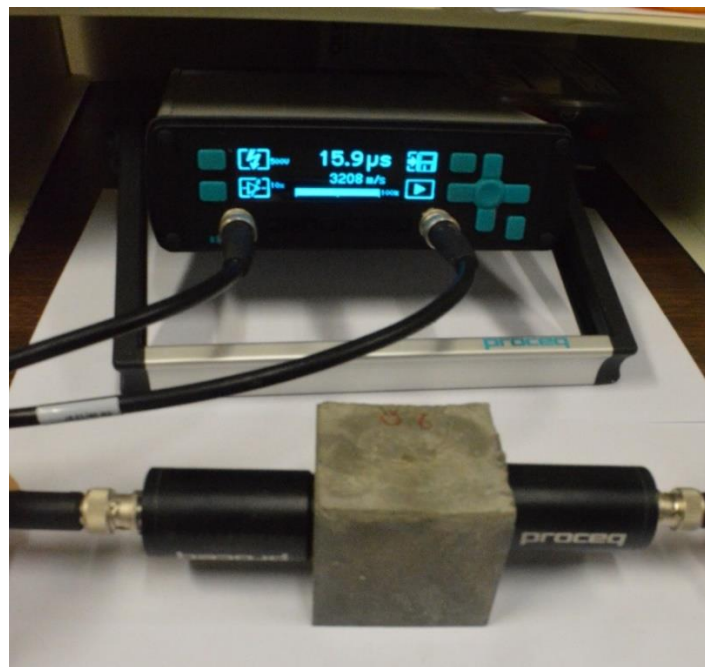


Figure 81: Ultrasonic cement testing being carried out.